UNDERSTANDING THE EFFECTS OF PERIPHERAL ALKYL SUBSTITUENTS ON EXCITON DIFFUSION PROPERTIES OF PORPHYRIN THIN FILMS FOR ORGANIC PHOTOVOLTAIC APPLICATIONS

by

Meesha Kaushal

A dissertation submitted to the faculty of
The University of North Carolina at Charlotte
in partial fulfillment of the requirements
for the degree of Doctor of Philosophy in
Nanoscale Science

Charlotte

2019

Approved by:

_____
Dr. Michael G. Walter, Chair

_____
Dr. Jordan Poler

_____
Dr. Thomas Schmedake

_____
Dr. Christopher Bejger

_____
Dr. Yong Zhang

ABSTRACT

MEESHA KAUSHAL. Understanding the Effects of Peripheral Alkyl Substituents on Exciton Diffusion Properties of Porphyrin Thin Films for Organic Photovoltaic Applications. (Under the direction of DR. MICHAEL G. WALTER)

Understanding exciton diffusion is a crucial step in the engineering and fabrication of organic photovoltaic (OPV) devices. We studied a variety of organic dyes in our research lab including various derivatives of carboalkoxyphenylporphyrins in solution-cast nanometer thick films. We have established basic guidelines on how the exciton diffusion is affected by the arrangement and packing of peripheral alkyl groups in carboalkoxyphenylporphyrin solution-cast nanoscale thin films. The overall goal of this work is to link the molecular organization to singlet exciton diffusion parameters. Photoluminescent (PL) lifetime decays (τ_s) and quenching efficiencies (Q) of solution-cast thin porphyrin thin films lightly doped with [6,6]-phenyl-C61-butryic acid methyl ester (PCBM) have been measured. These data have been used with a 3D exciton eDiffusion Monte Carlo simulation model to generate the exciton diffusion parameters and nanocomposition in the thin films. The length and branching of the peripheral alkyl groups in carboalkoxyphenylporphyrins influence the excited-state dynamics in a thin film. Using longer and linear peripheral alkyl chains increase the PL decay lifetimes and exciton diffusion lengths (L_D). Structural studies such as Grazing Incidence Wide Angle X-Ray Scattering (GIWAXS) and X-ray diffraction (XRD) have indicated that molecular arrangement from longer and linear peripheral alkyl chains leads to nematic packing on the surface of thin films which is favorable for exciton diffusion in carboalkoxyphenylporphyrin thin films. Preliminary data collected for current-voltage

curves measured from ternary OPV devices fabricated using these carboalkoxyphenylporphyrins along with poly-3-hexylthiophene (P3HT) and PCBM also supports our previous exciton diffusion studies. Porphyrin derivatives with longer PL decay lifetimes (τ_s) and exciton diffusion lengths (L_D) have shown higher photocurrents and improved power conversion efficiencies. Our findings are an important step towards a deeper understanding of the exciton diffusivity and molecular packing relationship in order to improve the power conversion efficiency of thin film organic solar cells.

DEDICATION

This thesis is dedicated to my father Vijay Kaushal in India and my husband Kunal Kalia for their continuous support and faith in me. I would also like to dedicate this work to my family in India who have always been there for me and never let me give up when I was struggling with major health issues. Lastly, I would also like to dedicate my work to my grandfather and grandmother who we lost during the course of this study. This thesis is a proof that no obstacles can stop you from achieving your goals in life if you are determined and are ready to put the hard work and hours required.

ACKNOWLEDGEMENTS

Foremost, I would like to acknowledge my advisor Dr. Michael G. Walter for his immense support and unparalleled guidance throughout my thesis work. His faith in me to let me handle the projects and giving me some wonderful opportunities on the way has helped me become a better learner. I would like to thank Dr. Angy Ortiz for introducing me to this project and help me getting started in the lab in my first year. I would also like to acknowledge my fellow lab mates Dawn Marin, Dan Cohen for their inputs and valuable suggestions during this thesis. I am so thankful to the undergraduate researchers Praveen Srinivasamurthy, Camilla Middleton and Jaclyn Stiller who worked with me during several projects and helped me in synthesizing and analyzing the compounds as well as testing the device data. I am also grateful to Babar Hussain, Josue M. Hardigree and Gaurav Singh for helping me with data collection. I am very grateful to my thesis committee members for giving their valuable inputs and time to help me improve my knowledge. We sincerely acknowledge the use of eDiffusion software provided by Oleksandr Mikhnenko, http://mikhnenko.com/eDiffusion to calculate the exciton diffusion parameters. Lastly, a huge thank you to the Chemistry Department at UNC Charlotte and NSF for funding my work at some point in my degree. I am grateful to my committee members for very graciously agreeing to review my work and giving me their valuable feedback and time.

TABLE OF CONTENTS

LIST OF TABLES

LIST OF FIGURES

LIST OF STANDARD ABBREVIATIONS AND ACRONYMS

1. OPV - Organic Photovoltaics
2. OSC - Organic Solar Cells
3. BHJ - Bulk Heterojunction
4. HOMO - Highest Occupied Molecular Orbital
5. LUMO - Lowest Unoccupied Molecular Orbital
6. UV Vis - Ultraviolet Visible
7. ITO - Indium Tin Oxide
8. FTO - Fluorine doped Tin Oxide
9. TCPP - 5,10,15,20-tetrakis-(4-carboxyphenyl)porphyrin
10. TCM_4PP - 5,10,15,20-tetrakis-(4-carbomethoxyphenyl)porphyrin
11. TCB_4PP - 5,10,15,20-tetrakis-(4-carbobutoxyphenyl)porphyrin
12. TCH_4PP - 5,10,15,20-tetrakis-(4-carbohexoxyphenyl)porphyrin
13. TCO_4PP - 5,10,15,20-tetrakis-(4-carbooctoxyphenyl)porphyrin
14. $TCEH_4PP$ - 5,10,15,20-tetrakis-(4-carboethylhexoxyphenyl)porphyrin
15. TCSPC - Time Correlated Single Photon Counting
16. DMF - Dimethyl Formamide
17. THF- Tetrahydrofuran
18. AFM - Atomic Force Microscopy
19. PL Decay -Photoluminescent Decay
20. PCBM - Phenyl-C61- butyric acid methyl ester
21. C_{60} - Fullerene

22. MALDI- Matrix Assisted Laser Desorption Ionization

23. NMR – Nuclear Magnetic Resonance

24. SSE -Steady-State Emission

25. XRD -X-Ray Diffraction

26. GIWAXS -Grazing Incidence Wide Angle X- Ray Scattering

27. CV - Cyclic Voltammetry

28. DSC - Differential Scanning Calorimetery

29. EQE- External Quantum Efficiency

30. SMU -Source Measure Unit

31. P3HT- Poly-3- hexylthiophene

32. J_{sc} -Short Circuit Current Density

33. I_{sc} -Short Circuit Current

34. V_{oc} -Open-Circuit Voltage

35. P_{in} -Power In

36. P_{max} -Maximum Power

37. FF- Fill factor

38. J_{mp}- Maximum Current Density

39. V_{mp}- Maximum Voltage

40. L_D -Exciton Diffusion Length

41. D - Diffusion Coefficiet

CHAPTER 1. INTRODUCTION AND BACKGROUND

1.1 Motivation and Origin of Solar Energy

The increasing global population demands an alternative energy source that is sustainable, renewable, environment-friendly and cost-effective. Currently, non-renewable resources like oil, coal and natural gas supply most of the energy across the world.[1,2] There are potential environmental hazards related to both renewable and non-renewable energy resources.[3] Out of all the available renewable resources such as wind, geothermal, and hydroelectric, solar energy and wind energy are often considered cleanest and sustainable energy resources. According to the data collected by National Renewable Energy Laboratory (NREL) in the 2017 energy data book, the overall electricity generated worldwide using renewable resources was 24%. In the United States, 12.7% energy production originated from renewable resources. Out of all the available renewable resources, solar energy is an increasingly popular area for researchers today owing to its potential carbon free energy benefits and cheaper alternatives. **Figure 1.1** shows the total energy production and consumption in the United States in 2017 taken from NREL website energy data book. The data shows the actual percentage of the energy produced and consumed in 2017 from both renewable and non-renewable resources.[4] In general, renewable energy production and consumption has come a long way from where it was ten years ago.[4] However, in order to obtain sustainable and green energy alternatives that are beneficial for our ecosystem, a lot more research in to solar energy technology is needed. The surface of the earth receives

1.75×10^{17} W of energy from the sun in an hour which is sufficient to fulfill worldwide energy demands for one year. Therefore, harvesting sunlight and converting energy directly into electricity using photovoltaic (PV) device is a promising energy solution.[5]

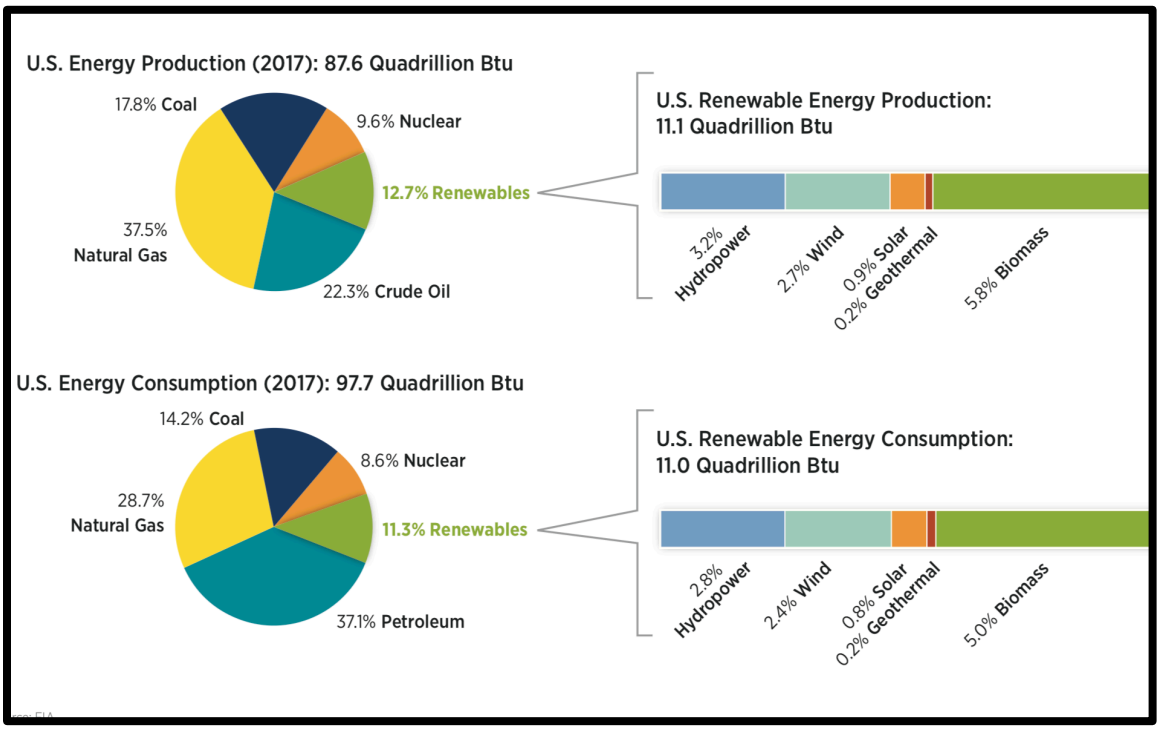

Figure 1.1 Energy production and consumption (2017) from NREL energy data website

Photovoltaic science dates back to as far as the 1870's when William Grylles Adams first exposed selenium cells to sunlight in 1876 and found that those cells had the ability to convert sunlight directly into electricity through the photovoltaic effect.[6] But it was only in the early 1950's that the first silicon solar cells were made by Bell Labs.[7] Scientists at Bell Labs were the first ones to revolutionize the field of semiconductors and photovoltaics using silicon, afterwards, the silicon solar cells were made commercially available by the year 1956.[8] The traditional mono or multi-crystalline silicon solar cells are categorized as first generation solar cells.[9] The silicon solar cells were expensive and had tedious manufacturing steps making them expensive for daily usage. The price of the

silicon solar panel has since then reduced and significant improvements have been made to make silicon solar cells more affordable. These are still the most popular solar cells to date accounting for 75% photovoltaic market.[10] The second-generation thin film solar cells used amorphous silicon and inorganic materials such as copper indium gallium selenide (CIGS) and cadmium telluride (CdTe). This class of materials offered a cost-effective solution to the already existing expensive silicon solar cells but at a much lower power conversion efficiency.[3] The third-generation solar cells use new highly processable materials, such as carbon nanotubes, quantum dots, organic dyes, and conjugated polymers. This class of solar cell is also referred to as organic solar cells and is the focus of this dissertation.

Organic Photovoltaics (OPV) constitutes a class of organic electronic materials or semiconductors, which can be exploited for their potential to replace traditional inorganic semiconductors with low manufacturing cost using a flexible substrate.[11,12] OPVs offer advantages like low-cost, solution casting, roll-to-roll processing with tunable optical and electronic properties. These molecular materials form what is called organic/plastic solar cells.[10,13] The many advantages of OPVs have attracted massive enthusiasm in their field and significant amounts of research have been carried out to increase the power conversion efficiency (PCE) of these devices.[14-16]

For a single layer solar device, the theoretical power conversion efficiency (PCE) limit is 33% and is commonly referred to as the Schockley-Queisser limit, which describes the maximum possible efficiency of a single layer solar cell under the illumination of 1 Sun (1.5 AM solar spectrum).[17,18] Recently power conversion efficiencies (PCE) of approximately 16.2% have been achieved in single and multi-

junction OPVs.[19-21] However, by combining various junctions and making multi-layered photoactive layer in the organic solar cells, much higher efficiencies can be theoretically achieved. The major energy losses are contributed by two different sources, these sources could be either extrinsic or intrinsic. Carrier recombination, impurities, and absorption from unwanted layers, etc. are examples of extrinsic losses whereas below band-gap and thermalization losses contribute to the intrinsic losses.[17] The composition and assembly of organic solar cells have been discussed in detail in the next section with a brief introduction to all the important information that is related with this research.

1.2 Introduction to Organic Semiconductors

Organic semiconductors have been studied since the 1950's when Akamatu, Inokuchi and Matsunga published the discovery of semi-conducting polycyclic charge-transfer complexes with iodine and bromine.[14] Afterwards in 1970's, polyacetylene's conductivity was measured upon doping with halogens and this started the trend of studying conducting polymers. Heeger, MacDiarmid and, Shirakawa received the Nobel Prize in Chemistry in the year 2000 for their breakthrough research in electrically conductive polymer research.[22-24] **Figure 1.2** shows some of the commonly studied organic semiconductors for OPV applications. Organic semiconductors have delocalized π-electron clouds capable of absorbing photons from sunlight with tunable optoelectronic properties and can be used to convert solar energy to electrical energy, the mechanism of this conversion will be discussed in more detail in the next section.[25] The conjugated π-electron backbone in such organic materials makes them suitable materials for charge-transport layers in OPV applications which can be wet processed by spin-coating or doctor blading. In order to understand how organic solar cells work, it is extremely

important to understand the science behind the light absorption in organic semiconductor and its conversion into electrical energy.[26,27] The conjugated aromatic backbone of organic semiconductors possesses electrons in the p_z orbital of carbon which overlaps with electrons present in the adjacent p_z orbitals forming a delocalized cloud of π-electrons across the molecule.[28] Such delocalized π-electron cloud results in high polarizability in organic semiconductors.[28] The charge carrier mobility in organic semiconductors is much lower than inorganic semiconductors which impact the efficiency of organic solar cells.[28,29]

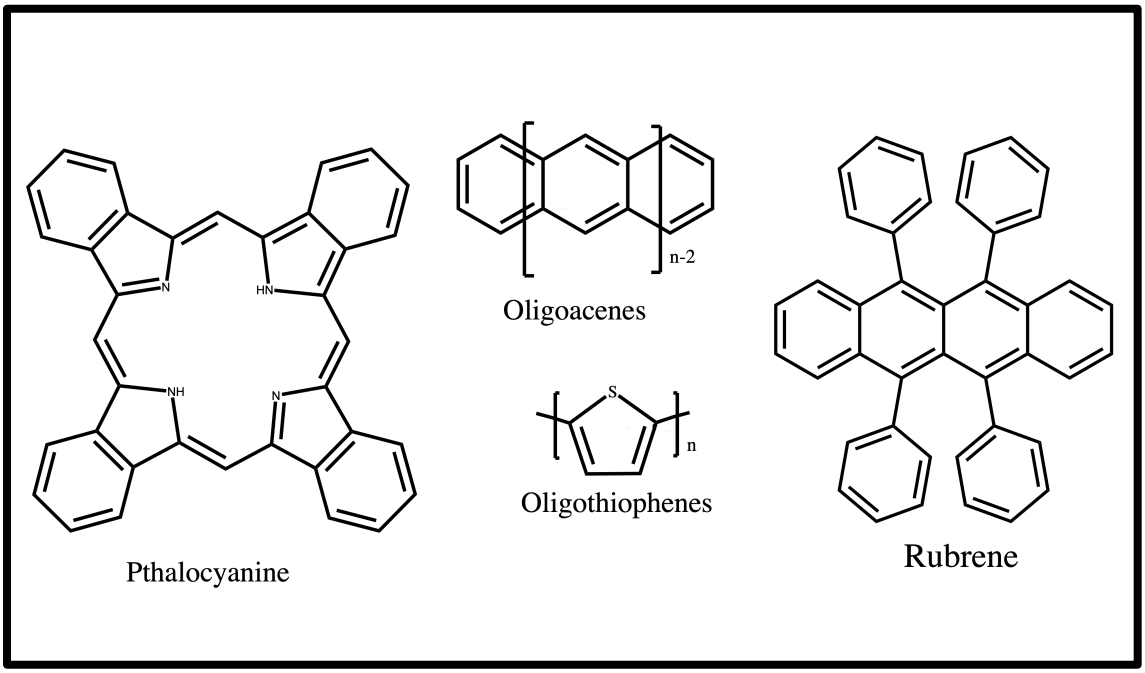

Figure 1.2 Commonly studied organic semiconductor materials

The band structure in organic semiconductors can be compared to inorganic semiconductors where highest occupied molecular orbital (HOMO) and lowest unoccupied molecular orbitals (LUMO) can be compared with valence band and conduction band in an inorganic semiconductor.[30] HOMO and LUMO energy levels of an organic semiconductor are assigned to the different types of π orbitals.[25,30] Upon

receiving energy from an outside source such as sunlight an electron is excited from HOMO energy level to the LUMO energy level of the organic semiconductor, this happens due to the presence of delocalized π-electron cloud in the organic semiconductors.[30] The mechanism of energy transfer in organic semiconductors takes place via Förster resonance energy transfer (FRET)W by hopping mechanism and is discussed later in this chapter whereas in inorganic semiconductors the energy transfer occurs through the movement of free charge carriers.[30] Following **Figure 1.3** shows the bonding and antibonding interactions that take place in an organic semiconductor when HOMO and LUMO energy levels are formed. In the next section, the constituent layers of organic solar cells have been explained with an emphasis on the HOMO and LUMO energy levels in these respective layers. The interactions in organic semiconductors are primarily covalent and weak intermolecular interactions.

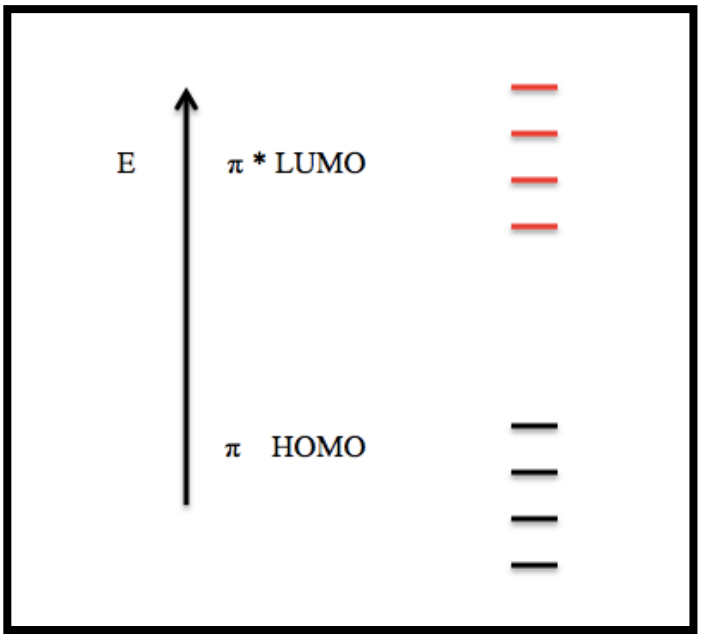

Figure 1.3 Bonding and antibonding interactions in HOMO and LUMO of an organic semiconductors[30]

1.3 Working Mechanism of Organic Solar Cells

1.3.1 Constituents of Photoactive layer in Organic Solar Cells

Photoactive materials are light-sensitive materials that have light absorbing properties due to the wide absorption range.[31] A photoactive layer in the organic solar cell generally consists of a donor layer consisting of conjugated π-electrons systems and an acceptor layer made from high electron affinity materials. Fullerenes are the most common materials to be used as acceptors in organic solar cells. The donor layer upon irradiation by outside light source generates a bound excited species which has an electron and hole held together by electrostatic forces and is known as an exciton.[23,30] The excited state should either be generated at the interface or should be able to migrate to heterojunction or interface in order to successfully complete the process of charge separation and generate energy.[32,33]

1.3.2 Mechanism of Charge Transfer in Donor-Acceptor layer in Organic Solar Cell

There are four major steps involved in the formation of excited state to energy conversion in organic photovoltaic devices. In order to have good photoconversion efficiency (PCE) in organic solar cell, all of these four steps should be completed efficiently.[30]

a. Light Absorption

b. Exciton Diffusion

c. Free Charge Carrier Generation (exciton dissociation)

d. Charge (electron/hole) Transport to the opposite electrodes

The formation of an excited state to the extraction of charges in an organic semiconductor is often considered one of the most critical steps and is highly responsible for the

performance of a photovoltaic device. Upon illumination, an electron in the HOMO energy level is excited to the LUMO energy level of the organic semiconductor. The electron and holes do not dissociate as the coulombic interactions between electron and hole are strong because of localized π-electrons and lower dielectric constants of organic semiconductors.[30] The binding energy of an exciton in an organic semiconductor is of the order of 0.3-1.4 eV, which is orders of magnitude higher than in inorganic semiconductors where electron and holes are easily dissociated since the binding energy of charge carriers generated in inorganic semiconductor is below 25 meV range.[30] Once the excited states (excitons) are generated, the next step is the exciton diffusion followed by exciton dissociation and formation of free charge carriers. Since the electron and hole pair is bound by some binding energy, Tang et al. suggested to create a junction using two different types of organic materials to assist in charge separation.[30,34,28,35] **Figure 1.4** shows that LUMO energy level of the acceptor is right below the LUMO level of donor and the energy gap between the two LUMO levels of acceptor and HOMO level of the donor is smaller than the potential energy of an exciton. The energy difference between two LUMO energy levels of the donor and acceptor material should be higher than the binding energy of the exciton generated in order to favor exciton dissociation at the interface. **Figure 1.4** shows the band alignment of two different organic semiconductors donors and acceptors and the exciton dissociation at the interface.

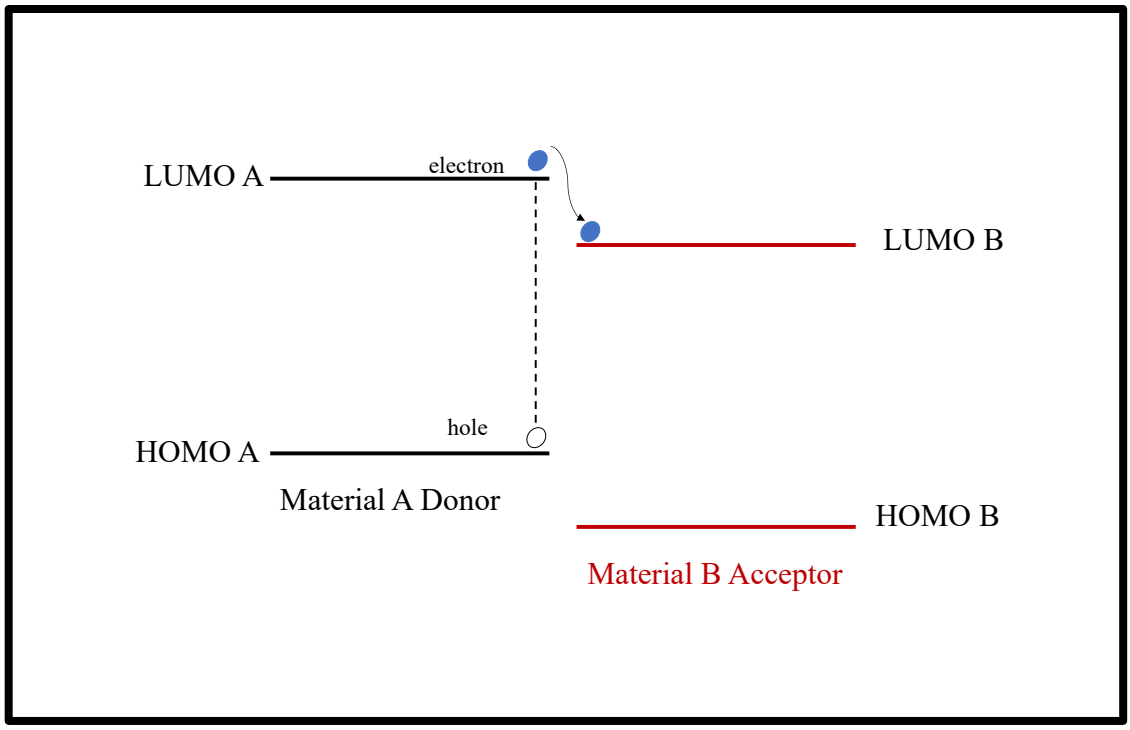

Figure 1.4 Energy levels of donor and acceptor materials in a heterojunction[30]

Due to the transfer of an electron from material A into material B due to the dissociation of an exciton at the interface, material A is referred to as the donor. Since the electron is transferred into material B because of the LUMO energy level, material B is referred to as the acceptor. This charge transfer takes place at the heterojunction of the photoactive layer on a femtosecond timescale.[30]Another possible process that is feasible at the heterojunction is radiative recombination. Since radiative recombination occurs on a nanosecond scale, exciton dissociation is more favorable before the recombination can take place. The exciton diffuses a certain distance by hopping and this distance is called the exciton diffusion length (L_D). The electron and hole form a charge pair at the interface, and this pair of charges is coulombically interacting at this point and are called a geminate pair.[30]

The potential gradient due to the difference in the work function of anode and cathode is responsible for the transport of the free charge carriers.[25] Normally a high work function anode and low work function cathode are chosen in order to create enough potential gradient that can aid in the movement of charges to the electrodes and will directly impact the photocurrent density (J_{sc}).[30] The process of drifting charge carriers in response to the potential gradient of the two electrodes is called carrier movement due to drift currents.[30] Another very significant phenomenon responsible for carrier transport is due to the diffusion current, which occurs because of the increased population of electrons and hole at the bulk-heterojunction, which drives the charge carriers through the concentration gradient, and the charge carriers move away from heterojunction.[30] The diffusion currents influence the charge carriers when the externally applied voltage is greater than the internal electric field generated whereas drift currents influence charge carriers when internal electric field is large.[30] Interestingly, excitons are neutral and are unaffected by an applied bias. The work function of anode should be close or equal to the HOMO of the donor and the work function of cathode should be close or equal to the LUMO of the acceptor in order to minimize the potential barrier created at the active layer heterojunction.[30] A good ohmic contact is reached by using high work function metals such as gold (Au, 5.2 eV) as the anode and low work function metal such as aluminum (Al, 4.2 eV) as the cathode. **Figure 1.5** shows all the steps that take place in an organic solar cell.[30] The efficiency of all the steps combined is known as external quantum efficiency (EQE). The EQE is the efficiency of each step involved from light absorption to charge collection in the solar cell and is given by Equation. 1.1:[30]

$$\eta_{eqe} = \eta_A . \eta_{diff} . \eta_{diss} . \eta_C \quad \text{…. ……} \textit{Equation 1.1}$$

Where,

$\eta_{A=}$ Photon absorption,

η_{diff} =number of excitons diffusing to interface

η_{diss}=number of excitons that dissociate to electron and hole

η_C=number of charge carriers extracted at the electrodes

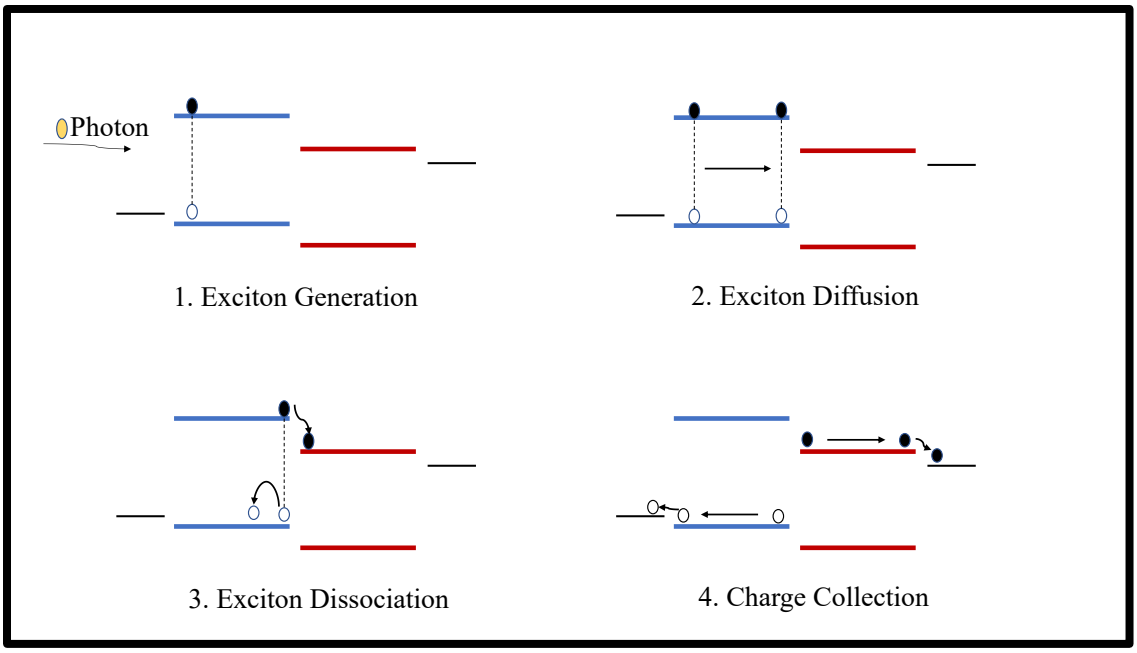

Figure 1.5 Summary of the steps involved in organic solar cell modified from the original.[30]

1.3.3 Fluorescence

When light is absorbed by a molecule's ground state to reach a higher energy excited state and longer wavelength light is emitted upon returning back to the ground state, the emitted light while returning to the ground state is called fluorescence.[36] The three important events leading to fluorescence are excitation of an electron by an incoming photon which happens at a femtosecond timescale, vibrational relaxation from an excited state to ground state occurs at picosecond timescale and emission of longer wavelength photon occurs at nanosecond timescale. **Figure 1.6** shows the Jablonski diagram

elaborating all the possible pathways that an electron can opt upon excitation from the ground state to higher excited state and while coming back to the ground state with timescales of all the phenomenon involved in the above process. The difference between absorbed wavelength and emitted wavelength is called the Stokes shift.

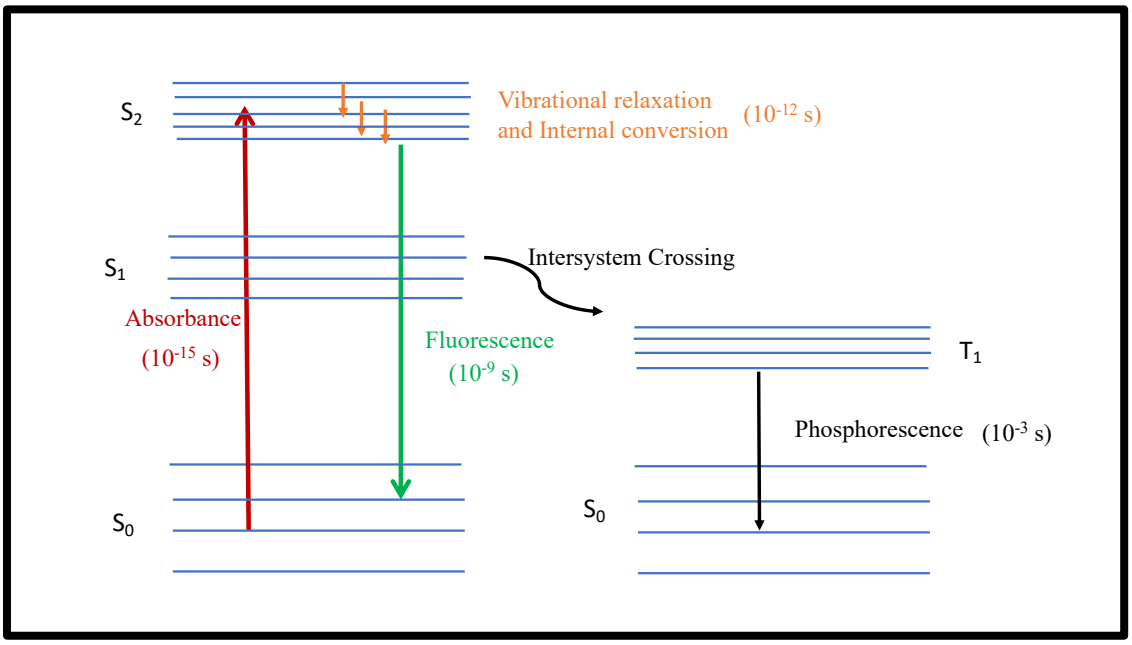

Figure 1.6 Jablonski diagram summarizing energy levels and transitions

During the excitation process, if the two electrons maintain their spin, they are referred to as singlet excited states. However, if the excited state goes through intersystem crossing and the spin of the electron is reversed, a triplet excited state is formed (**Figure 1.6)**. The triplet excited state is lower in energy than the singlet excited state. Fluorescence quenching is often referred to as a decrease in the quantum yield or emission intensity of a fluorophore upon interacting with a quencher molecule. There are two major categories of quenching, dynamic and static quenching. Dynamic quenching can take place when the molecule is in the excited state and interacts with another molecule facilitating non-radiative energy transfer resulting in the decrease of a fluorescent lifetime. However, if the molecule is quenched in its ground state by the formation of a non-fluorescing

complex between fluorophore and quencher, no decrease in a lifetime is observed and the phenomenon referred to as static quenching.[37]

1.3.4 Energy Transfer Mechanisms in Organic Semiconductors

After the exciton is formed the excess energy in the system is transferred throughout the conjugated system. The donor and acceptor material can both generate excited states and these excitons are required to diffuse to the interface for dissociation. Exciton migration in organic semiconductors can happen by three different pathways:

Cascade Energy Transfer (Radiative Energy Transfer): The cascade energy transfer is also called the radiative energy transfer and is followed by emission of a photon by the photo-excited state, which is absorbed by the next molecule, and this is how energy is transferred in the system. The cascade energy transfer occurs in thin films where the absorption and emission spectra overlap with each other.[38,39]

Dexter's Energy Transfer: The Dexter energy transfer involves the orbital-orbital overlap for the purpose of energy transfer upon absorbing a photon. This mechanism involves the direct electron exchange which required overlapping electron densities.[38]

Förster's Resonance Energy Transfer: In the majority of molecular semiconductors excitons diffuse by Förster's resonance energy transfer (FRET), which is a non-radiative energy transfer process, where no direct electron exchange takes place.[38] The energy transfer takes place via coulombic coupling and the electromagnetic fields of donors and acceptor molecular dipoles.[40] FRET is inversely proportional to distance between dipole-dipole interactions and becomes strong when the distance decreases.[38] This molecular dipole distance dependence is shown in following equations 1.2 and 1.3. Singlet exciton diffusion via FRET is also limited by the lifetime of the excited state. [41]

$$k_F(d) = \frac{1}{\tau}\left(R_o/d\right)^6 \quad \text{.....Equation 1.2}$$

$$R_o^6 = \frac{9\eta_{PL}K^2}{128\pi^5 n^4}\int \lambda^4 F_{D(\lambda)}\delta_A(\lambda)d(\lambda) \quad \text{.....Equation 1.3}$$

Where,

R_o is radius and is dependent on the orientation of molecular dipoles (K)

λ is spectral overlap integral

F_D is normalized fluorescence of the donor

σ_A is the absorption cross-section of acceptor

η_{PL} is photoluminescence efficiency

1.3.5 Types of Organic Solar Cells based on Active Layer Architectures:

The incoming photons are absorbed in the photoactive layer made from an electron donor and an electron acceptor in organic solar cells. The interface where donor –acceptor materials come in contact with each other is of great significance and is commonly called heterojunction in organic photovoltaics (OPVs).[42] Based on the architecture of donor-acceptor heterojunction, OSC's can be categorized into three different types as Bilayer , Bulk-Heterojunction and Tandem Solar cells as shown in **Figure 1.7** below.

(a) Bilayer Organic Solar Cells

The bilayer OSC's have planar donor-acceptor layers where a very thin layer of donor material and acceptor material is used. Since the diffusion lengths of organic semiconductors are short in thin films (~10 nm) the possibility of exciton reaching the interface is low in such devices. If the thickness of the active layer is very small, this limits the amount of light absorption. Since the exciton diffusion length of most organic

semiconductors is much smaller than their absorption depths, bulk-heterojunction is a better morphology to achieve higher efficiency organic solar cells.[43]

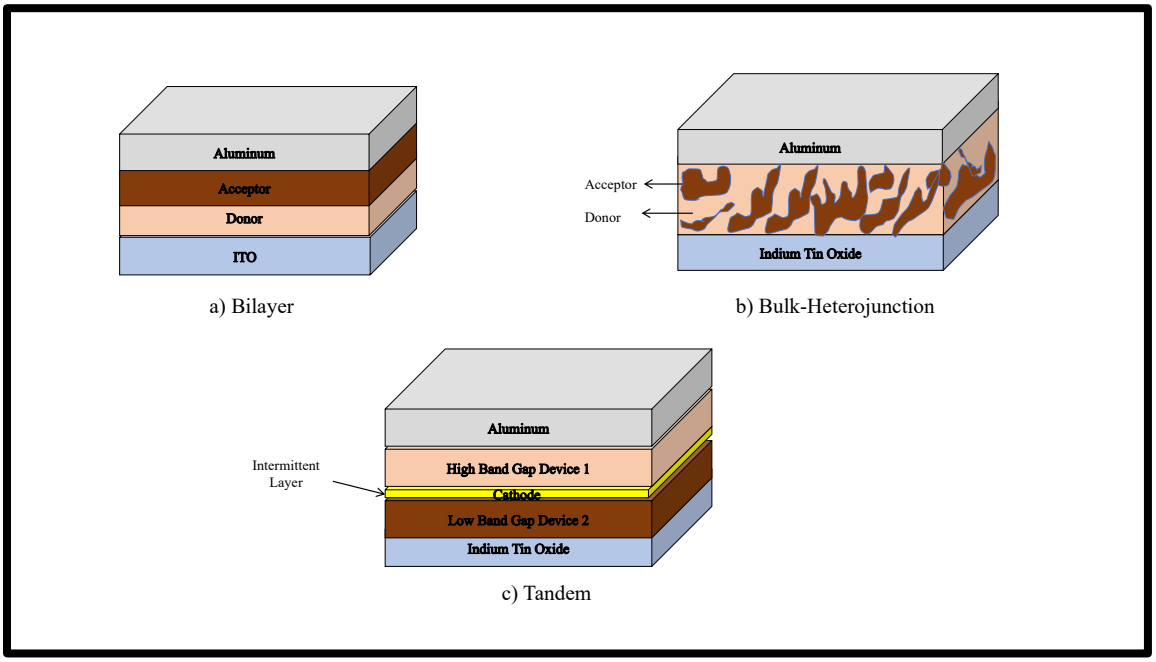

Figure 1.7 Types of organic solar cells based on heterojunction

(b) Organic Bulk-Heterojunction Solar Cells

The bulk-heterojunction OSC's have a photoactive layer where donor and acceptor materials are non-uniformly blended into each other.[31] The idea behind mixing the donor and acceptor is to create an interface closer to the exciton generation site. If the interface is closer to photogeneration site, the exciton has a smaller distance to diffuse in order to reach the interface. This increases the possibility of charge separation at the interface and reduces the possibility of recombination, which would ultimately lower the efficiency of the organic solar cell. It is one of the most important types of organic solar cell studied.

(c) Tandem Solar Cells

The category of organic solar cells where one or two devices are combined or stacked in a single solar cell to enhance absorption and photovoltaic properties of a solar cell is called a tandem solar cell. Hiramoto et al. introduced this specific kind of cell where a p-type (hole conducting) material with a co-deposited intermittent layer and then n-type (electron conducting) material. By stacking solar cells in series, the open-circuit voltage can be increased.[44]

1.4 Current-Voltage Curves of Resistors and Solar Cells

The current-voltage (I-V) curve explains the relationship between the current that flows in a solar cell device upon applying a certain voltage across the positive and negative ends in the circuit. I-V curves give important information such as the performance or power conversion efficiency of the photovoltaic device.[45] In a pure resistor, current and voltage are linear and follow Ohm's law which means as the voltage increases the current flowing through the resistor increases linearly.[46] The current flowing in such systems can be calculated by following equation:

$$I=V/R \quad \ldots\ldots\ldots\ldots\ldots\ldots\ldots\ldots \quad \textit{Equation 1.2}$$

Where I is the current flowing, V is the applied voltage and R is the resistance. An example of I-V curve in such systems can be seen in **Figure 1.8 (a).** Such systems with linear dependence between current and voltage are called ohmic systems. The current in first quadrant will be positive and in the third quadrant will be negative.[47,48]
However, the semiconductor devices are made of P-N junction diodes, therefore, such devices do not exhibit the linear relationship between current and voltage. The current

will flow in such systems only when the diode is forward biased and will be blocked when the diode is reverse biased as shown in **Figure 1.8 (b)**.[49]

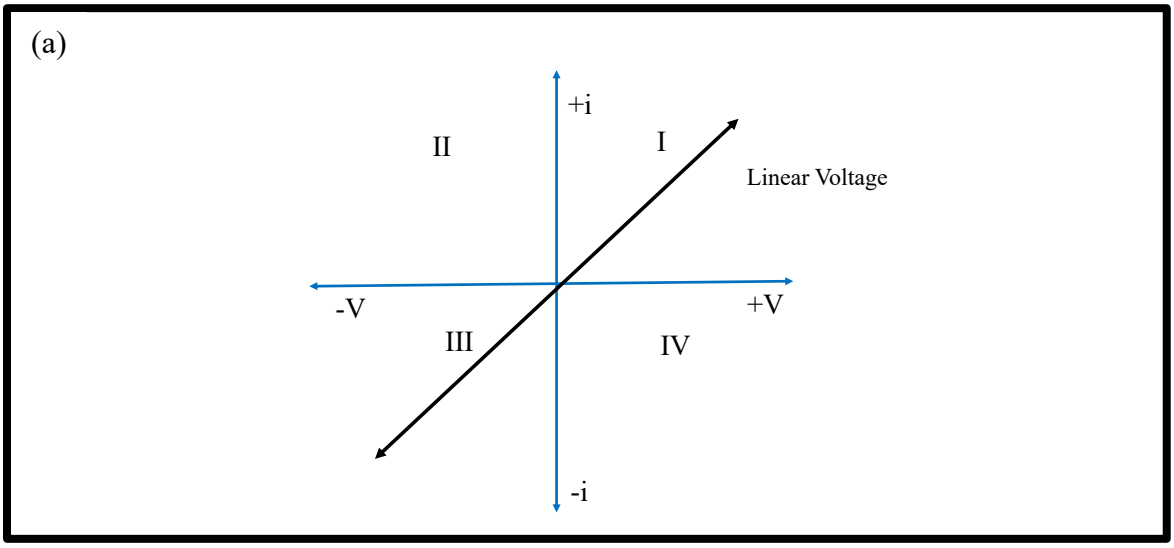

Figure 1.8 (a) Linear relationship between current and voltage in a resistor

In the first quadrant, positive current passes through the circuit and is often referred to as forward bias current where the anode is the positive end of the circuit. As the applied voltage surpasses the internal voltage of the system, the current increases sharply. Contrary to the first quadrant, when the P-N junction is reverse biased, there is very little current is passing through the circuit. After a certain voltage, the reverse bias is large enough that the current increases drastically and is referred to as the breakdown voltage.[48]

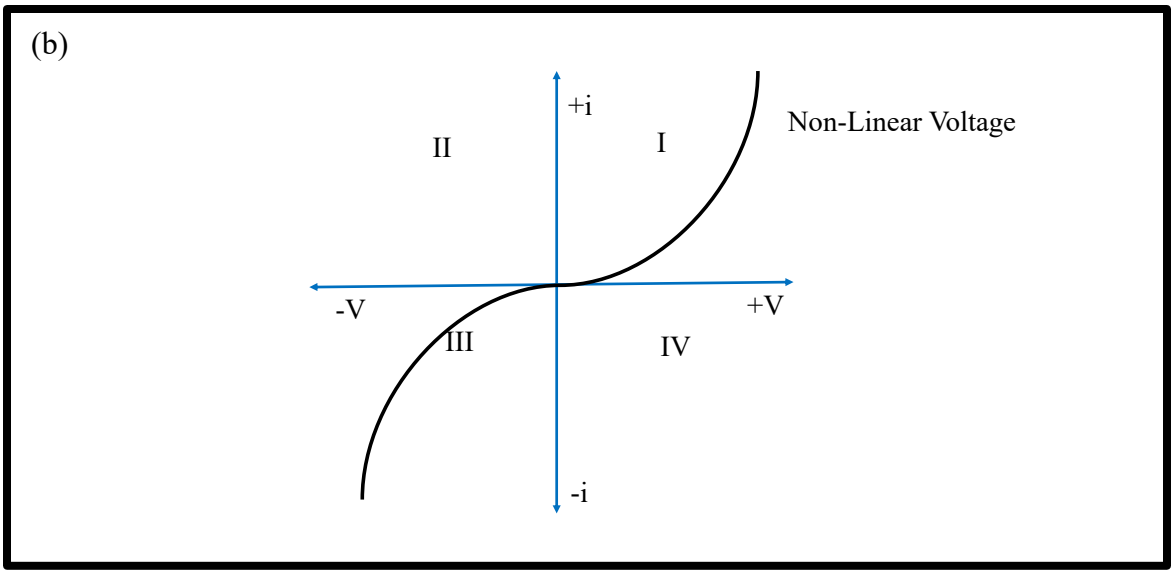

Figure 1.8 (b) curves in a semiconductor device showing non-linear relationship

The *J-V* curve of solar cells exhibits diode behavior as shown in **Figure 1.9**, the main parameters governing the efficiency of solar cells are maximum power (P_{max}), maximum voltage (V_{max}), short-circuit current density (J_{sc}), open-circuit voltage (V_{oc}) and Fill Factor (FF).

Short-Circuit Current Density (J_{sc}): A solar cell gives the maximum current when there is no resistance, which is a possibility only when there is a short circuit in the conduction pathway. This current is called the short circuit current density or J_{sc} and is measured when the voltage is zero. The short circuit current is dependent on the incident photon flux of the device and is also dependent on the absorption spectra of the photoactive material of the solar cell. For research purposes, AM 1.5 standard light intensity (100 mW cm^{-2}) is used to study the photovoltaic parameters. For the measurements, short circuit current density is used and is calculated by diving the short circuit current (I_{sc}) by the area of the illumination of a solar cell device.

Open-Circuit Voltage (V_{oc}): The other important parameter of a solar cell is open-circuit voltage (V_{oc}), which is the voltage when the current flowing in the system is zero.

Fill Factor (*FF*): Fill factor is the ratio of the maximum power output of the solar cell to the theoretical power. Fill factor determines the maximum power of a solar cell.

$$FF = \frac{J_{mp}\,V_{mp}}{J_{sc}\,V_{oc}} \quad \text{.....Equation 1.3}$$

Where J_{mp} and V_{mp} are maximum current and voltage in the device.

Power Conversion Efficiency (PCE) or (η): Power conversion efficiency decides how efficiently the device converted solar energy into electrical energy and is calculated by dividing the maximum power generated by the device (P_{max}) by the incident power (P_{in}).

$$PCE(\eta) = \frac{P_{max}}{P_{in}} \text{ or } \frac{J_{sc}\,V_{oc}FF}{P_{in}} \quad \text{.....Equation 1.4}$$

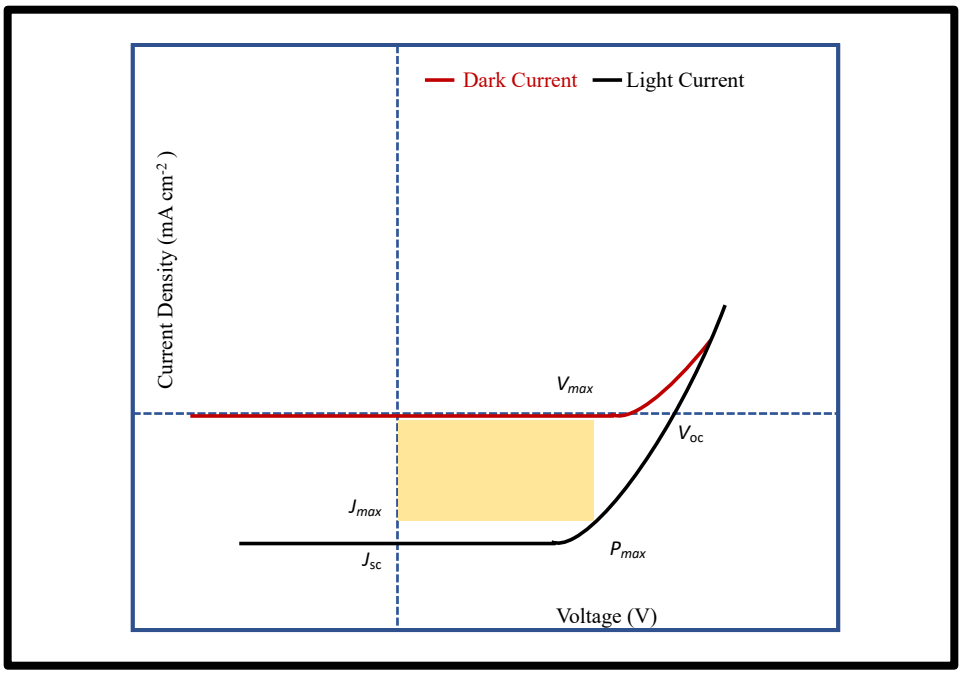

Figure 1.9 *J-V* Curve of a single junction solar cell

1.5 Porphyrins and their Importance in Organic Photovoltaics

Porphyrins are colorful light-harvesting macromolecules with excellent photophysical properties and large absorption coefficients in the visible region of the spectrum.[50] Porphyrins are structural analogs of chlorophyll responsible for all the energy production in plants and also form the backbone of the Heme found in hemoglobin in organisms.[51] In the past decade, extensive research has been done on porphyrins and their derivatives to use them as light-harvesting systems for OPV applications.[1,50] Porphyrins get their color and absorbance intensity from a highly conjugated π-electron system.[52] The extended π-conjugated structure of porphyrin ring provides an excellent pathway for electron transfer and makes them a great candidate for photovoltaic devices. If we take a look at absorption spectra of porphyrins and solar radiation, we see that more than half of the solar harvesting region falls under 700 nm in the spectrum. Porphyrins absorption spectra overlap the sun's absorption spectra region and hence intense absorption bands in the visible region.[23]

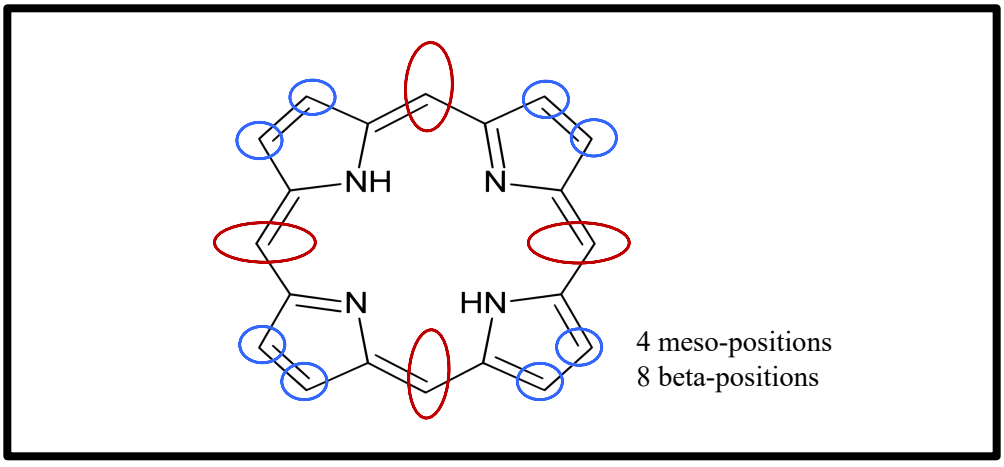

Figure 1.10 Structure of free base porphyrin showing meso and beta positions modified [31]

Since porphyrin-based chromophores exhibit fast and efficient energy transfer in plants during photosynthesis, many studies were initially carried out to synthesize

porphyrins and use them as sensitizers in solar cells for artificial photosynthesis. [53] There has been a lot of interest in the electronic structure of porphyrins pertaining to their biological, catalytic and photophysical properties. Porphyrins have been studied in artificial light-harvesting antennas, donor-acceptor (dyads), donor-acceptor-donor or acceptor-donor-acceptor (Triads). The structure of porphyrin has two types of sites to functionalize the porphyrin; these are called meso- carbons and β – carbons. There are four meso positions and eight β- positions available on a porphyrin parent ring that could be easily functionalized as shown in the following **Figure 1.10**.[54] The parent ring of a porphyrin is very electron rich and highly conjugated consisting of 22 π-electrons, of which 18 electrons form the aromatic core according to Huckle aromaticity rule (4n+2) rule where n =4.[50]

If we look into the absorption spectra of a free-base porphyrin, it has intense absorption bands due to the presence of π-conjugation as seen in **Figure 1.10**. The first and most intense band is seen in 380-500 nm region or ultraviolet region and is called Soret or B- band which corresponds to $S_0 \rightarrow S_2$ transition followed by series of weaker but significant bands (less intense than B-band) corresponding to $S_0 \rightarrow S_1$ transition in the 500-750 nm region or visible region and these bands are called Q-bands. The molar extinction coefficient for B-band and Q-band is 10^5 $M^{-1}cm^{-1}$ and 10^4 M^{-1} cm^{-1} respectively.

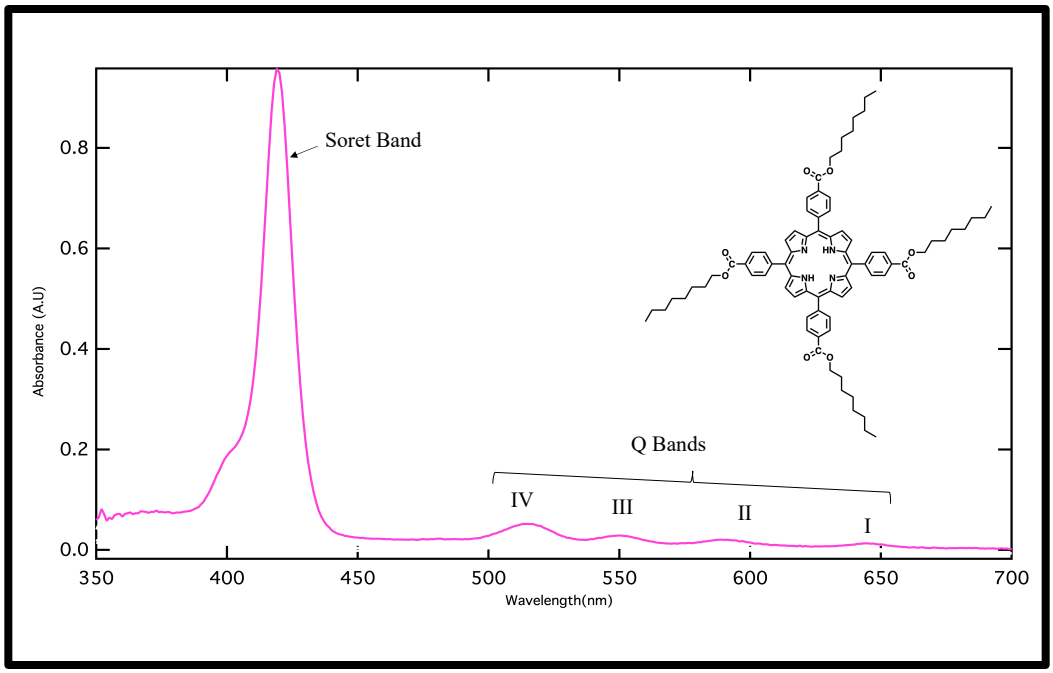

Figure 1.11 UV-visible spectrum of porphyrins with four Q bands in the spectrum[52]

In order to understand why porphyrins, absorb at a certain specific wavelength we need to understand the transitions occurring once they are illuminated. The highest occupied molecular orbitals (HOMO) and lowest unoccupied molecular orbitals (LUMO) in a porphyrin are shown below in **Figure 1.12**.[52,55] Martin Gouterman explained the absorption spectra using a Four Orbital model where two HOMOs (π) and two LUMOs (π*) are present as seen in **Figure 1.12**. The two HOMOs are a_{1u} and a_{2u} whereas LUMOs are degenerate orbitals e_g. Upon excitation, the transition between HOMO and LUMO occur and orbital mixing takes place which results in two types of energy states; one with higher oscillator strength resulting in B or Soret-band and the other with lower oscillator strength resulting in Q bands.[52]The intensity of Q-bands depends on the position and nature of the substituent on the porphyrin ring. The four meso and eight beta positions available and the center of porphyrin can host various metals in order to form metalloporphyrins

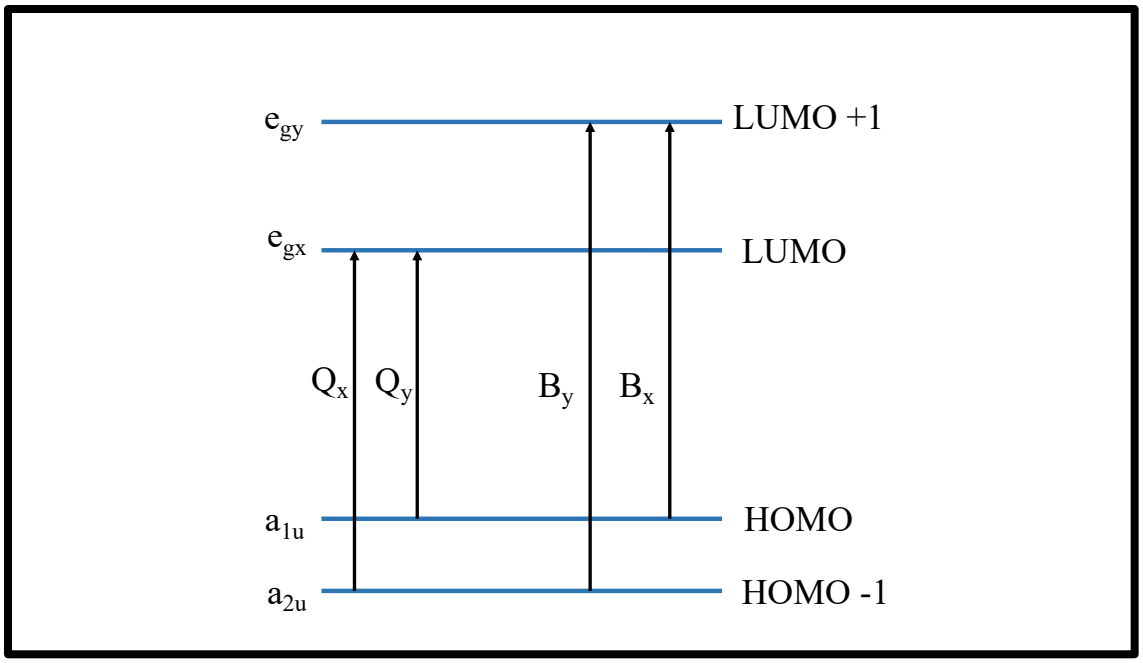

Figure 1.12 Energy levels of the four Gouterman orbitals shown[52]

The linkers and binding groups can be attached to the porphyrin molecule in order to tune its photophysical properties.[56]

1.6 Porphyrins in Dye-Sensitized Solar Cells and their mechanism

Due to their optoelectronic properties porphyrins have been under tremendous research for use in dye-sensitized solar cell (DSSC) using Ru-polypyridyl dyes adsorbed on mesoporous titania surface.[57,58] In a typical DSSC, dye-sensitized TiO_2 nanoparticles provide conduction and are used as a photoanode and Pt electrode is used as a counter electrode.[59] The I^-/I_3^- electrolyte is used as a redox shuttle between the TiO_2 photoanode and the counter electrode. The TiO_2 layer is deposited on FTO coated glass and then a monolayer of dye is introduced. Upon illumination, the electrons from dye molecules are excited and are injected into the conduction band of TiO_2, which leaves the dye in an oxidized state. The redox couple I^-/I_3^- provides an electron to the dye and restores its

ground state. The electron moves through the circuit and reaches the counter electrode where I_3^- is reduced to I^- and the cycle is completed (**Figure 1.13**).[13,59] The initial DSSC's were built using ruthenium bipyridyl dyes and were 11% efficient however the cost of Ru based dyes was a major limitation.[59] Since then, significant research has gone into developing efficient dyes. The sensitizer required should have a wide absorption range, be cost-effective and possess high molar absorption coefficient.[31] Since porphyrins exhibit such a fast energy transfer in photosynthesis, they have been successfully used as the sensitizers in these kinds of solar cells. The most common porphyrins used are free base porphyrins and Zn- derivatives of meso-benzoic acid substituted tetracarboxyphenylporphyrin (TCPP).[12,57] A Zn-porphyrin sensitizers (YD2-0C8) combined with another organic dye (Y123) was found to be 13% efficiency.[13,22,54]

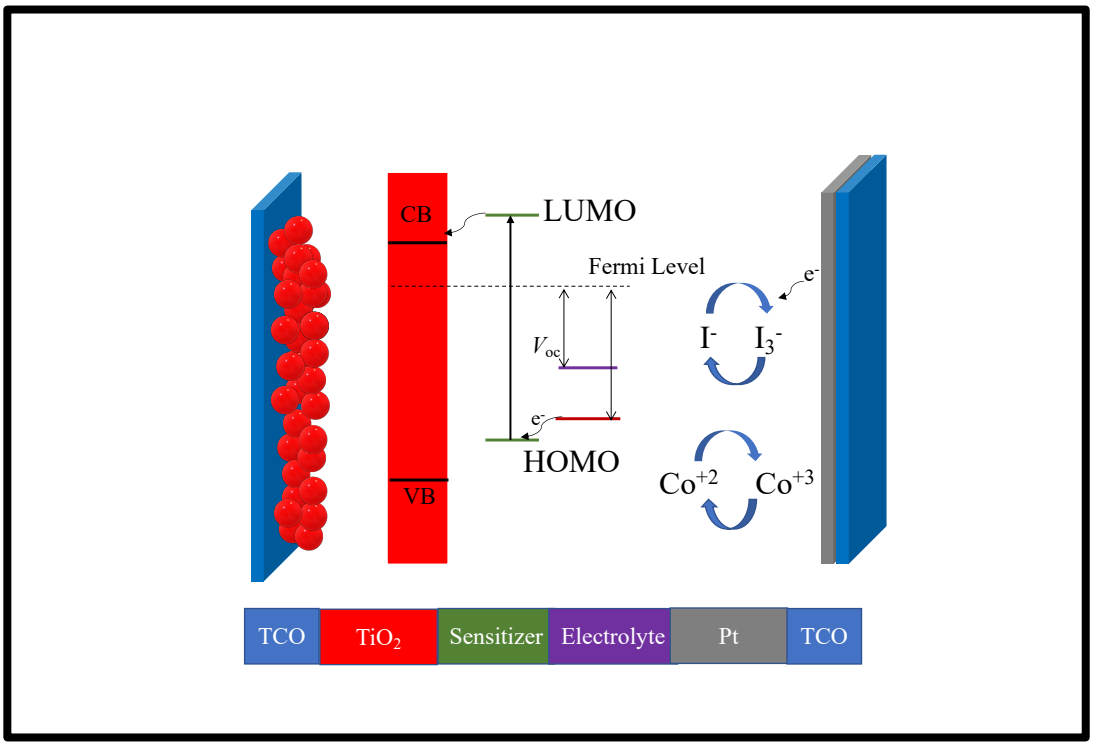

Figure 1.13 Principle of dye-sensitized solar cell[54]

1.7 Porphyrin –Fullerene Bulk Heterojunction Solar Cells

The main difference between organic solar cell and an inorganic solar cell is the nature of the charge carrier generation. In an organic solar cell, electron and hole are electrostatically bound in the form of excitons, while in an inorganic solar cell free charge carrier are formed directly upon the absorption of light. The nature of excited states in these kinds of solar cells is decided primarily by the dielectric constant of the semiconductor as mentioned earlier. The other factor playing an important role is Bohr's radius of the charge carrier. The lower dielectric constants and weaker non-covalent interactions in organic semiconductors make the wavefunction of electrons spatially restricted and localized as compared to the strong interactions in inorganic semiconductors. [60,59]

The small molecule solar cell has multi-stacked heterojunction which has a nanometers thick interface for the ease of exciton diffusion. Phthalocyanines, porphyrins, perylenes and buckminsterfullerene (C_{60}) are the common materials used for small molecule organic solar cell. The bulk-heterojunction has donor and acceptor material intermixed and the interface has a high surface area.[60] The porphyrin and fullerene derivatives are common materials studied in organic solar cells where porphyrin acts as a donor and fullerene derivatives acts as acceptor.

1.8 Research Objectives:

The objective of this research is to understand the effects of peripheral alkyl groups on the molecular orientation of free base porphyrins and how molecular orientation and packing around periphery of carboalkoxyphenylporphyrin affects their exciton diffusion properties in thin films. We are trying to establish basic guidelines on

how the exciton diffusion is affected by rearrangements and packing in carboalkoxyphenylporphyrin thin films.

In Chapter 2, the photophysical properties of free-base porphyrin having linear and branched peripheral alkyl groups were investigated in solution cast thin films. The properties like absorbance, photoluminescent (PL) lifetime (τ_s) and steady-state emission (SSE) were measured and used to calculate relative quenching efficiencies (Q), diffusion constant (D) and diffusion length (L_D) using Monte-Carlo eDiffusion simulations model. Five different free base tetrakis-carboalkoxyphenylporphyrin (TCR_4PP) derivatives were synthesized, characterized and tested for their photophysical properties. These derivatives include Tetra(4-carbomethoxyphenyl)porphyrin (TCM_4PP), Tetra(4-carbobutoxyphenyl)porphyrin (TCB_4PP), Tetra(4-carbohexoxyphenyl)porphyrin (TCH_4PP), Tetra(4-carboethyhexoxyphenyl)porphyrin ($TCEH_4PP$), Tetra(4-carbooctoxyphenyl)porphyrin (TCO_4PP). The diffusion coefficient (D) and exciton diffusion lengths (L_D)were calculated for all the above derivatives and the effect of longer alkyl chain with and without branching was studied on their singlet exciton diffusion. An increase in the observed exciton diffusion length was seen from 15 nm for TCM_4PP to 25 nm for TCH_4PP whereas this trend of increase in L_D with chain length was not seen in branched alkyl chain derivatives. Structural studies suggested that linear alkyl groups favor homeotropic arrangements of porphyrin molecules in thin films which enhances exciton diffusion. However, having branched alkyl groups around periphery favors slip-stack assembly of porphyrin molecules in thin films making these molecules less favorable for exciton diffusion. We conclude that in addition to the chain length several different factors like rearrangements of the alkyl chains influence the exciton diffusion in

such compounds.

In Chapter 3, the effects of peripheral alkyl groups and thermal annealing on the exciton quenching efficiency in bilayer porphyrin-fullerene thin films have been investigated. The UV-vis absorption spectra, steady-state fluorescence emission, differential scanning calorimetry and X-Ray Diffraction data of three different derivatives of carboalkoxyphenylporphyrin have been studied. The steady-state quenching efficiencies of these three derivatives have been calculated from their steady-state emission using pristine spin-cast films and films with an evaporated C_{60} bilayer. Structural analysis studies have been performed using X-ray diffraction (XRD), Grazing Incidence Wide Angle X-Ray Scattering (GIWAXS), UV-visible spectroscopy. Thermal properties were studied using differential scanning calorimetry measurements (DSC). Annealing the films caused significant structural changes and these were observed in the UV-visible absorbance spectra and XRD diffraction patterns. Prior to thermal annealing, quenching efficiencies for the TCH_4PP and TCO_4PP (hexyl and octyl derivatives) were greatest, which is in agreement with previous bulk quenching experiments.[61] After annealing, the hexyl derivative (TCH_4PP) showed the lowest bilayer quenching efficiency and indicated evidence of significant molecular rearrangements.[15]

In Chapter 4, Polymer:Porphyrin:PCBM ternary devices were fabricated to study the effect of varying alkyl groups length and branching on the device parameters in the ternary assembly of solar cell. The Polymer:Porphyrin:PCBM blend composition by weight was kept at 1:1:4 for the active layer. Poly(3-hexylthiophene) (P3HT), [6,6]-phenyl-C61-butyric acid methyl ester (PCBM) and previously used porphyrin derivatives Tetra(4-carbobutoxyphenyl)porphyrin (TCB_4PP), Tetra(4-carbohexoxyphenyl)porphyrin

(TCH_4PP), Tetra(4-carboethylhexoxyphenyl)porphyrin ($TCEH_4PP$), Tetra(4-carbooctoxyphenyl)porphyrin (TCO_4PP) were used for the OPV devices. UV-Visible spectra of the ternary blend were measured in order to realize the spectral response of porphyrin in P3HT:PCBM blend. In order to measure the HOMO-LUMO levels of the materials of the active layer, cyclic voltammetry data was used to measure the oxidation and reduction potential of the porphyrins. The HOMO and LUMO levels of the P3HT and PCBM were taken from the literature. *J-V* curves collected from these devices were used to calculated open-circuit voltage (V_{oc}), short-circuit current density (J_{sc}), fill factor (*FF*) and photoconversion efficiency (PCE) or (η). Ternary solar cells with porphyrins that have linear and symmetrical peripheral alkyl groups displayed significantly improved solar cell performance. The open-circuit voltage was similar for all the solar cells, however, short circuit current density significantly improved as the peripheral alkyl chain length was increased linearly in the devices. The performance of these solar cells helped validate our previous hypothesis that exciton diffusion and power conversion efficiency is influenced by the molecular arrangement and packing of peripheral alkyl group in the carboalkoxyphenylporphyrins in thin films. This study is critical in linking molecular arrangement and packing in different derivatives of carboalkoxyphenylporphyrin in thin film assembly to solar cell efficiency.

CHAPTER 2. ENHANCING EXCITON DIFFUSION IN PORPHYRIN THIN FILMS USING PERIPHERAL ALKYL CARBO ALKOXY GROUPS TO INFLUENCE MOLECULAR ASSEMBLY

2.1 Introduction

There has been a lot of interest in the electronic structure of porphyrins pertaining to their biological, catalytic and photophysical properties.[62] Porphyrins have been studied in artificial light-harvesting antennae's, Donor-Acceptor (dyads), Donor-Acceptor-Donor or Acceptor-Donor-Acceptor (Triads). Porphyrins are structural analogs of chlorophyll, which is the main pigment responsible for photosynthesis and exhibits very fast and efficient singlet-singlet energy and charge transfer during photosynthesis.[23,63] Chlorophyll uses sunlight to run various photo-catalytic processes involved in photosystem I and photosystem II, where oxygen and sugars are produced with the help of electron acceptor and electron donors. Porphyrins have deep colors and possess high molar absorptivity coefficient because of the π - π^* transitions which enables them to be an excellent candidate in extracting solar spectrum and hence solution processed bulk-heterojunction solar cells.[62] The artificial model system devised uses porphyrins as donors and fullerene-based acceptors in order to replicate the natural process of photosynthesis. Exciton formation, diffusion, and dissociation in such organic molecules is crucial to the performance of the bulk-heterojunction solar cell. Organic molecules possessing exciton diffusion length (L_D) greater than 10 nm have shown power conversion efficiencies of more than 10% in such solar cells.[64] Using bulk-heterojunction assembly enables the presence of multiple interfaces in the active layer making exciton transport more favorable by reducing the possibility of electron-hole recombination.

There are several techniques available to measure the exciton diffusion length of organic semiconductors. These techniques include photoluminescence (PL) surface quenching, time-resolved (PL) surface quenching, time-resolved (PL) bulk quenching with Monte Carlo simulation which is used in this chapter, exciton-exciton annihilation, time-resolved (PL) bulk quenching with Stern-Volmer equation and Förster resonance energy transfer (FRET) theory.[65]

We used long alkyl chain carboalkoxyphenylporphyrins compounds as the donor material to mimic this process of photosynthesis so that it can be used in organic photovoltaics (OPVs). Previously in our research group, the exciton diffusion properties of mixed substituent carbomethoxyphenylporphyrins were reported.[66] [6,6]-phenyl-C_{61}-butyric acid methyl ester commonly known as PCBM was used as a quencher in a very small amount (vol. frac. 0.06% and 0.2%) to determine bulk quenching efficiencies (Q). The mechanism of the exciton diffusion in these long alkyl chain phenyl porphyrins can be best explained by Förster resonance energy transfer mechanism, where excitons hop and transfer the energy to the next site. The Photoluminescent lifetimes were measured on a Ti-Sapphire laser and the lifetimes and quenching efficiencies were used in Monte-Carlo 3D eDiffusion simulation software to determine exciton diffusion coefficient. In this project, we measure and compare exciton diffusion lengths of long and short peripheral alkyl chain substituted carboalkoxyphenylporphyrins and relate their exciton diffusion properties to their molecular rearrangements and organization. We studied and compared the photophysical properties of four new porphyrin derivatives where alkyl chain lengths were varied. Upon increasing the length of the alkyl chain in free base carboalkoxyphenylporphyrins, the exciton lifetime and exciton diffusion lengths showed

an increment up to a certain alkyl chain length. The derivative with hexyl chains (6-carbon) around it showed exciton diffusion length (L_D) of 25 nm. Spectroscopic and XRD patterns suggest that the carboalkoxyphenylporphyrins favors nematic or homeotropic self-assembly when spin cast which results in improved exciton diffusion properties. We synthesize long alkyl chain carboalkoxyphenylporphyrins and measured the exciton diffusion properties in these porphyrins. The structure of the porphyrin derivative used is shown in **Figure 2.1** where we varied the R-group and studied the effects of varying this R-group on the exciton diffusion.

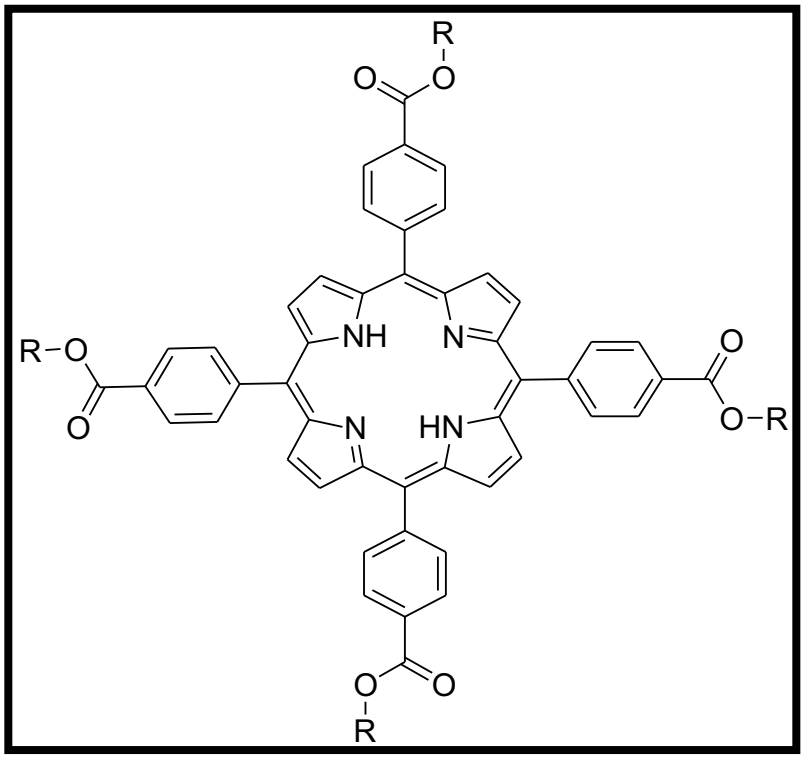

Figure 2.1 Structure of Tetrakis-5,10,15,20-(4-carboalkoxyphenyl) porphyrin

2.2 Experimental

2.2.1 Synthesis of tetrakis-5,10,15,20-(4-carboalkoxyphenyl) porphyrin (TCR_4PP):

Tetrakis-5, 10,15,20-(4-carboxyphenyl) porphyrin (0.08 g, 0.1 mmol) was reacted with an excess of 1-bromoalkane (0.6 mmol) and potassium carbonate (0.11 g, 0.8 mmol) in 15 mL anhydrous DMF at 80°C for 20 h under N_2. The reaction mixture was added to 300 mL of water and the dark purple precipitate was collected by filtration and rinsed with water. The product was purified by silica gel column chromatography eluting with DCM to yield a purple solid as TCR_4PP.[43,67,68]

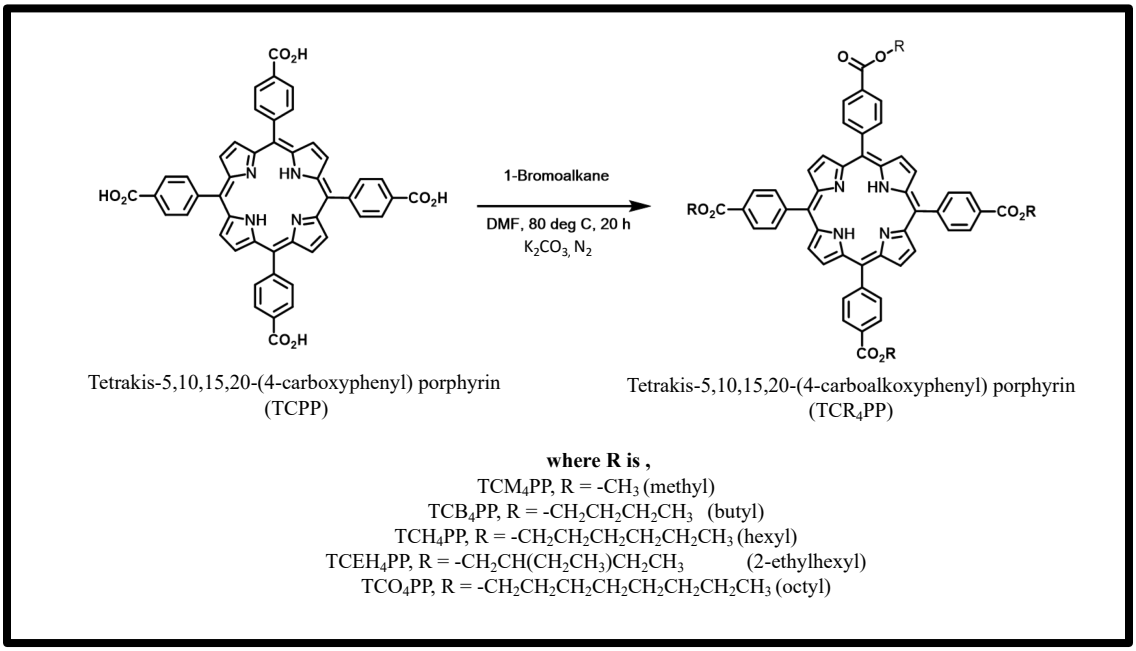

Figure 2.2 Synthesis of tetrakis-5,10,15,20-(4-carboalkoxyphenyl) porphyrin derivatives

Tetrakis-5,10,15,20-(4-carbobutoxyphenyl)porphyrin (TCB_4PP): Column chromatography using DCM afforded 0.098 g (96%) of purple solid was collected as **TCB_4PP** (matching previously reported).[69] **^{1}H NMR** (300 MHz, CH_2Cl_2, TMS, δ): 8.86 (s, 8H), 8.44 (d, J = 8.0 Hz, 8H), 8.31 (d, J = 8.3 Hz, 8H), 4.50 (t, J = 6.5 Hz, 8H), 1.90 (pnt, J = 7.0 Hz, 8H), 1.62 (sxt, J = 7.4 Hz, 8H), 1.07 (t, J = 7.3 Hz, 12H), -2.84 (s, 2H)

UV-Vis λ_{max} (THF, $\varepsilon = M^{-1}cm^{-1}$): 418 nm (ε = 444,000), 513 nm (ε = 20,000), 547 nm (ε = 8,000), 591 nm (ε = 5,000), 647 nm (ε = 3,000) **MALDI-TOF** (Calculated for $C_{64}H_{62}N_4O_8$: 1014.44 Found: M = 1014.36).

Tetrakis-5,10,15,20-(4-carbohexoxyphenyl)porphyrin (TCH_4PP): Column chromatography using DCM afforded 0.08 g (71%) of purple solid was collected as **TCH_4PP**. **^{1}H NMR** (300 MHz, CH_2Cl_2, TMS, δ): 8.86 (s, 8H), 8.44 (d, *J* = 8.0 Hz, 8H), 8.31 (d, *J* = 8.0 Hz, 8H), 4.49 (t, *J* = 6.6 Hz, 8H), 1.91 (pnt, *J* = 7.04 Hz, 8 H), 1.59 (m, 8H), 1.43 (m, 16H), 0.96 (t, *J* = 7.0 Hz, 12H), -2.84 (s, 2H) **UV-Vis λ_{max} (THF, $\varepsilon = M^{-1}cm^{-1}$):** 418 nm (ε = 653,000), 514 nm (ε = 29,000), 548 nm (ε = 13,000), 591 nm (ε = 8,000), 646 nm (ε = 5,000) **MALDI-TOF** (Calcd for $C_{72}H_{78}N_4O_8$: 1126.58 Found: M = 1126.2).

Tetrakis-5,10,15,20-(4-carbooctoxyphenyl)porphyrin (TCO_4PP): Column chromatography using DCM afforded 0.082 g (66%) of purple solid was collected as **TCO_4PP**. **^{1}H NMR** (300 MHz, CH_2Cl_2, TMS, δ): 8.86 (s, 8H), 8.44 (d, *J* = 8.3 Hz, 8H), 8.31 (d, *J* = 8.5 Hz, 8H), 4.49 (t, *J* = 6.6 Hz, 8H), 1.91 (pnt, *J* = 7.2 Hz, 8H), 1.6-1.38 (m, 40H), 0.91 (t, *J* = 6.8 Hz, 12H), -2.84 (s, 2H) **UV-Vis λ_{max} (THF, $\varepsilon=M^{-1}cm^{-1}$):** 418nm (ε=453,000), 514nm (ε=21,000), 548nm (ε=9,000), 590nm (ε=6,000), 647nm (ε=4,000) **MALDI-TOF** (Calcd for $C_{80}H_{94}N_4O_8$: 1238.71 Found: M = 1238.1)[43]

2.2.2 Thin Film Preparation

Glass microscope slides were washed and sonicated for 15 min each in glass-cleaning detergent, milliQ water, and isopropyl alcohol, dried with N_2 followed by UV-ozone treatment for 20 min to ensure the slides are free of contaminants.[43] Five different solutions of carboalkoxyphenylporphyrin derivatives were made in chlorobenzene under

nitrogen atmosphere inside the glove-box (approx. 6 mM for each derivative - TCM_4PP(control), TCB_4PP, TCH_4PP, $TCEH_4PP$, TCO_4PP) and stirred for 24 h before spin coating. For each derivative, solutions were doped with PCBM at volume fractions of 0.2% and 0.06% (v_{frac}). The doped porphyrin solutions with PCBM were stirred for 15 min before spin coating. Spin-cast films were formed by casting the porphyrin solutions at 2000 rpm for 60s under N_2 atmosphere. Porphyrin solutions and glass slides were warmed to 70 °C prior to spin coating to encourage uniform film formation. The spin-cast film thicknesses were found to be between 20 nm to 25 nm as measured by atomic force microscopy (AFM). Photobleaching during photophysical measurements was avoided by encapsulating the films under N_2 using epoxy and a coverslip shown in **Figure 2.3**. The PCBM v_{frac} (total volume occupied by PCBM molecules versus the blend volume) was calculated using previously reported methods, with porphyrin densities found experimentally to be ~0.97 g cm^{-3}. The PL (t) decay lifetime of each porphyrin film was measured using a Ti-Sapphire femtosecond laser with a repetition rate of 200 kHz with excitation at 410 nm and emission was collected at 650 nm. PL(t) data were fit to double and triple exponential decays using Igor Pro 6.3 software. The fitted PL decays, quenching efficiencies and v_{frac} were used to obtain exciton diffusion coefficients (D) using Monte Carlo eDiffusion Software simulations.

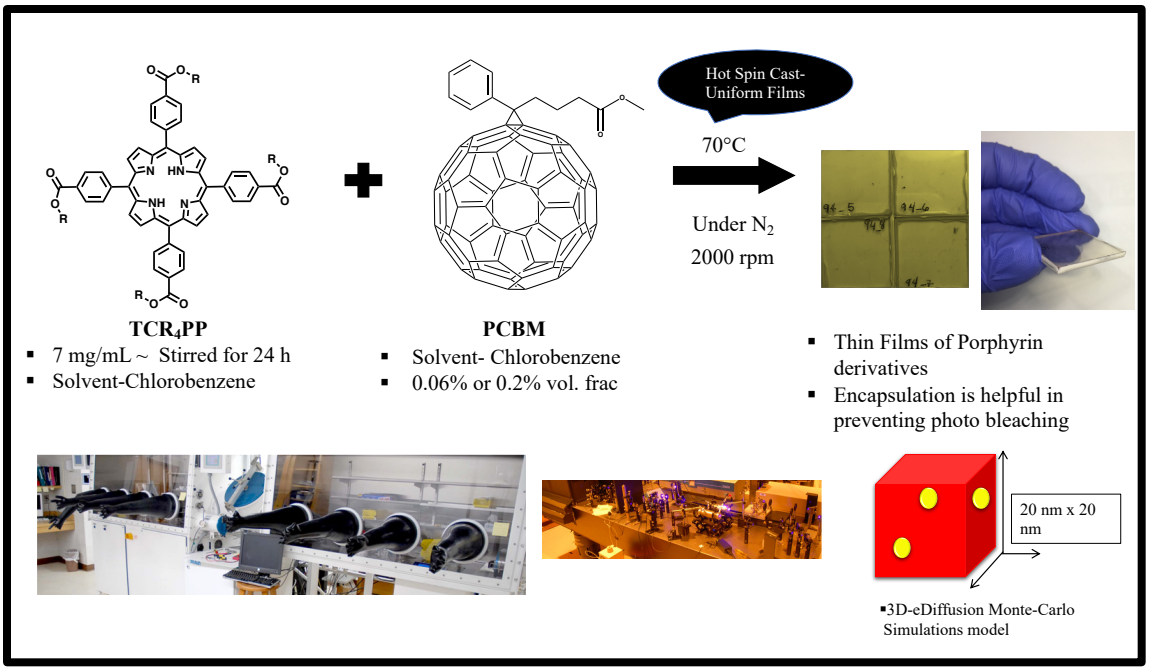

Figure 2.3 Thin film preparation in the glovebox and encapsulation procedure for PL decay and Monte-Carlo eDiffusion modelling

2.3 Results and Discussions:

2.3.1 UV-Visible Absorption

The two most important methods of achieving higher efficiency organic solar cells are by either expanding the spectral range where absorption of photons takes place or by manipulating the lifetime, diffusion length and charge-separation of generated excitons. UV- visible absorption spectra of thin films of all the porphyrin derivatives were tested for additional structural information. Previously in our research lab, tetrakis-5,10,15,20-(4-carbomethoxyphenyl)porphyrin (TCM_4PP) was investigated for its photophysical and optoelectronic properties. It was seen that TCM_4PP doesn't have good solubility in common organic solvents used for organic solar cell fabrication. However, replacing the methoxy group on the periphery by butoxy, hexoxy, ethylhexoxy and octoxy significantly improved the solubility from 6 mg mL^{-1} to 80-100 mg mL^{-1}. The

absorption spectrum provides us further information about how these different alkyl chain derivatives assemble in a thin film. The absorption spectra for thin films as well as solutions of porphyrin were studied, and significant differences were observed. The absorbance spectra of carboalkoxyphenylporphyrin film and solution (inset) are shown in the **Figure 2.2.** In solution, the Soret peaks (418 nm - 419 nm) (ε= 400-500 x 10^{-3} M^{-1} $cm^{-}1$) representing a strong S_0-S_2 transition, for all the derivatives are seen aligned on top of each other with no significant shifts and additional features. The four Q bands known as Q_4 (514 nm), Q_3 (548 nm), Q_2 (591 nm), Q_1 (647 nm) representing S_0-S_1 transitions are also seen. The similar spectra are attributed to the presence of an identical core structure in all the derivatives and the absence of molecular interactions in the solutions. The spin-cast thin films of porphyrins have broad and red shifted Soret peaks and significant differences when alkyl chain is varied which is attributed to π-π porphyrin macrocyclic interactions.[70] TCM_4PP thin film has the most red-shifted Soret peak at 434 nm. As the length of the alkyl chain increases the red shift decreases as seen in TCO_4PP (422nm) and $TCEH_4PP$ (421nm). These peaks suggest that long alkyl chains and branching contribute to molecular orientation and an increased average spacing between two porphyrin molecules when spin-cast. Also, the four Q-bands in both solution as well as thin films have different trends suggesting evidence of molecular assembly. The intensity of Q-bands increases from Q_1-Q_4 in solutions whereas in films Q_1 absorbance (650 nm) is more intense than Q_2 (600 nm) suggesting molecular self-assembly as the carbon chain length is increased. The behavior of Q bands in solutions is similar to an etio-type spectrum of porphyrins previously reported in the literature. Stronger Q_2 band than Q_1 band suggests molecular self-assembly which is absent in solution.[71] However, TCM_4PP

also show etio-type behavior when spin cast but is absent in higher derivatives. The comparison of solution absorbance and thin film absorbance of porphyrin derivatives tells us about the possible macrocyclic interactions occurring in thin films, which are absent in porphyrins when they are in solutions. Lastly, a small feature found on absorption spectrum of TCH_4PP was a peak at 400 nm, which could be due to a strong excitonic coupling between porphyrin molecules stacked on top of each other in a thin film assembly.[72] This feature suggests high organization and molecular packing in hexyl porphyrin derivative.

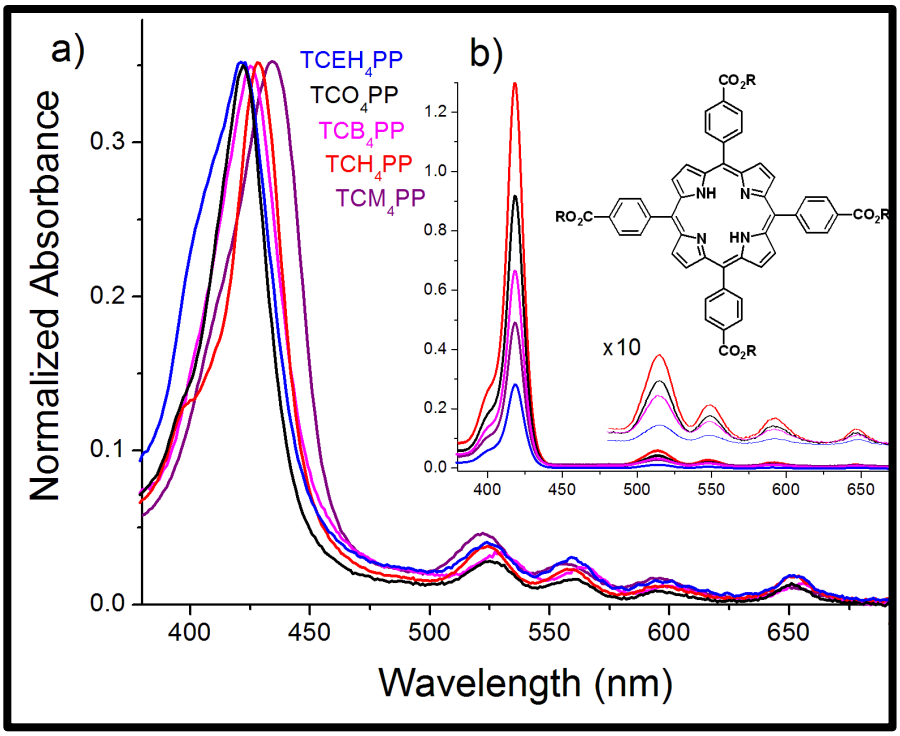

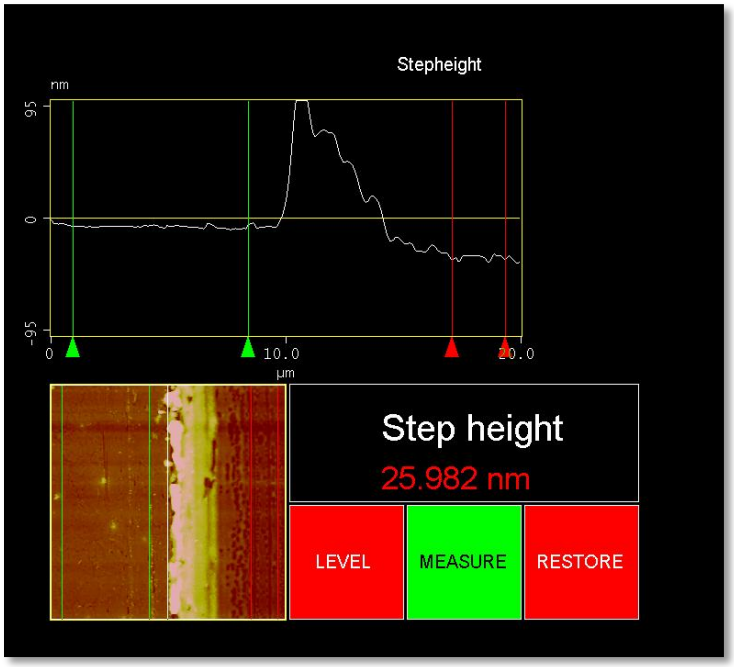

Figure 2.4 A. Normalized absorption spectra of (a) spin-cast thin films (b) solutions (inset) with in a concentration range from 1-5 mM of TCM_4PP (–), TCB_4PP (–) and TCH_4PP (–) $TCEH_4PP$ (–), and TCO_4PP (–); film thickness ranges from 20-25 nm (B) Average step height or thickness of the films using AFM

2.3.2 Photoluminescent Lifetimes of Thin Films and Exciton Diffusion Constants

As discussed in section 1.3.4 in Chapter 1, the energy transfer in the molecular semiconductors upon excitation takes place by the excitons diffusing or random walk hopping by a non- radiative process called the Forster resonance energy transfer (FRET) In order to measure exciton diffusion parameters in pristine porphyrin thin film and porphyrin-PCBM doped thin films, we used a time-resolved bulk-quenching model and ran Monte-Carlo eDiffusion simulations. This is a proven technique used in polymers and porphyrins to calculate the exciton dynamics.[73] PCBM is the most commonly used quencher because of its high electron affinity and solubility in organic solvents.[16] The lifetimes of pristine and doped films were measured using time-correlated single photon counting (TCSPC) method. The data were fitted using Igor Pro 6.3 software.

The eDiffusion model simulates the conditions on a doped film inside a 20x20x20 nm simulation box where excitons hop from one site to another until it meets a quencher molecule. We need to know what volume fraction of quencher molecule that was added in the donor thin films for this simulation, photoluminescent lifetimes (τ_s) of the pristine porphyrin and porphyrin-PCBM thin films as shown in **Figure 2.5**. The eDiffusion simulation discussed in section **2.3.3** keeps running until the PL decays converges with the exciton diffusion model which gives us the hop size (H) which is used to calculated diffusion coefficient (D) and diffusion length (L_D)

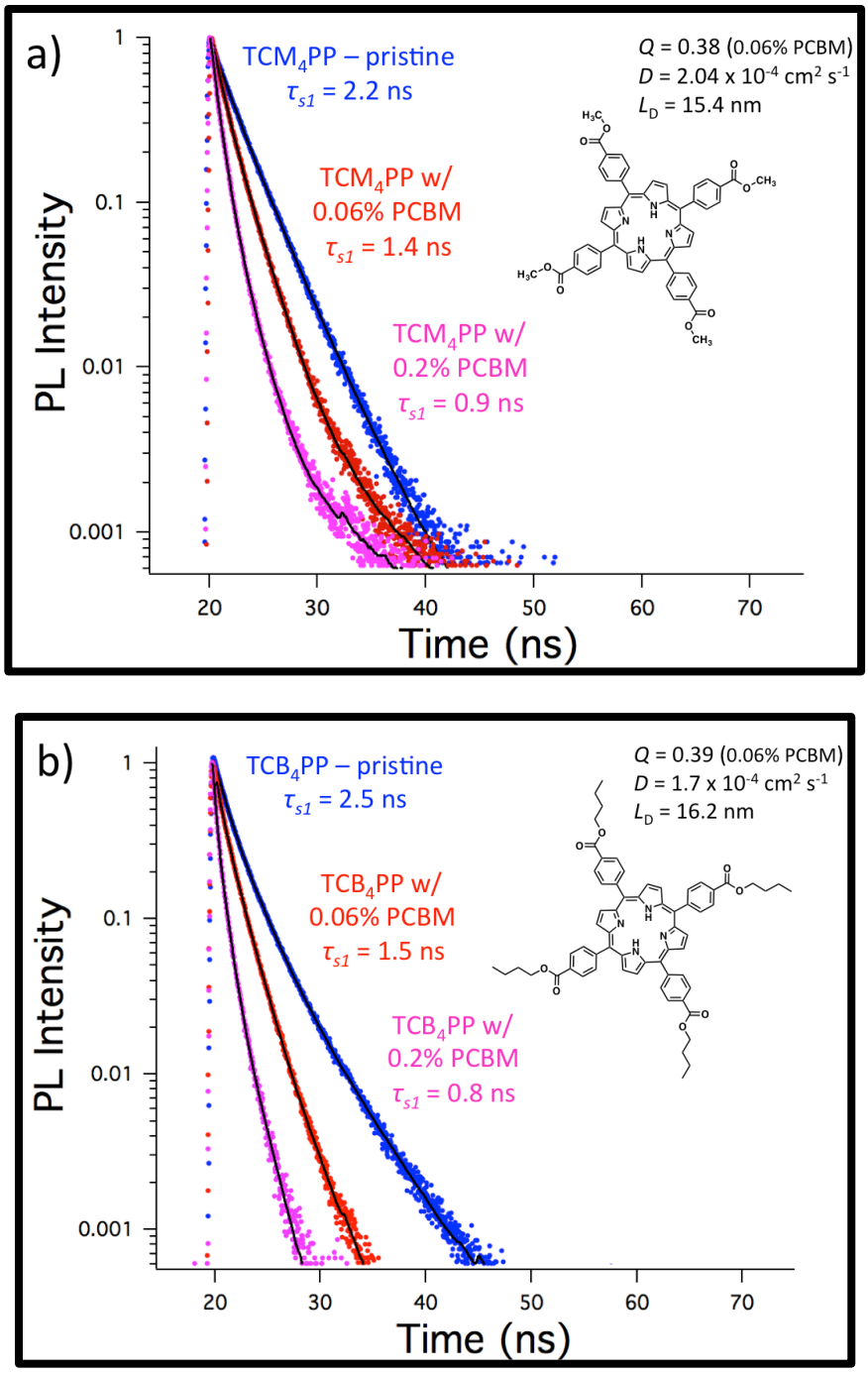

Figure 2.5 Photoluminescent lifetimes and exponential fits of all the derivatives from TCSPC of pristine (a) TCM_4PP (b) TCB_4PP doped with 0.2% and 0.06% PCBM with quenching efficiencies (Q), diffusion coefficients (D) and diffusion lengths (L_D)

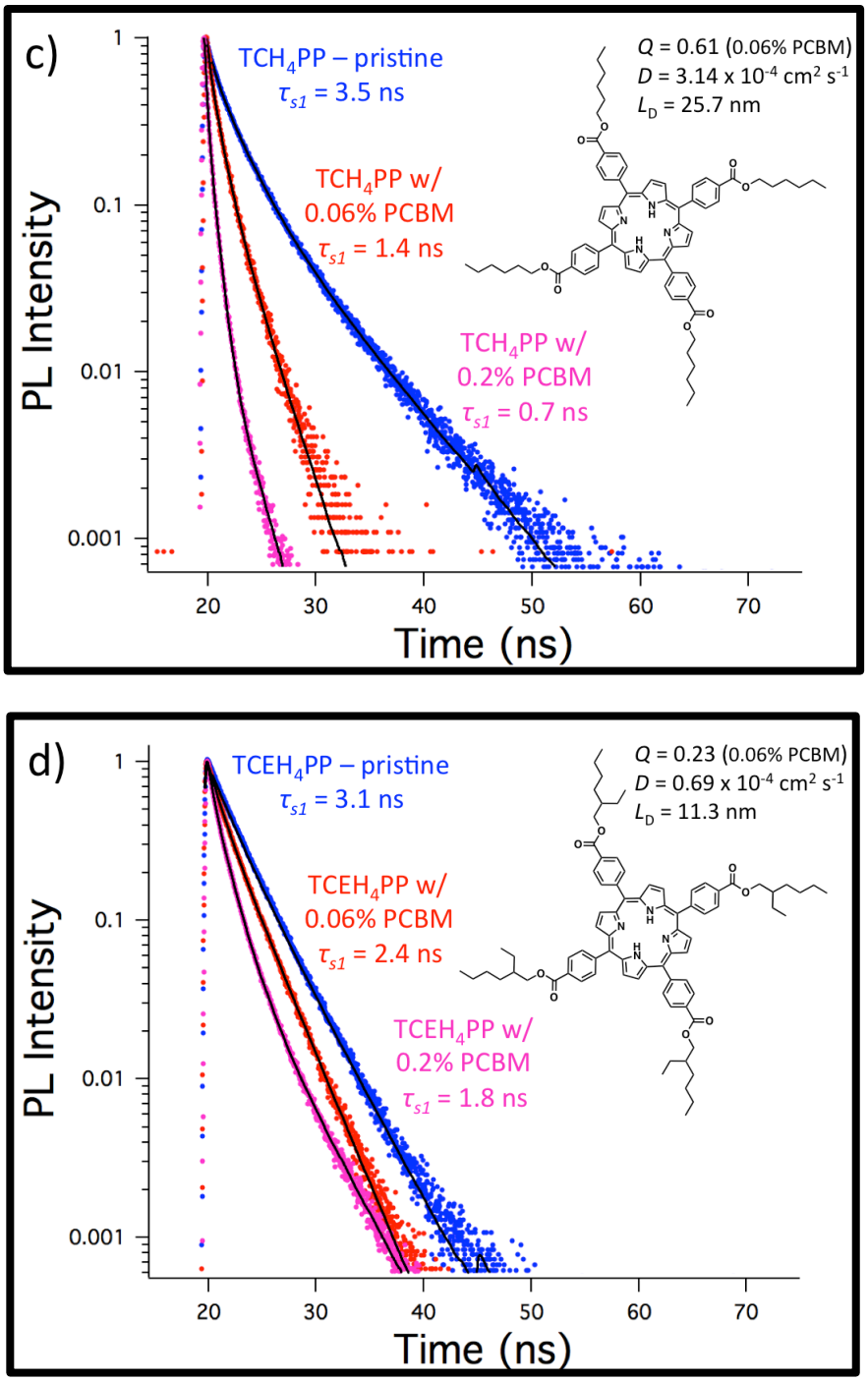

Figure 2.5 Photoluminescent lifetimes and exponential fits of all the derivatives from TCSPC of pristine (c) TCH_4PP (d) $TCEH_4PP$ doped with 0.2% and 0.06% PCBM with quenching efficiencies (Q), diffusion coefficients (D) and diffusion lengths (L_D) continued

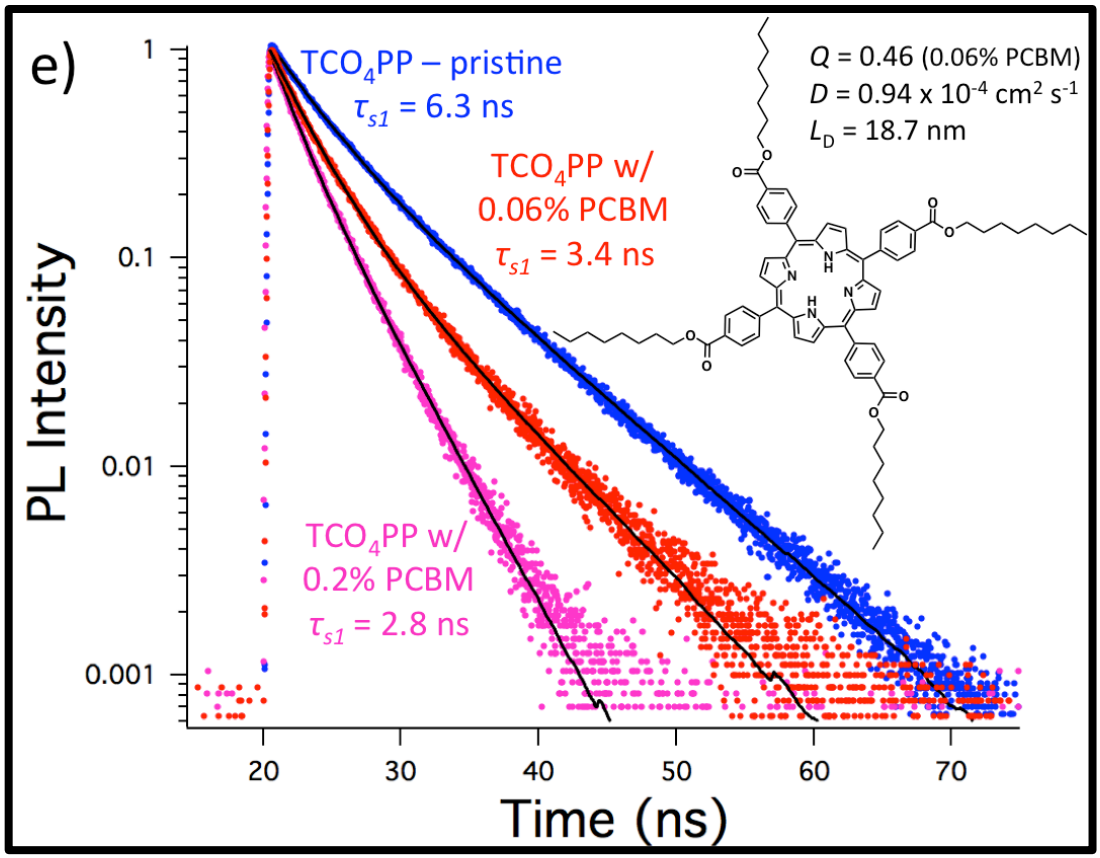

Figure 2.5 Photoluminescent lifetimes and exponential fits of all the derivatives from TCSPC of pristine (e) TCO_4PP doped with 0.2% and 0.06% PCBM with quenching efficiencies (Q), diffusion coefficients (D) and diffusion lengths (L_D) continued

2.3.3 Monte-Carlo eDiffusion Simulations used in calculating Diffusion parameters

In order to calculate the exciton diffusion parameters such as diffusion length (L_D), quenching efficiency (Q_{eff}) eDiffusion software was used to model the process of diffusion and provide the hopsize (H) in a thin film. The excitons diffusion length (L_D) gives critical information of how far the excitons have to diffuse before they reach the interface to undergo exciton dissociation. The Monte-Carlo Simulations in eDiffusion software by Oleksandr Mikhnenko enables modeling of photoluminescent decays (PL Decays) of pristine as well as blended organic semiconductor, polymer solar cells, etc. As

mentioned before, PCBM is a commonly used acceptor material, which is used to make polymer acceptor blends. Any exciton diffusion simulation needs two samples one quenched and the other one pristine. The procedure has been modified from eDiffusion simulation guide in order to explain each and every step of the simulations in detail. The lifetime of both the samples can be used to find the relative quenching efficiency 'Q' using the formula

$$Q = 1 - \int {}^{PL_{blend}\, dt}/_{PL_{pristine}}\, dt \quad \text{.....} \textit{Equation 2.1}$$

The relative quenching efficiency depends on PCBM concentration and the morphology of the semiconductor and PCBM blend. This information can be used to determine the diffusion constant which in turn will help in determining exciton diffusion length in a semiconductor:PCBM blend as well as in the pristine sample.

The software was developed in c++ and is equally efficient in WindowsXP, Windows7 and MacOs. The PL decay lifetimes of pristine and blended samples where the concentration of PCBM was known were measured. The instrument response function (IRF) is also required while collecting the PL decay lifetime data for deconvolution of the actual decay plot. It is important that IRF should be collected with exactly the same parameters (except for the emission wavelength) as the lifetime measurements. While modeling the semiconductor:PCBM blend we used two separate volume fractions 0.06% and 0.2% in our experiment (v_f);

$$v_f = \frac{\text{Volume of PCBM molecule } (V_{PCBM})}{\text{Volume of semiconductor:PCBM blend}} \quad \text{.....} \textit{Equation 2.2}$$

We can calculate the concentration of PCBM molecules using equation 2.3;

$$C_{PCBM} = {}^{v_f}/_{V_{PCBM}} \quad \text{.....} \textit{Equation 2.3}$$

Assuming the PCBM molecules are spherical in geometry, therefore, volume of the PCBM molecule is given by equation 2.4.

$$V_{PCBM} = \frac{4}{3}\pi r^3 \quad \text{..... } \textit{Equation 2.4}$$

Assuming the radius of each PCBM is 0.5 $x10^{-7}$ cm, the density of PCBM molecule is given by equation 2.5. Where M_{PCBM}= 911g/mol, N_A is Avogadro's number.

$$\rho_{PCBM} = C_{PCBM}\frac{M_{PCBM}}{N_A} g/cm^3 \text{.....} \textit{Equation 2.5}$$

Therefore, mass fraction can be written as equation 2.6. Where $\rho_{semiconductor}$ is density in g/cm^3.

$$m_{frac} = \frac{\rho_{PCBM}}{\rho_{PCBM}+\rho_{semiconductor}} \text{.....} \textit{Equation 2.6}$$

Next step is configuring and editing the experiment. The common parameters for all the experiments need to go in the software first and the window will display the number of excitons simulated which is 10^4excitons per generation. The gen_num "number" will determine the duration in which the simulation occurs. In order to obtain smooth PL decays gen_num value should be 500. The coefficients a_1, t_1, a_2 and t_2 will determine mono or bi-exponential PL decays in pristine films of porphyrins in our experiment.

Afterwards, the radius of exciton and quencher is selected. PCBM is spherical and has a radius of 0.5 nm^3. So, E_{radius} and Q_{radius} was set at 0.5 nm^3 for our experiment assuming they both have a similar size. QAS is size of action sphere centered at quencher molecule. Action sphere is where excitons are generated and considered quenched so QAS radius =0.

A simulation box of 20x20x20 nm is used to map the quencher molecule in 3D Boolean grid. A Boolean 3D grid of 0.05nm size is superimposed with a simulation box

and a value of true or false is assigned to 3D grid depending upon the fact if it overlaps with a PCBM molecule or not. dT is the time discretization where random exciton is moved

$$D = \frac{\delta s^2}{6\delta t} \text{ ..... } \textit{Equation 2.7}$$

The time interval dT is chosen in such a way so that the δs is much smaller than the size of quencher used

$$\delta s = \text{hopsize x } dT < \text{Qradius} \text{ ..... } \textit{Equation 2.8}$$

$$\text{hopsize} = \frac{\delta s}{\sqrt{dT}} \text{ ..... } \textit{Equation 2.9}$$

Hopsize determines the diffusion coefficients and is critical to our measurements and is independent of dT.

$$D = \frac{\text{hopsize}^2}{6} \text{ ..... } \textit{Equation 2.10}$$

$$L_D = \sqrt{aD\tau} \text{ ..... } \textit{Equation 2.11}$$

After running the Monte-Carlo simulations, hopsize was calculated and was used for all the derivatives in order to measure the exciton diffusion parameters summarized in Table 2.1.

The change in the trend of average PL lifetime (τ_s) was observed from TCM_4PP (1-carbon chain derivative) to TCO_4PP (8-carbon chain derivative) in thin films. An increase in the PL lifetime was observed as the peripheral alkyl chain progresses to longer alkyl groups; TCM_4PP (2.2 ns), TCB_4PP (2.5 ns); TCH_4PP (3.5ns), TCO_4PP (6.1 ns) as shown in **Table 2.1**. Upon doping the pristine porphyrin films with two different volume fractions (0.06% and 0.2%) of PCBM, PL lifetimes were shortened due to the quenching of excitons at porphyrin-PCBM surface. This trend was observed both in steady-state emission and PL quenching. The quenching efficiency increased with an increase in chain length from

methyl derivative to hexyl derivative from 0.35 to 0.38 to 0.42. However, the branched derivative with ethyl hexyl chain showed the lowest quenching efficiency of 0.30 when 0.06% PCBM was added to $TCEH_4PP$ solution during spin casting.

Table 2.1 Alkylated TCR_4PP summary of average lifetime decays (τ), relative quenching efficiency (Q), exciton diffusion coefficient (D), diffusion length (L_D), and steady-state quenching efficiency (Q_{ss})

	τ_{S1} (ns)	τ_Q[a] (ns)	Q[a]	D x 10^{-4} $cm^2\ s^{-1}$	L_D (nm)	Q_{SS}[b]	Q_{SS}[c]
TCM_4PP (Control)	2.20	1.43± 0.27	0.35± 0.12	1.9 ± 0.6	15.4 ± 4.5	0.30	0.57
TCB_4PP	2.53±1.0	1.57 ±0.09	0.3 ± 0.03	1.7 ± 0.2	16.0 ± 1.2	0.53	0.59
TCH_4PP	3.50±3.0	1.73 ±0.27	0.52 ± 0.07	2.2 ± 0.7	21.3 ± 3.4	0.70	0.79
$TCEH_4PP$	3.10±1.6	2.19± 0.21	0.30 ± 0.07	1.0 ± 0.4	13.8 ± 2.7	0.40	0.57
TCO_4PP	6.25 ±2.7	3.45± 0.71	0.45 ± 0.11	0.9 ± 0.5	18.7 ± 4.8	0.82	0.96

The octyl derivative (TCO_4PP) showed lower quenching efficiency than the hexyl derivative (TCH_4PP). TCH_4PP also gave us the longest exciton diffusion length of 21 ± 3.4 nm when calculated from the equations used in Monte Carlo eDiffusion simulations. The octyl derivative showed the lowest diffusion constant (D=0.9x10$_{-4}$ $cm^2\ s^{-1}$) but due to very long lifetimes of octyl derivative, the diffusion length was calculated at 18 .7 ± 4.8 nm. The hexyl derivative (TCH_4PP) demonstrated the highest exciton diffusion lengths (L_D), diffusion coefficients (D) and relative quenching efficiencies (Q) out of all the derivatives. TCO_4PP showed the longest lifetimes out of all the derivatives. These are some of the longest diffusion lengths for porphyrin derivatives ever reported but the

diffusion coefficients were similar to the previously reported in porphyrin systems in literature. Finally, steady-state quenching efficiencies of TCH_4PP and TCO_4PP were also higher than TCM_4PP, TCB_4PP. $TCEH_4PP$ showed the lowest quenching efficiencies of all the porphyrin derivatives.[74]

2.3.4 Calculating exciton diffusion using Stern-Volmer equation

The Stern-Volmer equation can also be used to quantify quenching data and calculate the exciton diffusion parameters for compounds that exhibit single exponential decays. Most of the PL decay with quencher PCBM were fitted using bi or tri exponentials in Igor Pro. Software. The Stern-Volmer equation is often used to determine Stern-Volmer constant and is given by:

$$\frac{I_o}{I} = 1 + K_{sv}\,[Q] \quad \text{.....Equation 2.12}$$

Where,

I_o fluorescence intensity in the absence of quencher and I is the fluorescence intensity in the presence of quencher

K_{sv} is Stern-Volmer constant

Q is the concentration of quencher

In a bimolecular reaction, K_{sv} is given by K_q. τ_o where K_q is bimolecular quenching which is proportional to diffusion coefficient and τ_o lifetime of an excited state in the absence of quencher.[75,76]

The average PL decays were used and the calculated the diffusion coefficients for all the carboalkoxyphenylporphyrin derivatives in pristine and blended thin film assembly were calculated. For this purpose, the concentration on each blend in the thin film was calculated as 0.00042 M for 0.06% vol. fraction and 0.0018M for 0.2% vol. fraction. The

distance of the exciton to organic semiconductor was assumed to be 1 nm based on our literature survey and the radius of PCBM molecule. Once the concentration and distance of the exciton-exciton was established the data was fitted into Stern-Volmer equation.

$$\frac{1}{\tau} = \frac{1}{\tau_F} + 4\,\pi r D c \ldots\ldots\ldots\ldots\ldots\ldots\ldots\ldots \textit{Equation 2.13}$$

Where,
τ *is* PL lifetime of the blended film

τ_F is the PL lifetime of the pristine film

r is the distance between exciton

D is the diffusion coefficient, and

C is the concentration of quencher in the thin film

Table 2.2 shows the diffusion coefficients calculated using both Stern-Volmer equation and Monte-Carlo eDiffusion simulation model

	τ_{S1} (ns)	τ_Q[a] (ns)	Q[a]	D x 10^{-4} $cm^2\ s^{-1}$(SV)	L_D
TCB_4PP	2.53±1.0	1.57 ±0.09	0.3 ± 0.03	1.64±0.2	15.6± 1.2
TCH_4PP	3.50±3.0	1.73 ±0.27	0.52 ± 0.07	2.5± 0.7	22.9± 3.4
$TCEH_4PP$	3.10±1.6	2.19± 0.21	0.30 ± 0.07	1.28± 0.4	15.4± 2.7
TCO_4PP	6.25 ±2.7	3.45± 0.71	0.45 ± 0.11	1.77± 0.5	25.7± 4.8

The values for diffusion coefficients(D) and exciton diffusion length (L_D) are in good agreement with the Monte-Carlo calculations with some variations which could be attributed to the nature of the exponential fit of the PL decays. Stern-Volmer equation generated higher exciton diffusion lengths (L_D) for TCO_4PP as the equation relies heavily on PL lifetime decays. This method is more useful for single exponential PL decay fit and

bilayer assembly which assumes there is 1-D interface between donor and acceptor.[36] The values in **Table 2.2** are preliminary calculations done only to see the relativity of two different techniques in order to calculate diffusion coefficients. We believe the Monte-Carlo simulations provide much more realistic data by simulating the actual conditions such as number of quencher molecules present in the thin films.

2.3.5 Photoluminescent Lifetimes of Porphyrin Solutions

The photoluminescent lifetime decays of all the porphyrin derivatives in dichloromethane (DCM) solutions were measured and very similar PL lifetime (τ_s) decays were observed for all the porphyrin derivatives. The lifetime of the excitons in the porphyrin derivatives with alkyl chain length from methyl to octyl was very similar unlike the thin films of all of these derivatives, where the lifetimes varied significantly indicating the increasing alkyl chain has very little to no effect on singlet exciton PL lifetime in the carboalkoxyphenylporphyrins All of the PL lifetime (τ_s) decays were between 8.5-9.0 ns as shown in **Figure 2.6**. This behavior could be attributed to the presence of similar core in all the derivatives and similar molecular interactions in the solutions unlike thin films.

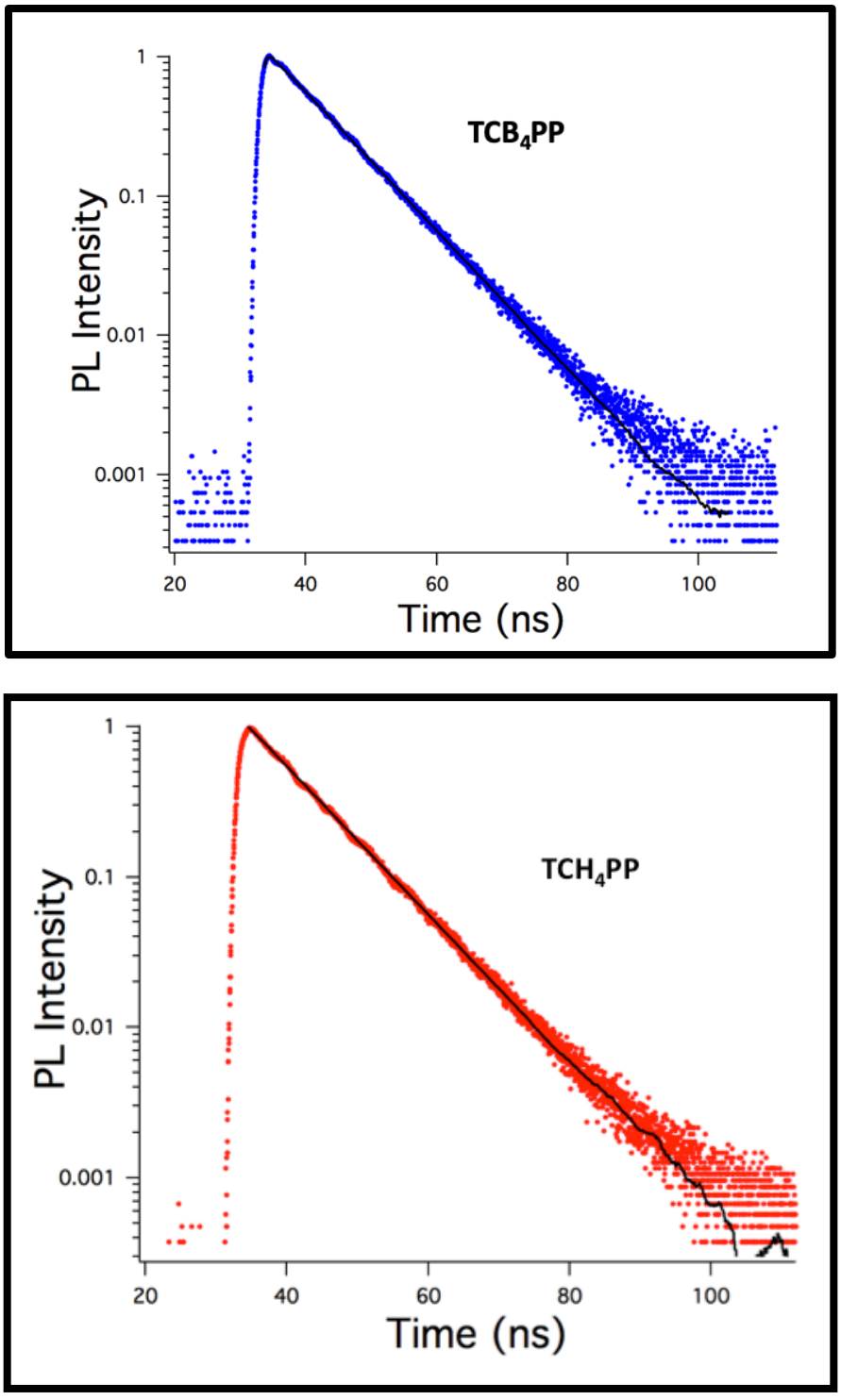

Figure 2.6 PL lifetimes and exponential fit of all porphyrin derivatives in a dichloromethane

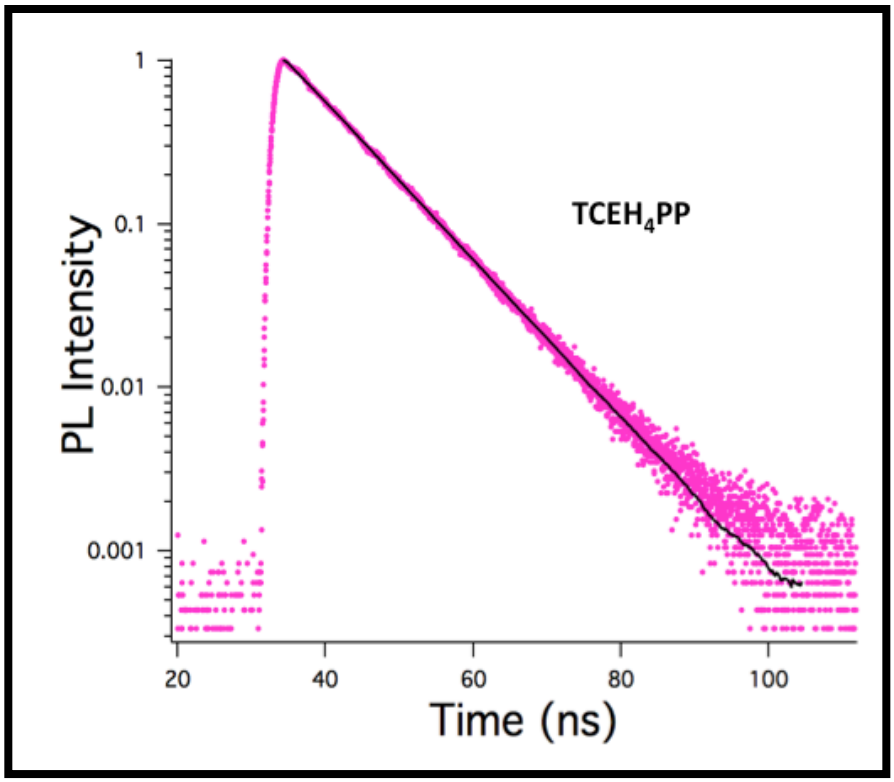

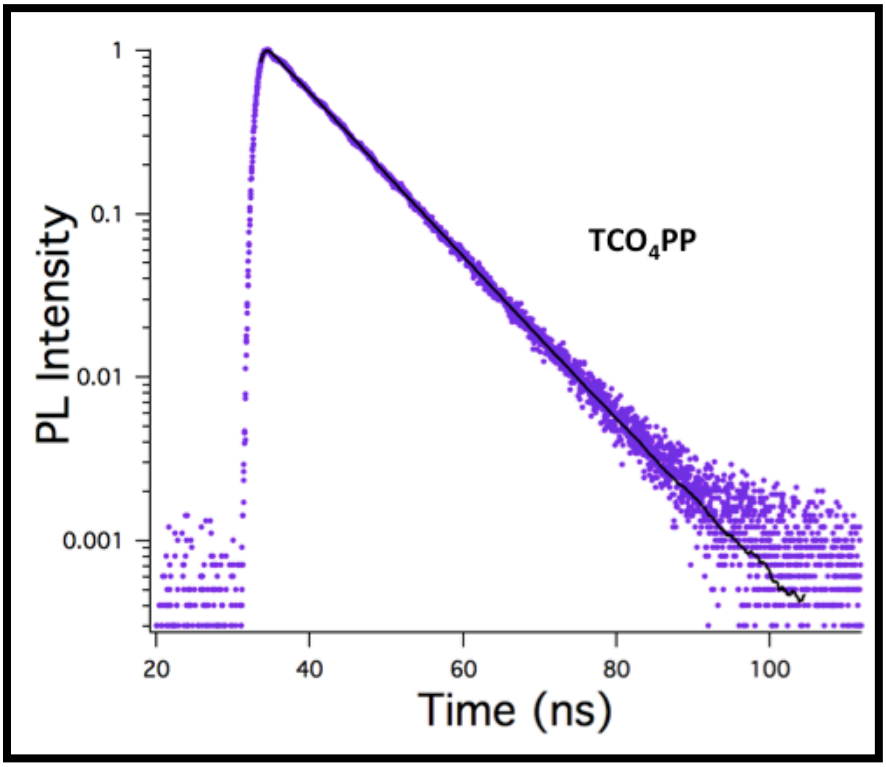

Figure 2.6 PL lifetimes and exponential fit of all porphyrin derivatives in a dichloromethane continued.

2.3.6 Steady-State Emissions

The steady-state emission of all the derivatives is shown in **Figure 2.7**.

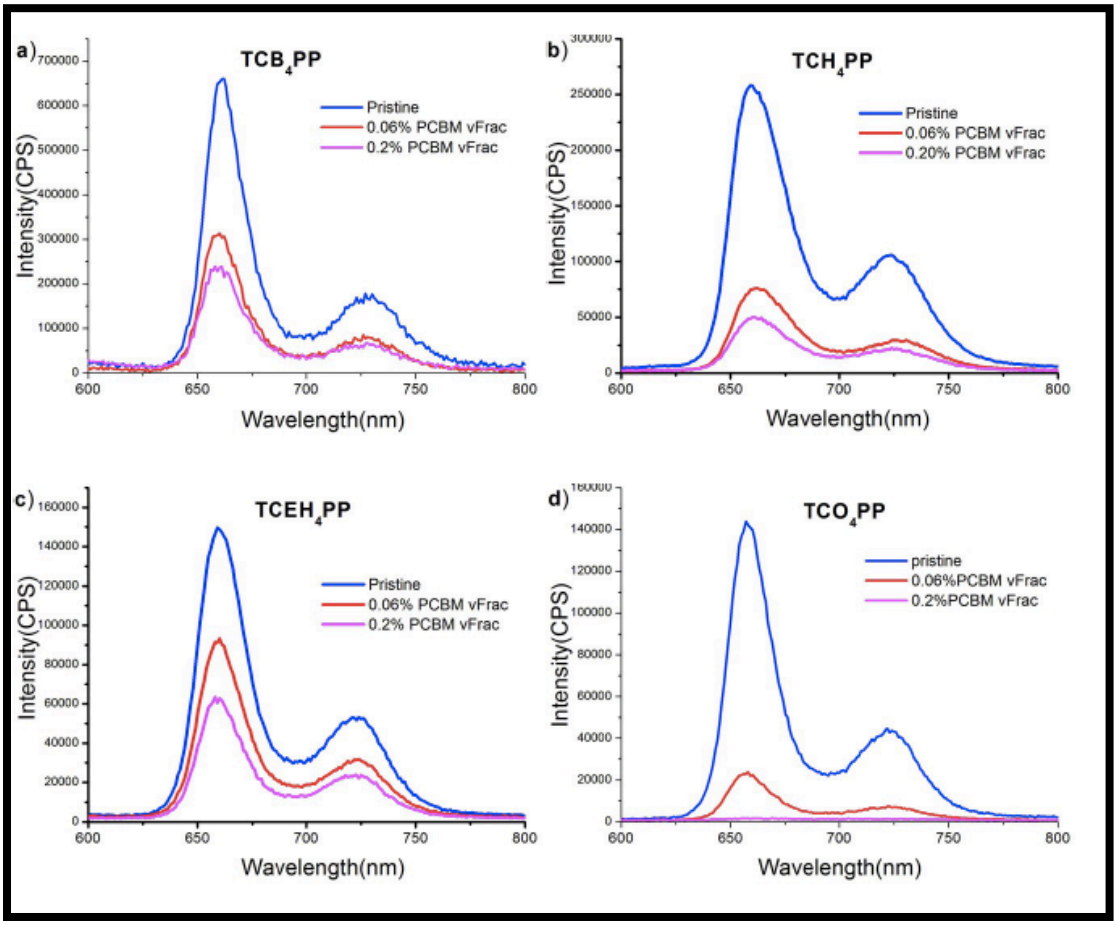

Figure 2.7 Steady-State emission of (a) TCB_4PP pristine and with 0.06%, 0.2% PCBM (b) TCH_4PP pristine and with 0.06%, 0.2% PCBM (c) $TCEH_4PP$ pristine and with 0.06%, 0.2% PCBM (d) TCO_4PP pristine and with 0.06%,0.2% PCBM

The emission spectra of all the pristine and porphyrin:PCBM blended derivatives with 0.06% and 0.2% PCBM have been shown. The excitation wavelength of 425 nm was used for all the derivatives since the highest absorption intensity for the carboalkoxyphenylporphyrin derivatives falls in that range. The intensity of the emission for pristine derivative decreases as the volume fraction of quencher/ acceptor material

increases and is seen in the following figure. TCO_4PP showed the highest steady-state quenching efficiency and the data has been summarized in **Table 2.1.**

The relative quenching efficiencies were calculated by integrating the area under the pristine porphyrin emission curves and pristine-PCBM doped porphyrin emission curves using the following equation

$$Qss = 1 - \int \frac{PL_{blend}\, dt}{PL_{pristine} dt} \quad \text{.....Equation 2.14}$$

2.3.7 X-Ray Diffraction Analysis: Thin films

The structural rearrangements of porphyrin thin films on the glass substrate was studied using x-ray diffraction (XRD) data and additional information regarding the organization of porphyrin thin films were obtained as shown in **Figure 2.6**. The smallest alkyl chain derivative TCM_4PP showed one broad peak at 2θ = 10 °-35 ° with no other intense peaks, which means there is little to no order present in TCM_4PP. As the length of the alkyl chain was increased the intensity of XRD peaks increases. The broadened peak at 2θ = 10 °-35 ° is also found in the XRD spectra for TCB_4PP, TCH_4PP, and was previously observed in thin films containing tetrabutylphenylporphyrins indicating minimal periodic structure.[70]

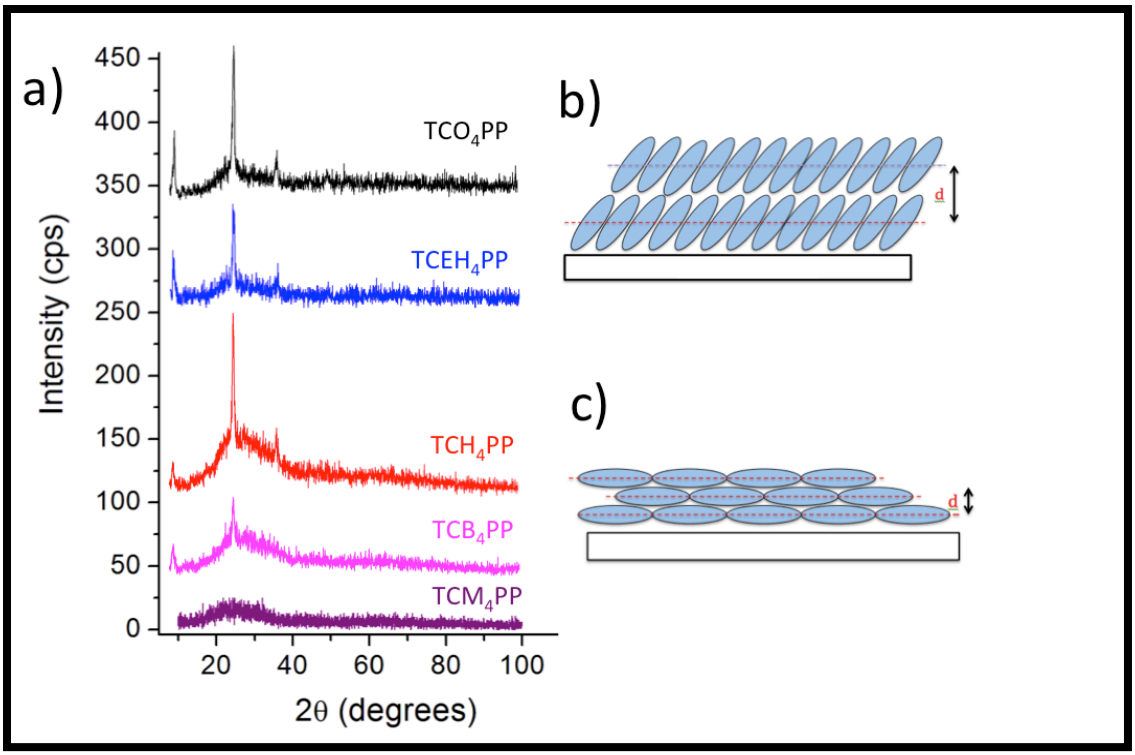

Figure 2.6 X-ray diffraction patterns of solution-cast thin films of TCM_4PP (−), TCB_4PP (−) and TCH_4PP (−) $TCEH_4PP$ (−), and TCO_4PP (−), film thickness: 20-25 nm. Porphyrin stacking in solution-cast thin films b) nematic assembly and a) slip-stack assembly

Three intense peaks were seen in the XRD spectra with different relative intensities for thin films of TCH_4PP, $TCEH_4PP$, and TCO_4PP derivatives (at approximately 2θ = 6 °, 22 °, and 34 °) with an exception of TCB_4PP as it didn't have the peak at 2θ=34 ° and showed only two peaks at 2θ = 6 ° and 22 °. This data indicates the diffraction peak ranging from 2θ = 5.9 ° - 6.3 ° indicating self-assembled stacks of organization of porphyrin molecules aligned perpendicular to the surface with a calculated d-spacing between the porphyrin stacks ranging from 13.99 Å to 15.31 Å respectively.[72] The d-spacing values are in good agreement with previous reports of solution-cast thin tetraphenyl porphyrin films which also show interplanar stack distances

of 14 Å. [72] Literature survey showed reports of tetraphenylporphyrins and zinc-octaethylporphyrin suggesting surface stacking and molecular orientations at angles between 23 ° and 50 °.[77] Interestingly, the $TCEH_4PP$ branched alkyl chain derivative showed largest calculated d-spacing of 15.3 Å, while the TCO_4PP octyl alkyl derivative exhibited the closest d-spacing of 13.9 Å The ratio of relative intensities of the peaks at the 2θ = 6.0 ° to the more intense peak at 2θ = 22 ° was found similar and roughly calculated at 2:1 for thin films containing TCB_4PP, $TCEH_4PP$, and TCO_4PP porphyrin derivatives. The ratio of relative intensities of the same peaks was nearly 5:1 in the XRD spectrum of the TCH_4PP derivative. This data suggested that the TCH_4PP (hexyl-containing) film has a higher order and crystalline domains and majority of the aligned porphyrin molecules stacked on the surface in a well packed, nematic/homeotropic arrangement.[70,78] Although TCB_4PP also shows evidence of an organized assembly of the molecular thin film; there are likely greater regions of disorder or aggregation within the films as summarized from literature and data collected. **Table 2.2** summarizes the XRD peaks with d-spacings and relative intensities.

Table 2.3 XRD Data for TCB_4PP, TCH_4PP, $TCEH_4PP$, TCO_4PP

TCB_4PP			
XRD peaks (2θ)	6.08	22.28	N/A
d-spacing(Å)	14.54	3.99	N/A
Intensity	34	83	N/A
Relative Intensity(%)	41	100	N/A
TCH_4PP			
XRD peaks (2θ)	5.98	22.38	34.23

d-spacing(Å)	14.78	3.97	2.62
Intensity	41	206	77
Relative Intensity (%)	20	100	37
$TCEH_4PP$			
XRD peaks (2θ)	5.78	22.13	34.38
d-spacing(Å)	15.30	4.02	2.61
Intensity	31	56	24
Relative Intensity (%)	55	100	43
TCO_4PP			
XRD peaks (2θ)	6.33	22.63	34.23
d-spacing(Å)	13.97	3.93	2.61
Intensity	64	141	46
Relative Intensity (%)	45	100	33

The largest relative peak intensities for 2θ = 6.0 ° were observed for thin films containing TCO_4PP and $TCEH_4PP$ indicating a preferentially stacked arrangement with porphyrin edge-on alignment observed previously with self-assembled coordinating porphyrins.[43] The XRD data suggests that TCH_4PP derivative is very closely packed and stacks in a nematic/homeotropic assembly, which explains its longest diffusion lengths, and strong excitonic coupling as it has more structural organization.

2.4 Conclusions

Exciton diffusion parameters of five carboalkoxyphenylporphyrin derivatives with varying peripheral alkyl groups were investigated. Time-correlated single photon counting was used to measure the photoluminescent lifetime decays of these singlet

excitons. We conclude that the exciton diffusion is sensitive to the molecular packing and rearrangements in these derivatives, which is also influenced by the size of alkyl groups on the porphyrin ring in thin films. X-ray diffraction showed a difference in molecular packing in various different alkyl group leading to more organized pattern and approaching single crystal structures as we increase the alkyl chain length. XRD data indicates the presence of nematic/ homeotropic assembly in hexyl chain derivative (TCH_4PP) exhibiting strong excitonic coupling. This particular derivative gave us the longest exciton diffusion length and high exciton diffusion parameters. The derivative with branching (-ethylhexyl) on the porphyrin ring $TCEH_4PP$ displays the shortest exciton diffusion length, which is due to slip-stacked molecular assembly. Spin-casted thin films of TCH_4PP showed the exciton diffusion length of 20-25 nm, which is double the exciton diffusion length of many organic semiconductors being currently used in OPVs. TCO_4PP derivative showed a significantly longer lifetime of 6.3ns however the diffusion rate was lower than other derivatives for TCO_4PP. We conclude that TCH_4PP has a balanced mixture of molecular packing/organization in thin films, which makes them better candidates than other derivatives. This study also demonstrates the sensitivity of how in porphyrin dye molecular packing and rearrangements can have a massive impact on their photophysical properties and exciton diffusion. Our results provide a deep insight into PL lifetimes, exciton diffusion lengths, quenching efficiencies and diffusion coefficients which will be useful in understanding and developing better performing porphyrin-based optoelectronic devices.

CHAPTER 3. FILM STRUCTURE MODIFICATIONS TO ENHANCE EXCITON DIFFUSION IN PORPHYRIN-FULLERENE BILAYER THIN FILMS AND STUDYING THEIR THERMAL PROPERTIES

3.1 Introduction and Background

There are various assemblies that could be used to fabricate an organic photovoltaic device such as bilayer where donor and acceptor material has a defined interface or bulk-heterojunction where donor and acceptor interfaces are intermingled. Bulk-Heterojunction (BHJ) assembly is one of the most common active layer assembly where donor and acceptor components are intermixed having several interpenetrating networks of interfaces.[79] The BHJ assembly is known to have a blended irregular interface of donor and the acceptor material with an advantage of increased surface area of the interface and reduced recombination sites for the excitons.[79] The exciton diffusion lengths (L_D) for most of the organic semiconductors are short (approx. 10 nm) requiring a multiple interfaces like in bulk heterojunction in order for excitons to reach the interface.[80,81] High efficiency organic solar cells are highly dependent on the efficiency of exciton diffusion mechanism at the interface in order to form free charge carriers that can be extracted at the respective electrodes. Another possible method to improve efficiency is to increase the exciton diffusion length of the organic semiconductor and form a layered interface by molecular self-assembly or stacking where donor and acceptor have a 1-D interface.[74,82] During this project we prepared bilayer assembly of porphyrin and fullerene thin film where porphyrin was spin coated and fullerene was evaporated under high vacuum on top of the porphyrin layer. The goal of this project was to study the effect of bilayer quencher molecules on the exciton quenching efficiencies (Q). While most of the cases of BHJ assembly have given higher efficiencies than a bilayer

assembly, there have been experiments performed when bilayer organic solar cells gave comparative power conversion efficiencies in organic solar cells.[83] **Figure 3.1** shows the bilayer thin film assembly and the derivatives used in this chapter for the structural modifications and annealing studies.

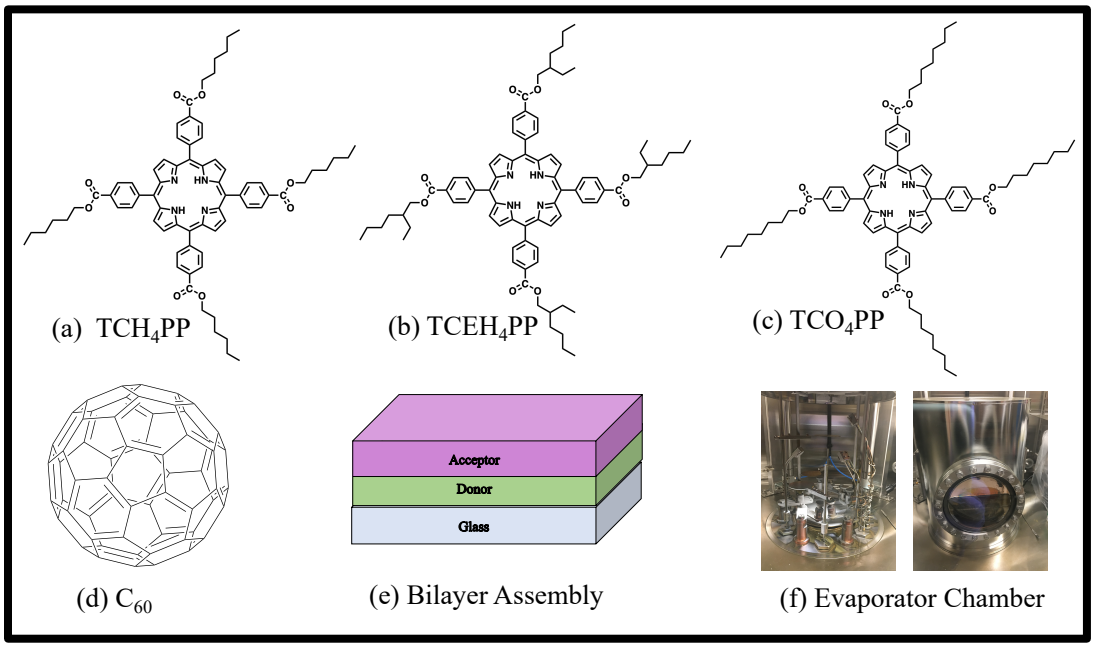

Figure 3.1 Porphyrin derivatives and fullerene used in bilayer thin film composition

The thin film UV-vis absorbance spectra, steady-state fluorescence emission, and thermal properties of three carboalkoxyphenylporphyrin derivatives before and after annealing have been studied: tetra(4-carbohexoxyphenyl)porphyrin (TCH_4PP), tetra(4-carbo-2-ethylhexoxyphenyl)porphyrin ($TCEH_4PP$), and tetra(4-carbooctoxyphenyl)-porphyrin (TCO_4PP). The quenching efficiencies of these three derivatives have been calculated from their steady-state emission using pristine spin cast films and films with an evaporated C_{60} bilayer. Structural analyses have been performed using X-ray diffraction (XRD), UV-vis spectroscopy, and thermal annealing properties were studied using differential scanning calorimetry measurements (DSC). Annealing the films caused

significant structural changes and these were also observed in the UV-vis absorbance spectra and XRD diffraction patterns. Prior to thermal annealing, quenching efficiencies are greatest for the TCH_4PP and TCO_4PP (hexyl and octyl derivatives), which is in agreement with previous bulk quenching experiments done to calculate exciton diffusion lengths.[61] After annealing, the hexyl derivative (TCH_4PP) showed the lowest bilayer quenching efficiency and indicated evidence of significant molecular rearrangements.[15]

3.2 Experimental

The studied porphyrin materials TCH_4PP, $TCEH_4PP$, and TCO_4PP were prepared as previously reported.[61,68] Fullerene, C_{60} (99.8%) was purchased from SES chemicals and was used as received. Microscope slides (2 cm x 2 cm) were thoroughly washed and sonicated for 20 min in alkonox, milli-Q water, isopropyl alcohol, dried with N_2 and followed by UV-ozone treatment for 20 min to obtain a clean surface free of contaminants for spin-casting. The slides were thoroughly checked for any surface contaminants before introducing them into the glove box for hot spin casting. Three pristine carboalkoxyphenylporphyrin derivatives solutions TCH_4PP, $TCEH_4PP$, and TCO_4PP were prepared in chlorobenzene under nitrogen atmosphere (approx. 6 mM). The studied derivatives showed excellent solubility in chlorobenzene for device purposed (100 mg mL^{-1}).[43] The solutions of each derivative consisting of TCH_4PP, $TCEH_4PP$, and TCO_4PP in chlorobenzene were stirred for 48 h before spin coating to ensure proper mixing. The solutions and glass slides were heated on hot plate inside the glove box at 70 °C for 10 -15 min prior to spin casting to make sure the solution and glass substrate is at same temperature to achieve uniform thin films. Films were spin cast at 2000 rpm for 45 s under controlled N_2 filled glove box. The hot spin casting ensures uniform porphyrin

film formation. C_{60} evaporation was done in an evaporation chamber inside the glove box and C_{60} layer thickness was monitored to achieve a 30 nm thickness. An aluminum oxide coated boat was used to evaporate C_{60} using 5 x 10^{-6} mbar pressure.

Two different sets of thin films were prepared for data collection. One set of thin films was spin-coated and introduced in to evaporation chamber for fullerene layer. The other set of thin films was annealed at 150 °C after spin coated for 15 min to collect thermal annealing data before evaporating fullerene layer. The absorbance spectra of the thin films were measured before and after evaporation of C_{60} layer for both sets of films on a Cary 300 spectrophotometer. Steady-state emission was measured for thin films before and after on a Jobin Yovin fluorolog. XRD patterns were obtained using a Panalytical X'Pert Pro MPD with Ni filtered Cu Kα radiation (λ = 1.541 Å) from a fixed anode at 45 kV, 40 mA. Data were collected with a 0.02 ° step size (5 ° < 2θ < 120 °), and a counting time of 0.35s per point. Differential scanning calorimetry (DSC) measurements were performed on Mettler Toledo using Al crucibles scanning 25 ° – 250 ° C at 10 C min^{-1} scan rate (forward and reverse cycles) using 2-3 mg of porphyrin TCH_4PP, $TCEH_4PP$, and TCO_4PP.

3.3 Results and Discussion:

3.3.1 Differential Scanning Calorimetry

In order to study the thermal behavior of the pristine porphyrins, glass transition temperatures (T_g) of all the derivatives were determined using differential scanning calorimetry technique. One heating and cooling cycle was performed to observe the phase transitions happening in the porphyrin derivatives at the rate of 10 °C/min as shown in **Figure 3.2**. The methyl chain derivative (TCM_4PP) showed no phase transition

pointing out absence of crystalline nature whereas the butyl derivative (TCB_4PP) showed a phase transition at 78°C in the forward cycle or heating cycle and two peaks in cooling or backward cycle during the measurement at 124 °C and 101 °C.

The hexyl derivative (TCH_4PP) showed only one phase transition during heating and cooling cycle at 130 °C whereas ethyl hexyl or branched derivative ($TCEH_4PP$) showed a phase transition at a very high temperature around 218 °C and at 129 °C during the cooling cycle. The longest alkyl chain derivative, octyl derivative (TCO_4PP) showed a peak at 208 °C during forward cycle and at 154 °C during cooling cycle. The heating and cooling cycles in all the thermograms forms a hysteresis and peaks indicates a transition from or towards crystallinity.[84] The forward peak seen in TCB_4PP, TCH_4PP, $TCEH_4PP$ and TCO_4PP indicates melting since melting is an endothermic process hence more heat is absorbed by the sample at this point and there is increase in heat flow seen when it is plotted against temperature and indicates melting point (T_m) of the specific porphyrin derivative during the heating cycle and the downward

The bend during the cooling cycle shows a crystalline exothermic transition and indicates the crystalline temperature of the porphyrin sample. This information was useful in selecting an appropriate annealing temperature for the porphyrin derivatives during thermal studies.

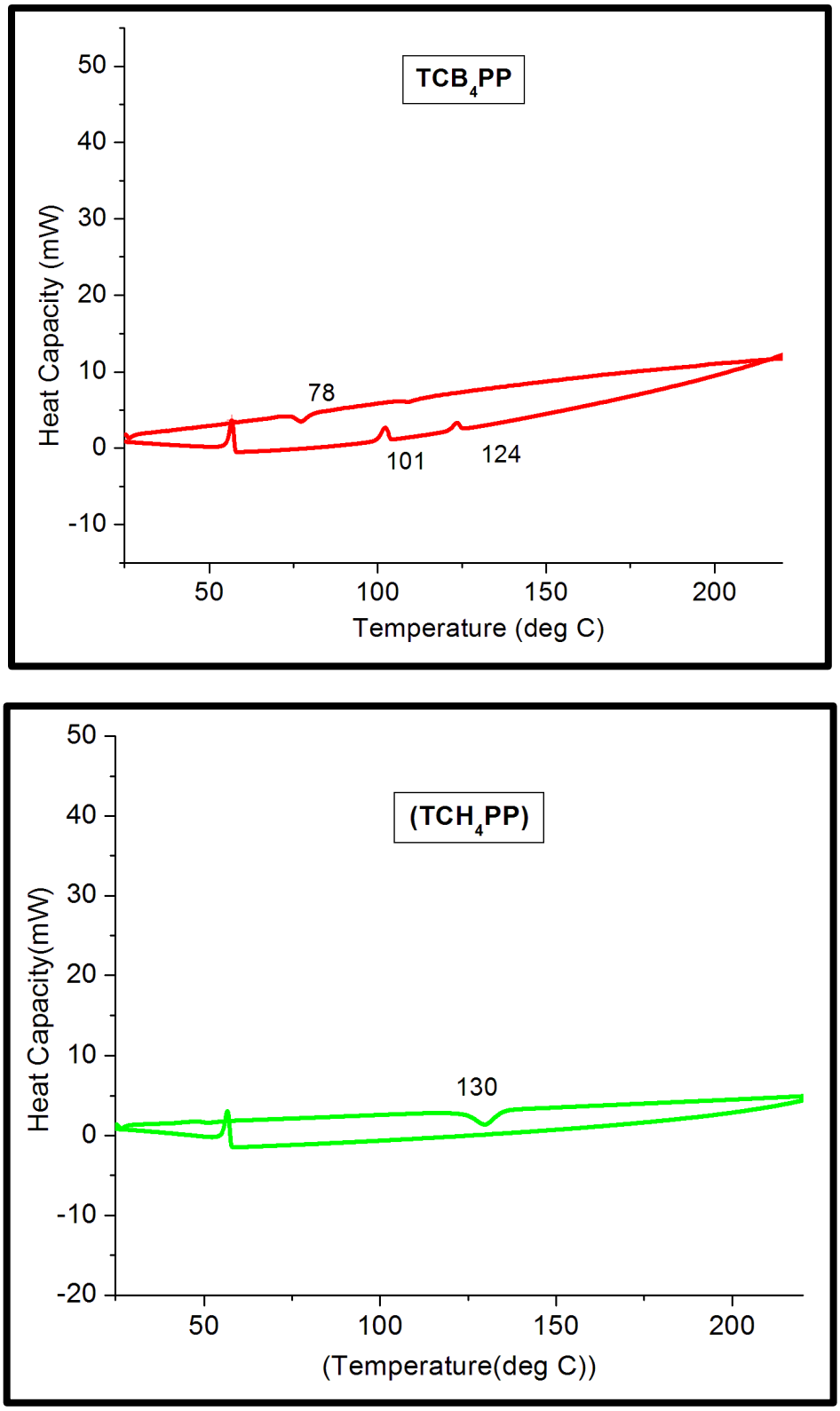

Figure 3.2 Differential Scanning Calorimeter measurements of pristine derivatives of TCB_4PP, TCH_4PP

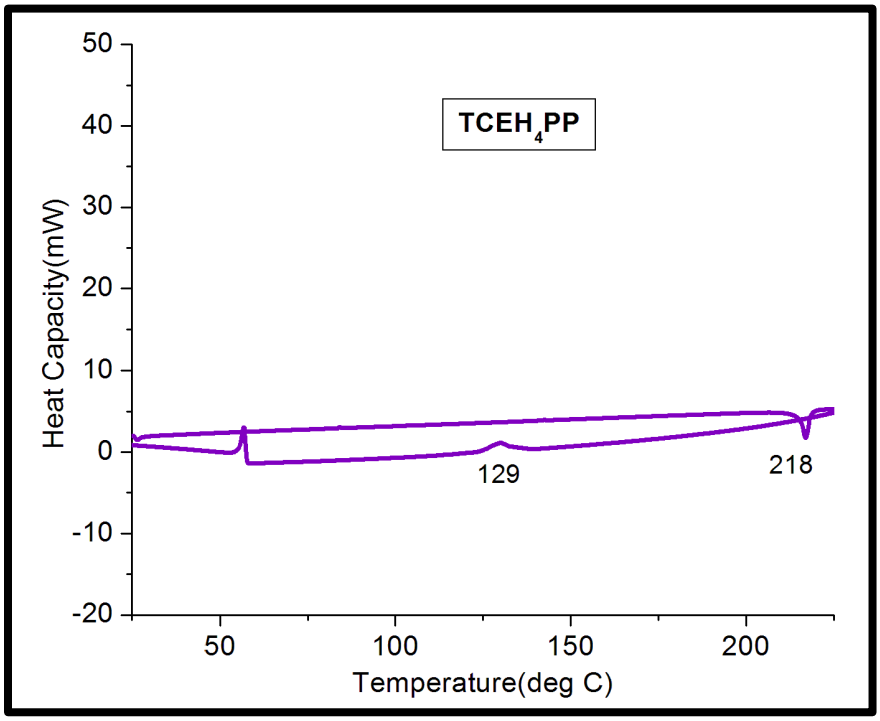

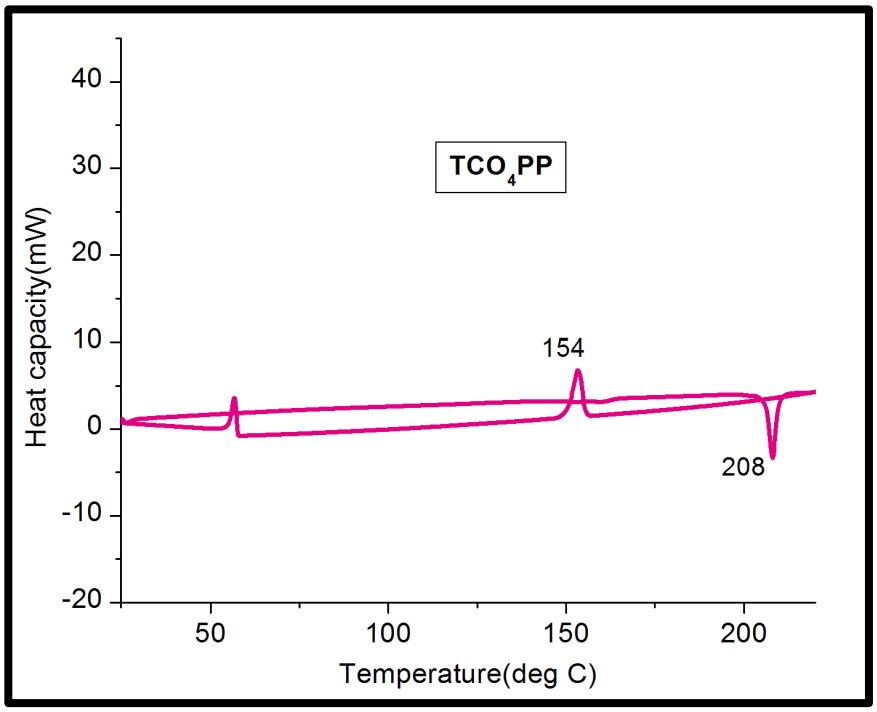

Figure 3.2 Differential Scanning Calorimeter measurements of pristine derivatives of $TCEH_4PP$, TCO_4PP continued.

3.3.2 Steady-State Emission and Quenching Efficiencies

We have previously reported the exciton quenching efficiencies of the carboalkoxyphenylporphyrin derivatives thin films in bulk-heterojunction assembly where porphyrin and PCBM solutions were blended in a solution to get a donor-acceptor solution.[43] During this project we explain the effects of distribution of quencher /acceptor to understand if it is interfering in the exciton transport dynamics. Therefore, we made a bilayer assembly of porphyrin and C_{60} thin films, where porphyrin solution was spin-coated similar to previous project but a thin layer of C_{60} was evaporated inside controlled atmosphere in evaporator chamber inside the glove box to obtain a planar heterojunction.

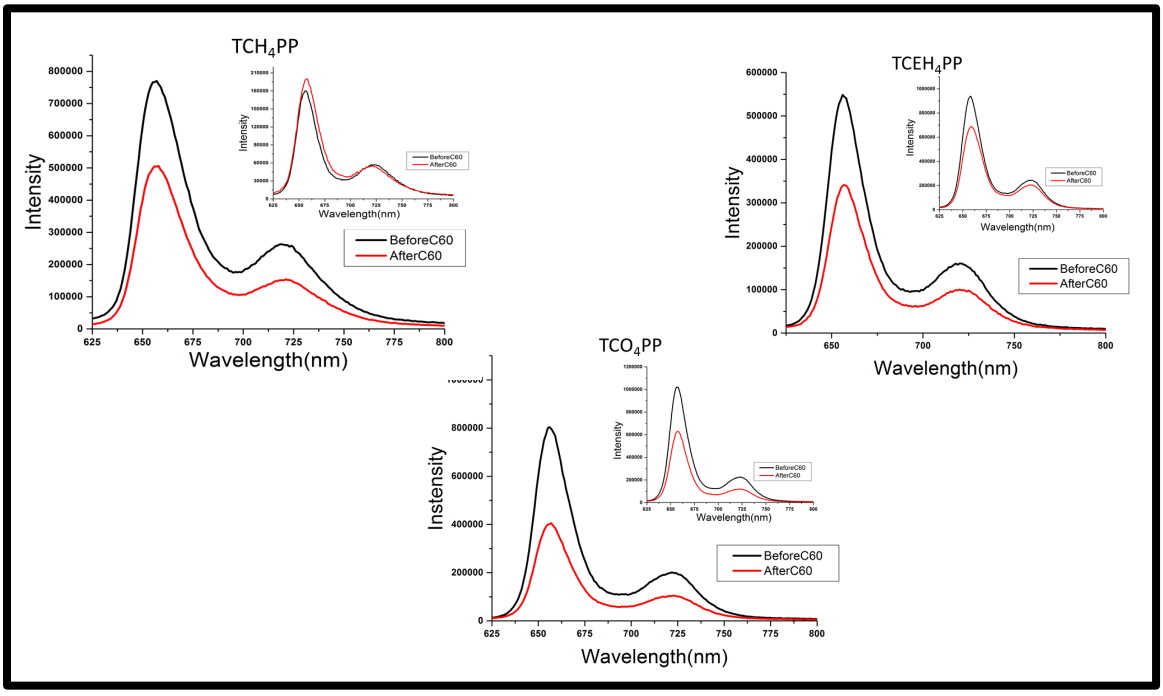

Figure 3.3 Steady-State emission of bilayer thin films with and without C_{60}, inset shows SSE of annealed films (150 °C)

The steady-state efficiencies (SSE) of pristine porphyrin thin films and bilayer porphyrin-C60 thin films were investigated at room temperature and at 150 °C as shown

in **Figure 3.3**. The results have been summarized in **Table 3.1**. The bilayer thin films were made to study the effect of distribution of acceptor or quencher molecules on exciton diffusion properties and quenching efficiencies in contrast to our previously studied bulk-heterojunction assembly.[43] The results from SSE of bilayer thin films shows similar trend from bulk-heterojunction assembly, which confirms that the distribution of acceptor does not affect the exciton diffusion. The results show an average steady-state quenching efficiency of 0.32 for TCH_4PP, followed by 0.25 for TCO_4PP and $TCEH_4PP$ showed least quenching efficiency of 0.22. This also provides good evidence that the higher rates of diffusivity seen for TCH_4PP were related to the exciton diffusivity and molecular organization, and not dependent upon the differences in PCBM distribution within the porphyrin thin films. The interfaces between each derivative and C_{60} is similar, however, absorbance and morphological data indicates changes in the molecular packing between these three porphyrin derivatives. Remarkably, after thermal annealing of the pristine porphyrin films, the quenching efficiency for the TCH_4PP derivative is significantly decreased to 0.14, whereas the average quenching efficiencies of TCO_4PP and $TCEH_4PP$ increased to 0.31 and 0.39 respectively.

Table 3.1 Quenching efficiencies obtained from steady-state emissions of bilayer porphyrin-C_{60} thin films at room temperature and at annealed temperature.

	Q_{ss} *(Room Temp.)*	Q_{ss} *(Heated – 150 °C)*
TCH_4PP	**0.32 ± 0.09**	**0.14[a]**
$TCEH_4PP$	**0.22 ± 0.1**	**0.31 ± 0.14**
TCO_4PP	**0.25 ± 0.1**	**0.39 ± 0.06**

Differential scanning calorimetry measurements indicate that only the TCH_4PP derivative shows a phase transition below the temperature that was used to anneal the films whereas $TCEH_4PP$ and TCO_4PP both show T_m endotherms above 200 °C. It was observed that above 180 °C, thin porphyrin films began to degrade, and therefore annealing temperatures were kept at 150 °C. **Table 3.1** shows decrease in quenching efficiency for TCH_4PP indicating major structural variations upon annealing whereas for $TCEH_4PP$ and TCO_4PP the values increased post annealing.

3.3.3 UV-Vis Absorption Spectra of Porphyrin-C_{60} Bilayer Thin Films

Additional information about bilayer thin films was obtained from the UV-vis spectra of the thin films. Figure shows the absorbance spectra of the thin films of TCH_4PP, $TCEH_4PP$ and TCO_4PP with C_{60} evaporated and without C_{60} evaporated. The absorbance was measure before and after annealing. The Soret peak in thin films between 420-430 nm suggests π-π porphyrin macrocyclic interactions.[70] The red shifted and broadened Soret peak was seen in thin films as explained in Chapter 1, which is likely

due to porphyrin-porphyrin molecular interactions aggregation and decreased average molecular spacing.[70] The absorbance was similarly measured after evaporating C_{60} film on the porphyrin thin film and very little to no shift in Soret peaks were seen. The C_{60} did not penetrate deep into the porphyrin thin films. The presence of C_{60} can be seen from the absorption spectra where an increase in the baseline starting from 650 nm to 400 nm after evaporation. TCH_4PP had the most red-shifted Soret peak at 431 nm as compared to $TCEH_4PP$ (427nm) and TCO_4PP (423nm). After the films were annealed in a controlled environment at 150 °C for 15 min, TCH_4PP had the largest blue shifted Soret peaks after annealing (8-10 nm) as compared to $TCEH_4PP$ and TCO_4PP.

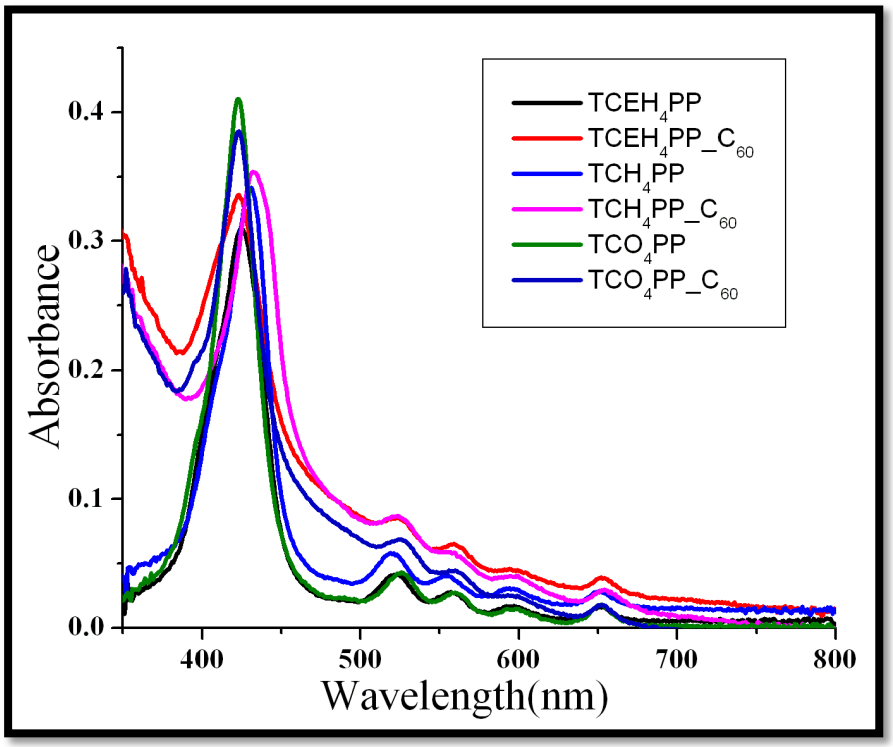

Figure 3.4 Absorbance spectra of TCH_4PP, $TCEH_4PP$ and TCO_4PP before and after C_{60} deposition at room temperature (2a) and films annealed at 150 °C (2b)

This suggests that TCH_4PP is more sensitive to annealing and underwent substantial molecular rearrangements or reorganization upon annealing which could be attributed to the ordered arrangement of porphyrins in TCH_4PP as explained in XRD data in Chapter 2.

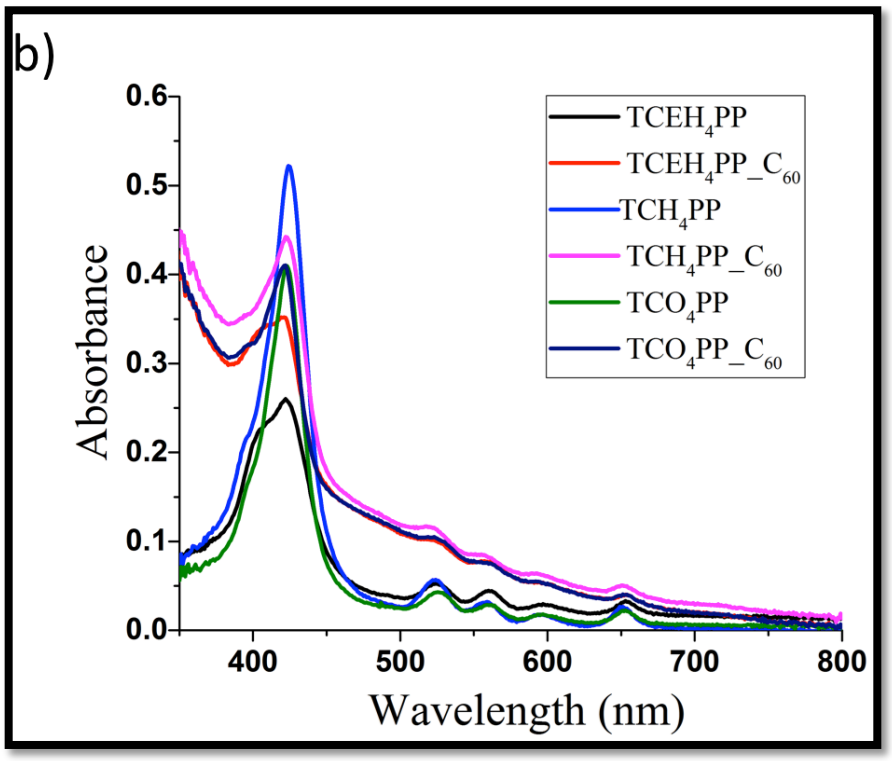

Figure 3.4 Absorbance spectra of TCH_4PP, $TCEH_4PP$ and TCO_4PP before and after C_{60} deposition at room temperature (2a) and films annealed at 150 °C (2b) continued.

3.3.4 XRD Analysis of Porphyrin Thin Films Before and After Annealing

The X-Ray diffraction analysis for the annealed and non-annealed thin films of TCH_4PP, $TCEH_4PP$ and TCO_4PP was done. The three peaks for all the respective derivatives were seen at 2θ=6 °, 22 ° and at 34 ° with the most intense peak at 2θ=22 ° as seen below in the figure. After the films were annealed for 15 minutes at 150 °C, the

XRD measurements were repeated and a decrease in peak height was seen. In addition, the peak at 2θ=34 ° could not be seen in annealed films as compared to non-annealed. The peaks for TCO_4PP and $TCEH_4PP$ broadened from the base suggesting less ordered packing in annealed films and more ordered packing in non-annealed films.

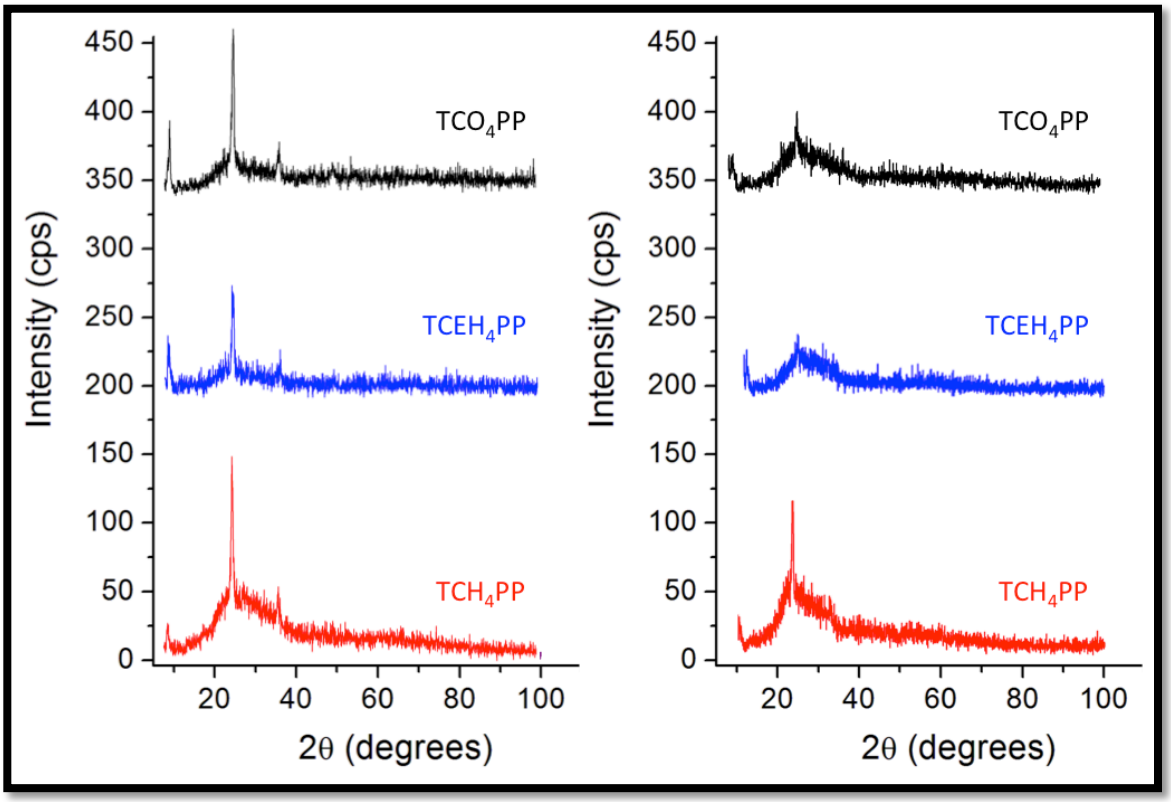

Figure 3.5 XRD peaks for annealed and non-annealed thin films of TCH_4PP, $TCEH_4PP$ and TCO_4PP

Crystallite size was calculated roughly using Scherrer's equation for annealed and non-annealed thin films using the full-width half maxima (FWHM).[85] Table 3.2 shows the size of crystallite calculated from equation 3.1 before and after annealing.

$$B(2\theta) = \frac{K\lambda}{Lcos\theta} \quad \text{.....Equation 3.1}$$

Where K is dimension factor normally considered close to unity

λ is wavelength of X-Ray

B is line broadening at FWHM in radians and is also denoted as B(2θ)

θ is bragg's angle

Table 3.2 Crystallite size using Scherrer's equation before and after annealing

Derivative	At R.T Size (nm)	Annealed @150°C
TCH_4PP (6-Carbon Chain)	114.1 nm	3.3 nm
$TCEH_4PP$ (Branched 6-Carbon Chain)	59.4 nm	7.8 nm
TCO_4PP (8-Carbon Chain)	56.4 nm	4.4 nm

3.4 Conclusions

The steady-state quenching efficiencies for bilayer thin films were investigated at room temperature and at 150°C. Three high performing porphyrin derivatives were chosen TCH_4PP, $TCEH_4PP$ and TCO_4PP. Out of the three derivatives chosen for this study TCH_4PP showed the highest quenching efficiencies at room temperature when a thin layer of C_{60} was deposited through evaporation. When the films of TCH_4PP were annealed to 150°C these films of TCH_4PP were most affected indicating significant structural changes. We also studied XRD patterns and absorbance data of these bilayer thin films at room temperature and the data completely support the fact that the acceptor (C_{60}) distribution

doesn’t have any impact on diffusion process in these derivatives. The peak at 2θ=6 ° suggests stacks of porphyrins on each other and is present in all the derivatives with varying intensities. At 2θ= 22 ° relatively intense peak is present and is indicative of nematic/homeotropic porphyrin molecules.

CHAPTER 4. TERNARY P3HT:PORPHYRIN:PCBM BULK-HETEROJUNCTION SOLAR CELL DEVICES

4.1 Introduction

Ternary assembly of polymer:fullerene along with a photoactive dye like porphyrin has recently attracted interest due to their tunable optical properties.[81] The broad spectral range of porphyrins makes them excellent candidates to be used in ternary blended bulk heterojunction (BHJ) thin film solar cells.[86] In addition, it is believed that such dyes can enhance the overall charge transport in the cell assembly by changing the surface morphology at the interface.[87] This chapter focuses on optimizing a ternary blended OPV device structure using four different derivatives of free base tetracarboalkoxyphenylporphyrin (TCR_4PP) in conjunction with poly-3-hexylthiophene (P3HT) as the donor material and 6,6-phenyl-C61-butyric-acid-methyl-ester (PCBM) as the acceptor in the active layer. Ternary blends with two compatible donor materials and with one acceptor material are emerging as a good alternative to improve the power conversion efficiency (PCE) problem faced by binary devices. As stated above, there are two ways a ternary blend can improve the efficiency of an organic device by increasing the solar absorption range or by enhancing free charge carrier separation and transport.

One of the common problems faced in bulk heterojunction solar cells is a high series resistance and recombination rates in the active layers. Porphyrins have inferior charge mobilities and longer exciton diffusion lengths as compared to some common organic semiconductors. Literature suggests increased short circuit current densities (J_{sc}) and tunable open-circuit voltage (V_{oc}) in ternary blends depending upon the composition of the ternary blend.[88] Since V_{oc} is limited by the difference between HOMO energy level

of the donor and LUMO energy level of the acceptor, there is little room for tuning the V_{oc} in binary systems and J_{sc} is limited by the absorption intensity. There have been experiments where V_{oc} was found to be tunable in such ternary blends but fill factor (*FF*) was lowered.[80,81,88,89] Research continues in this area to establish how ternary blends with porphyrins and conjugated ploymers affect solar cell device efficiencies.

We have previously studied the effects of changing length of peripheral alkyl group and molecular orientation in carboalkoxyphenylporphyrins on their exciton diffusion parameters in thin films. Our previous study showed an increase in exciton diffusion length and photoluminescent lifetimes as we increased the chain length on the meso-positions of these porphyrin derivatives. We hypothesized that this increase in chain length around the porphyrin molecule will have a positive impact on the efficiency of solar cells fabricated from these derivatives due to added stearic hinderance which is responsible for increasing charge separation distance in such bulky porphyrin derivatives and hence reduces the recombination rate.[87] The XRD analysis of our porphyrin derivatives revealed an interesting finding which helped us understand the orientation of these porphyrins in thin films. The derivatives with hexyl and octyl chains on their meso-positions are more likely to organize themselves in a homeotropic assembly which makes the exciton diffusion transport more efficient. However, the derivatives with branched chain ethylhexyl groups are more likely to organize themselves in a manner which is not very favorable for exciton diffusion. The nature of the molecular orientation and organization of these porphyrin derivatives heavily impact their exciton diffusion mechanism which is a critical phenomenon in the active layer of the OPV devices.

Therefore, we studied the effects of addition of four different porphyrin derivatives to a P3HT:PCBM organic solar cell and studied their device parameters and spectral responses. Poly-(3-hexylthiophene) P3HT has been chosen for its good hole mobilities as compared to porphyrins. Porphyrin derivatives provided an increase in the spectral range and have energy levels that are desirable for charge separation and electron transfer when mixed with the electron accepting material PCBM. The goal of this project was to investigate how the different porphyrins exciton diffusion length (L_D) would impact the device efficiency of a ternary blended organic solar cells. There are very few studies that relate the exciton diffusion properties and power conversion efficiencies to the molecular structures and arrangements in such ternary blends. We also studied the photophysical properties such as absorption and external quantum efficiency spectra of the ternary compositions thin films to understand the contribution of porphyrin in the ternary blended active layer of the solar cell.[88,89]

4.2 Experimental

4.2.1 Synthesis of free base carboalkoxyphenyl porphyrin:

Four free base carboalkoxyphenyl porphyrins were synthesized using already published synthesis scheme.[67] As explained in Chapter 2, four different derivatives of carboalkoxyphenylporphyrin derivatives were synthesized with varying alkyl chain at the meso positions such as TCB_4PP (carbobutoxy- 4 carbon chain),TCH_4PP (carbohexoxy- 6 carbon chain), $TCEH_4PP$(carboethylhexoxy- branched 6 carbon), TCO_4PP(carbooctoxy-8 carbonchain) from Tetrakis-5, 10,15,20-(4-carboxyphenyl)porphyrin.Tetrakis-5, 10,15,20-(4-carboxyphenyl)porphyrin (0.08 g, 0.1 mmol) was reacted with an excess of 1-bromoalkane (0.6 mmol) and potassium

carbonate (0.11 g, 0.8 mmol) in 15 mL anhydrous DMF at 80°C for 20 h under N_2. Reaction mixture was added to 300 mL of water and the dark purple precipitate was collected by filtration and rinsed with water. The product was purified by silica gel column chromatography eluting with DCM to yield a purple porphyrin derivatives.[43,67]

4.2.2 Solution Making and Thin Film Preparation from Ternary solutions

In order to measure thin film UV-Vis spectra of ternary blends of P3HT:Porphyrin:PCBM, microscopic glass slides measuring 2 cm x 2 cm were sonicated in alkonox, milliQ water and isopropropyl alcohol (IPA) for 15 min each and dried with N_2. The films were then treated in UV-ozone chamber for 20 m and were transferred to glove box immediately. Polymer:Porphyrin:PCBM thin films were drop-casted inside the glove box under ambient conditions (H_2O (0.1ppm); O_2 (0.6ppm). Approximately, 7mg/mL solution of each component of active layer (P3HT:Porphyrin:PCBM) was dissolved in o-dichlorobenzene and stirred for approx. 24 h inside the glove box . The vials were sealed with paraffin wax in order to avoid solvent evaporation. The ternary solutions were made by adding 100µL of each solution in a separate vial to obtain 1:1:1 volume ratio of each component. After mixing the active layer component solutions, the resulting solution was stirred for 1 h to ensure solubility. Before spin casting, both the solutions and glass slides were heated at 70°C for 15 min to ensure uniform films through hot spin-cast. The process was repeated for each derivative keeping the molar concentrations similar and the weight ratios consistent to obtain four different kind of thin film assemblies to measure UV- Vis of the resulting films.

4.2.3 Device Fabrication:

Ossila Patterned ITO glass slides with 20 Ω/ square resistance were sonicated and cleaned in alkonox, milliQ water, acetone and isopropyl alcohol for 15 min each. The slides were dried very carefully with nitrogen after each sonication step and tested for the conductive side using multimeter before introducing them in to UV-Ozone chamber to ensure the treatment of the correct side. The cells were treated in UV-ozone chamber for 20 min and were immediately spin-coated on a homemade spincoater using 70 µL of Ossila – Al 4093 PEDOT:PSS (~40 nm) outside of the glovebox. The slides were annealed at 120 ° C for 15 min to get rid of any water impurities. The slides were then immediately transferred to the glove box for active layer deposition. Three different solutions, P3HT (20 mg/mL), Porphyrin (20 mg/mL) and PCBM (20 mg/mL) were prepared in o-dichlorobenzene. Three solutions were mixed to obtain one ternary solution of 1:1:4 weight ratio to be used in the active layer. In order to obtain the above weight ratio, 20µL of P3HT solution was mixed with 20 µL of porphyrin solution and finally 160 µL of PCBM was added and was stirred for 30 min at 75° C inside the glove box to allow proper mixing. The slides with PEDOT:PSS layer on them were annealed again for 15 min before the hot spin cast in order to ensure the uniformity of layer. The spin-coater was set at 1000 rpm and 50 µL solution from the ternary blend was drop-casted for 60 s. This spin-coat step was repeated two more times to get a thick and dark active layer to make sure it generates enough excitons for *J-V* curve measurements.

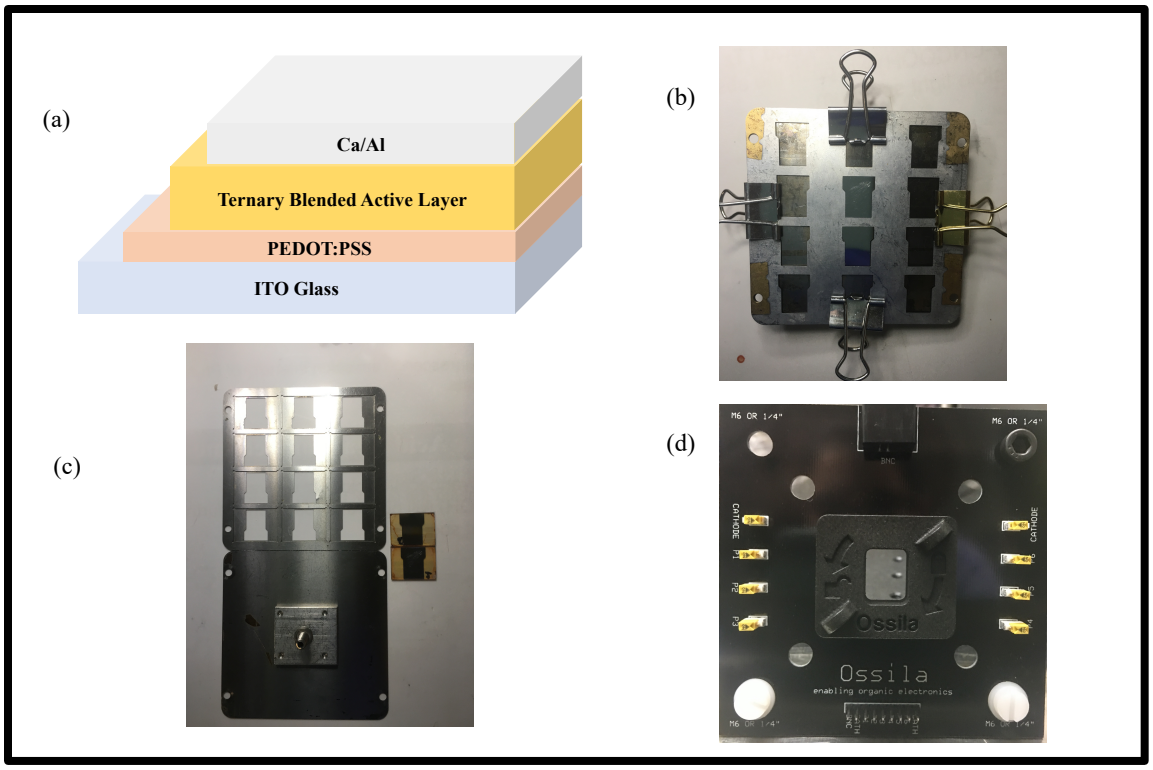

Figure 4.1 (a) Ternary device assembly (b) mask used in evaporator chamber for Ca/Al (c) finished device (d) Ossila push-fit test board for measuring *J-V* curves

The cells were then introduced in the evaporator chamber using mask on top of the active layer to deposit 20 nm calcium layer at the rate of 0.1 Å /s under $7x10^{-6}$ mBar. The deposition rate was controlled by SPC deposition controller. Ca was evaporated very slow in order to make sure there are no rough patches of calcium on the slides. **Figure 4.1** shows the assembly of ternary device made and image of completed device before measuring *J-V* curve in Ossila snapfit board. Lastly, the top contact aluminum was evaporated on top of the calcium layer in the evaporator inside the glove box under $7x10^{-6}$ mBar pressure conditions keeping the first 20 nm evaporation rate at 0.1 Å /s and then increasing the rate of evaporation to up to 1 Å /s. The total thickness of aluminum layer evaporated was 100 nm. The initial slow evaporation of aluminum ensures uniform deposition to avoid recombination pathways in the device assembly. Each layer in the

organic solar cells has to be very critically engineered in order to obtain a smooth and uniform thin film to avoid shorting of the final device.

The current density-voltage parameters of the final device were measured and plotted under conditions of AM 1.5 G simulated sun at an intensity of 100mWcm^{-2}. The devices were measured using Ossila Push-Fit Test Board made for pixelated anode substrates. Both the dark and the light current curves were measured. **Figure 4.2** shows the chemical structures of donor and acceptor materials used in the device fabrication.

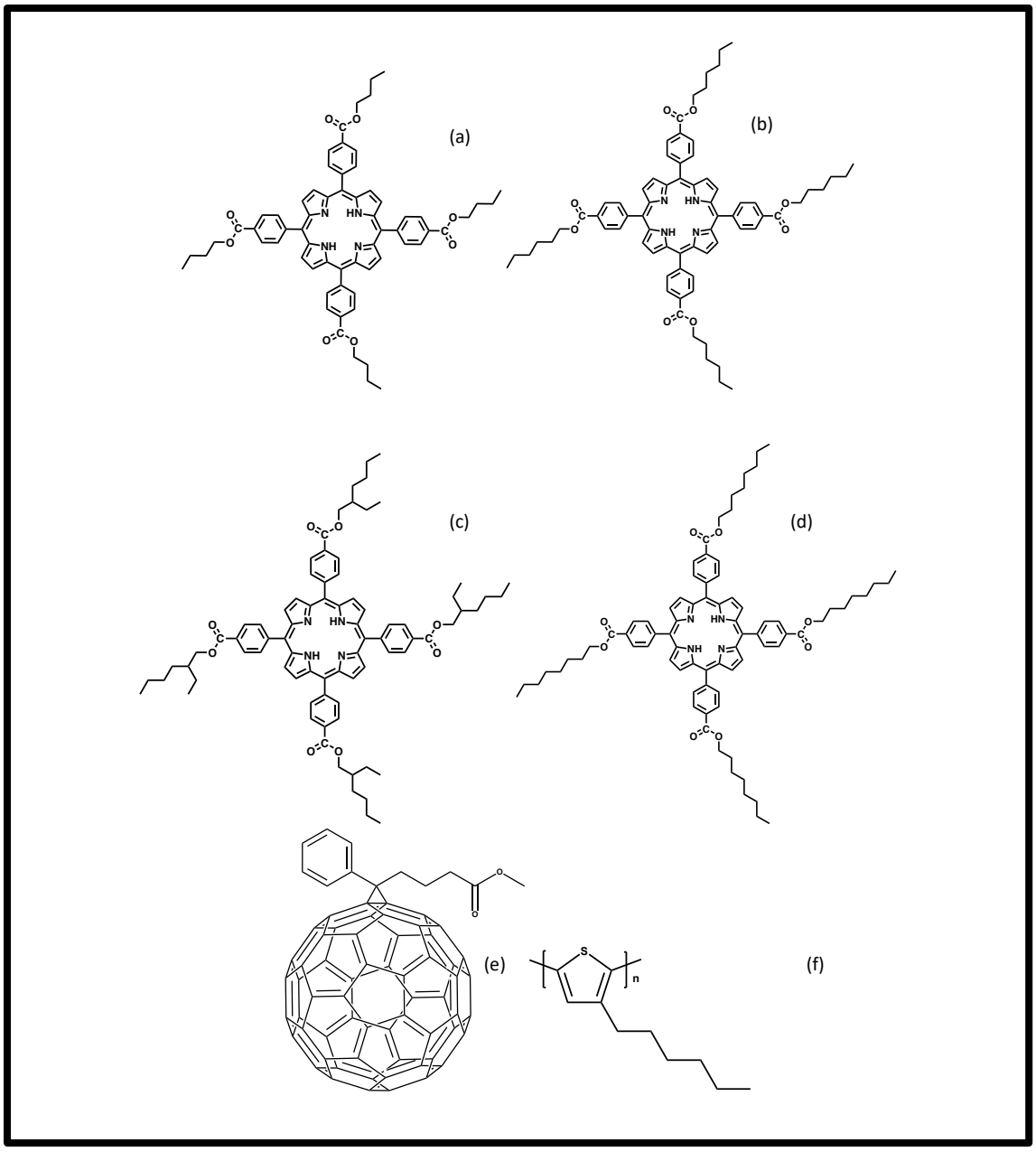

Figure 4.2 Donor and acceptor materials used (a) butyl derivative (b) hexyl derivative (c) ethyl hexyl derivative (d) octyl derivative (e) PCBM (f) P3HT

4.3 Results and Discussions:

4.3.1 UV-Visible Absorption:

Thin films of P3HT:Porphyrin:PCBM blends were measured for their absorbance to check the contribution of porphyrin in the absorbance spectra as shown in **Figure 4.3**.

P3HT thin film absorption spectra ranges from 400-650 nm region with highest absorption at 520 nm and two shoulders in the absorption peak at 570 nm and 610 nm which could be attributed to ordered crystalline features in the film.[90].

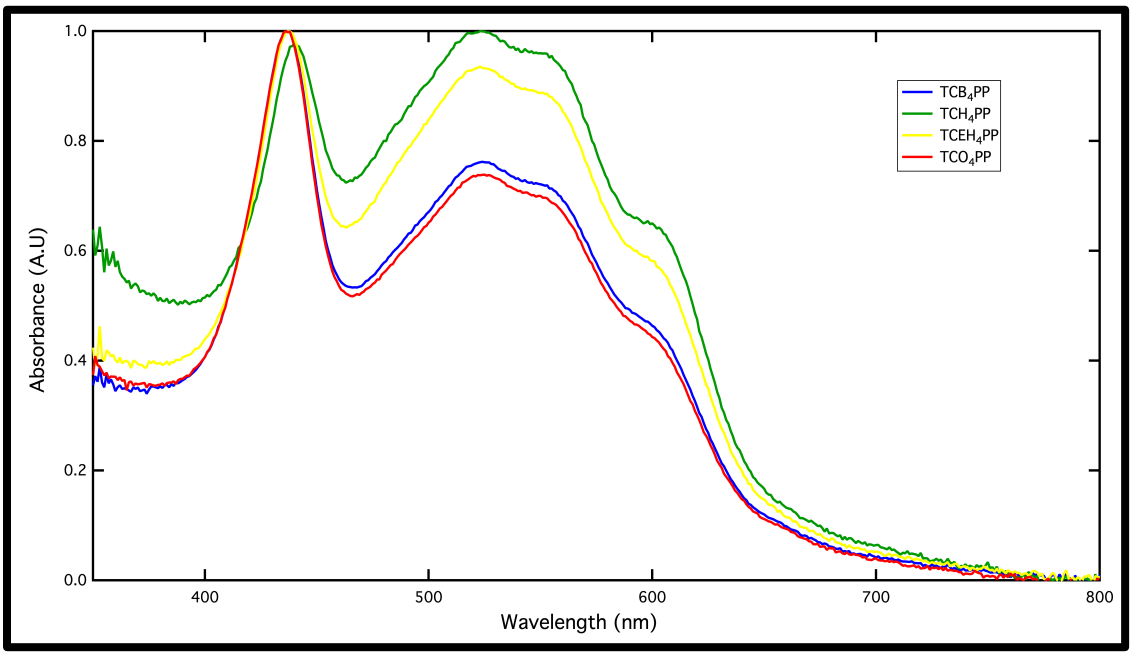

Figure 4.3 Normalized thin Film UV-vis spectra of P3HT:Porphyrin:PCBM ternary blend

Enhanced absorption because of the porphyrin in blended thin film is seen around 425 nm which is believed to contribute to the photocurrent in the device . The shape of the peak at 425 nm matches with the original shape of the Soret peak in the pristine porphyrin derivate absorbance spectra.[91,92] An additional peak due to the porphyrin in the P3HT will result in more excitons upon irradiation during the *J-V* curve measurement. The ratio of polymer to porphyrin has been kept 1:1 in this UV-Vis study and the overall ratio of the ternary blend has been kept at P3HT:Porphyrin:PCBM (1:1:4) for the device study.

4.3.2 Cyclic Voltammetry for Energy Band Diagram

In order to make a working organic photovoltaic device, the most critical step is selection of material used as donor and acceptor in the active layer of the device. The active layer is where all the processes from exciton generation to charge separation takes place. In an organic semiconductor, HOMO energy level signifies the amount of energy required to take out valence electron from the outermost shell of a molecule.[93] The energy level alignment of donor and acceptor material should be energetically favorable that encourages exciton dissociation so the charges can be extracted at the electrodes without recombination. Molecular electrochemistry techniques such as cyclic voltammetry helps to establish oxidation and reduction potential of organic materials and from there the HOMO and LUMO energies can be calculated. Oxidation potential corresponds to HOMO energy and reduction potential corresponds to LUMO energy level. In cyclic voltammetry, ferrocene is used as a known internal reference to calculate the redox potentials

$$E_{HOMO} = -e\,[E_{ox} + 4.4] \quad \text{.....} \textit{Equation 4.1}$$

$$E_{LUMO} = -e\,[E_{red} + 4.4] \quad \text{.....} \textit{Equation 4.2}$$

The difference between HOMO and LUMO energy levels is called band gapor energy gap. [94] In order to calculate the optical band gap of each derivative, the optical absorption was determined from the UV-visible spectra and converted into eV using following equation as cited.[94]

$$E_g = 1242/\lambda_{onset} \quad \text{.....} \textit{Equation 4.3}$$

The cyclic voltammetry data for this study was provided by Dr. Angy Ortiz.[95] All of the measurements were done on a Gamry potentiostat using a scan rate of 100 mV s^{-1}

with 0.1 M solution of tetrabutylammonium hexafluorophosphate($TBAF_6$) supporting electrolyte in dichloromethane under N_2. Two oxidation and two reduction peaks were observed in the CV scans of all the carboalkoxyphenylporphyrin derivatives as shown in **Figure 4.4**. [94,95] All four porphyrin derivatives show similar oxidation and reduction peaks and have very similar absorbance spectra in 10 μM solution of DCM. The absorbance spectra of the porphyrin derivatives in the solution was recorded to determine the optical band of the porphyrins as shown in **Figure 4.5**. The first onset of oxidation for the TCB_4PP and TCH_4PP are shown here and HOMO and LUMO levels have been calculated using ferrocene as the reference in above written equation. The band gap from CV measured values was calculated at 2.25eV for both TCB_4PP and TCH_4PP. The optical band gap for all the porphyrin derivatives was calculated at 1.89 eV.[94]

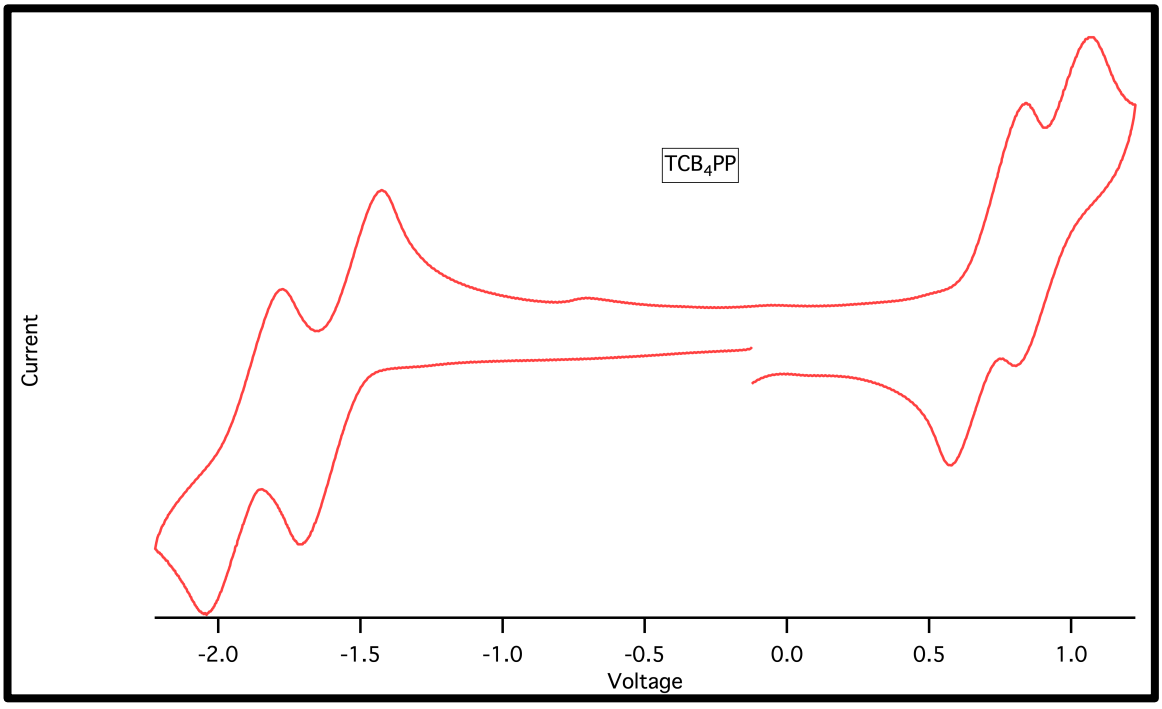

Figure 4.4 Cyclic Voltammetry scan of TCB_4PP, TCH_4PP showing similar oxidation and reduction peaks in 0.1 M $TBAPF_6$ in DCM

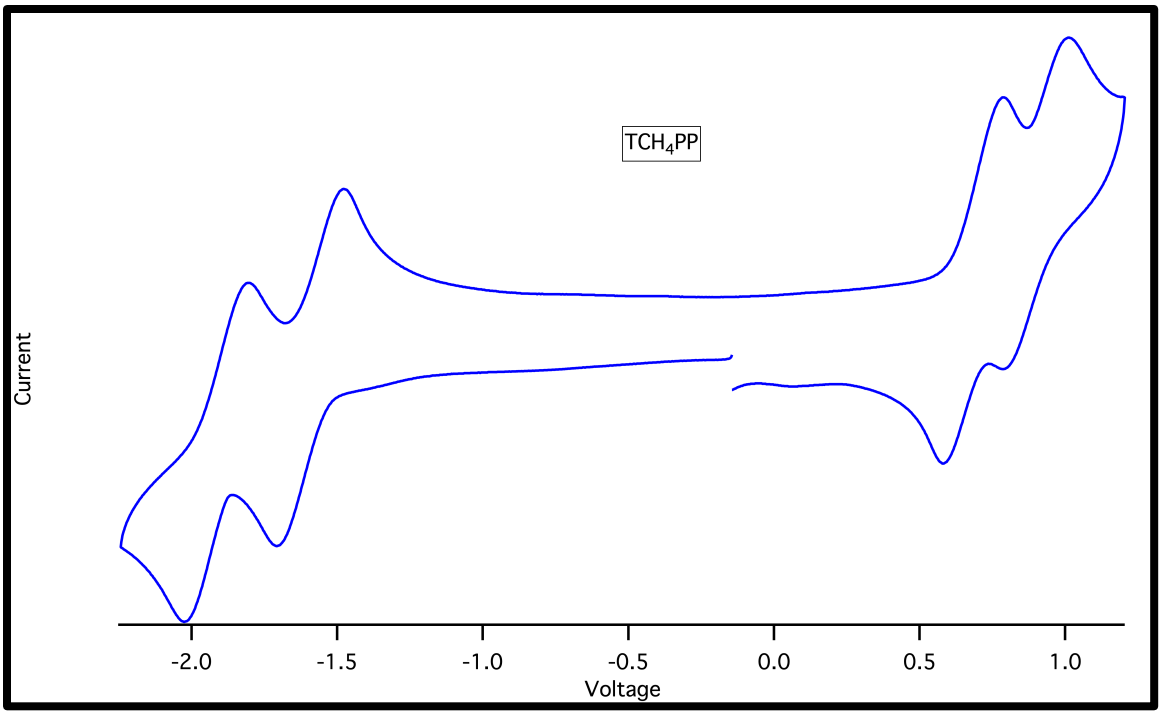

Figure 4.4 Cyclic Voltammetry scan of TCB_4PP, TCH_4PP showing similar oxidation and reduction peaks in 0.1 M $TBAPF_6$ in DCM continued

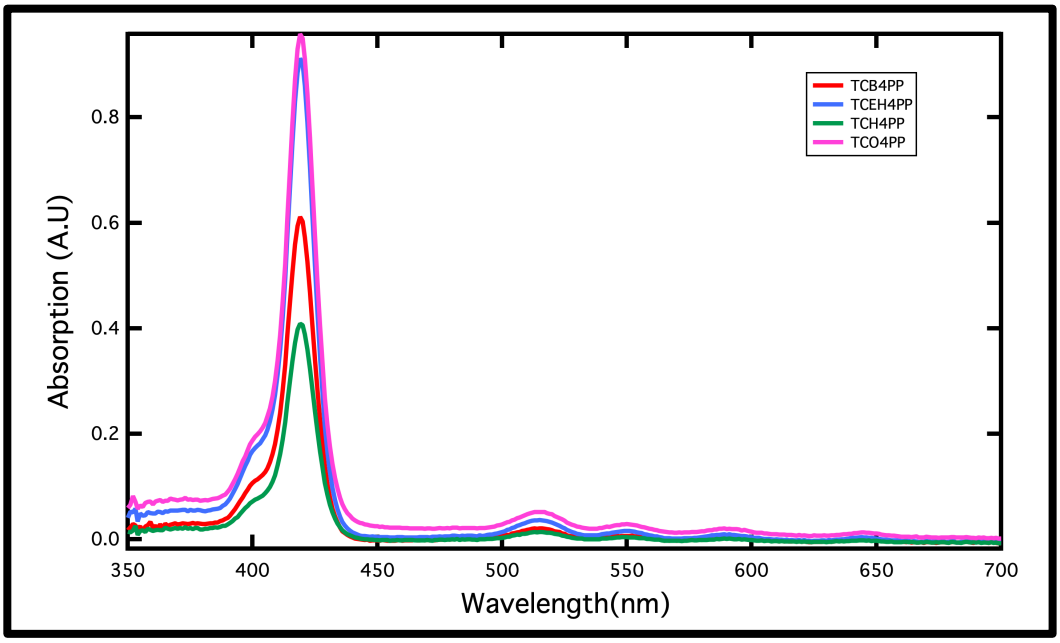

Figure 4.5 Normalized UV-vis Spectra of all porphyrin derivatives in dichloromethane

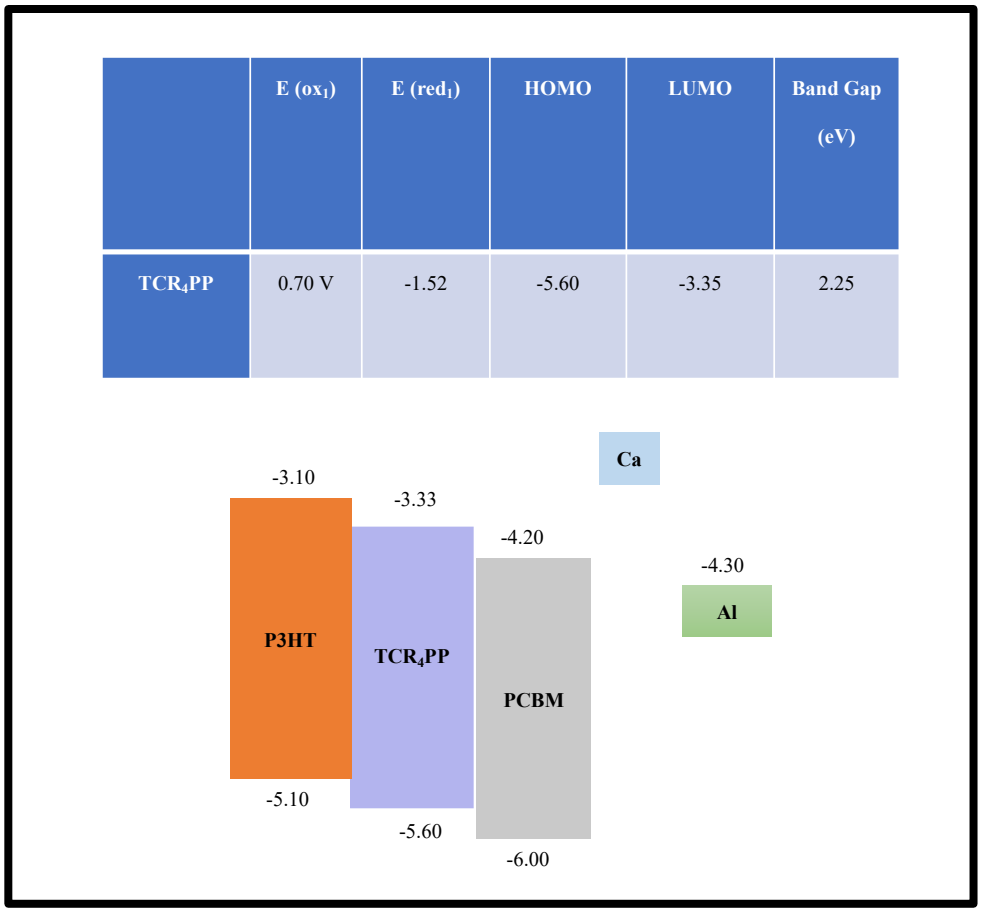

Figure 4.6 HOMO-LUMO levels of the active layer components derived from cyclic voltammetry

Figure 4.6 shows the table with oxidation and reduction onset values to calculate HOMO and LUMO energy levels in carboalkoxyphenylporphyrin derivatives. This data was used to construct an energy level diagram of the active layer components, electron transport layer and the metal contact used in the solar cell devices.

4.3.3 *J-V* Curve Measurements:

OPV devices were fabricated using two donor materials and one acceptor P3HT:TCB_4PP/TCH_4PP/$TCEH_4PP$/TCO_4PP: PCBM as the active layer for all the porphyrin derivatives. The preliminary current density and voltage (*J-V*) curves were studied for the bulk-heterojunction devices under AM1.5 G conditions at 100 $mWcm^{-2}$

intensity. **Table 4.1** provides a summary of the short-circuit current density (J_{sc}), open-circuit voltage (V_{oc}) and fill-factor (*FF*) and the power conversion efficiency (η) of the best devices made from the ternary blends. The J_{sc} ,V_{oc} and *FF* of the solar cell device increased using the hexyl derivative (TCH_4PP) but decreased significantly for ethylhexyl derivative ($TCEH_4PP$) as shown in **Figure 4.7**.

This increase in the J_{sc} and V_{oc} could be linked to our previous exciton diffusion studies and GIWAXS/XRD-analysis conclusions. It was observed that as we increase the alkyl chain length on the meso-position of free base porphyrin there is enhancement in the exciton diffusion parameters except for the ethylhexyl derivative which had less favorable molecular orientation in the thin film assembly which contributes to more recombination rate.[43] The V_{oc} for all the derivatives except for the octyl derivative is very low indicating recombination pathways in the ternary active layers. However, J_{sc} increases as we increase the length of the alkyl group with $TCEH_4PP$ as an exception where branching is present. The increase in J_{sc} could be attributed to improved morphology for longer alkyl group derivatives which improves the crystalline domains in the hexyl and octyl derivatives.

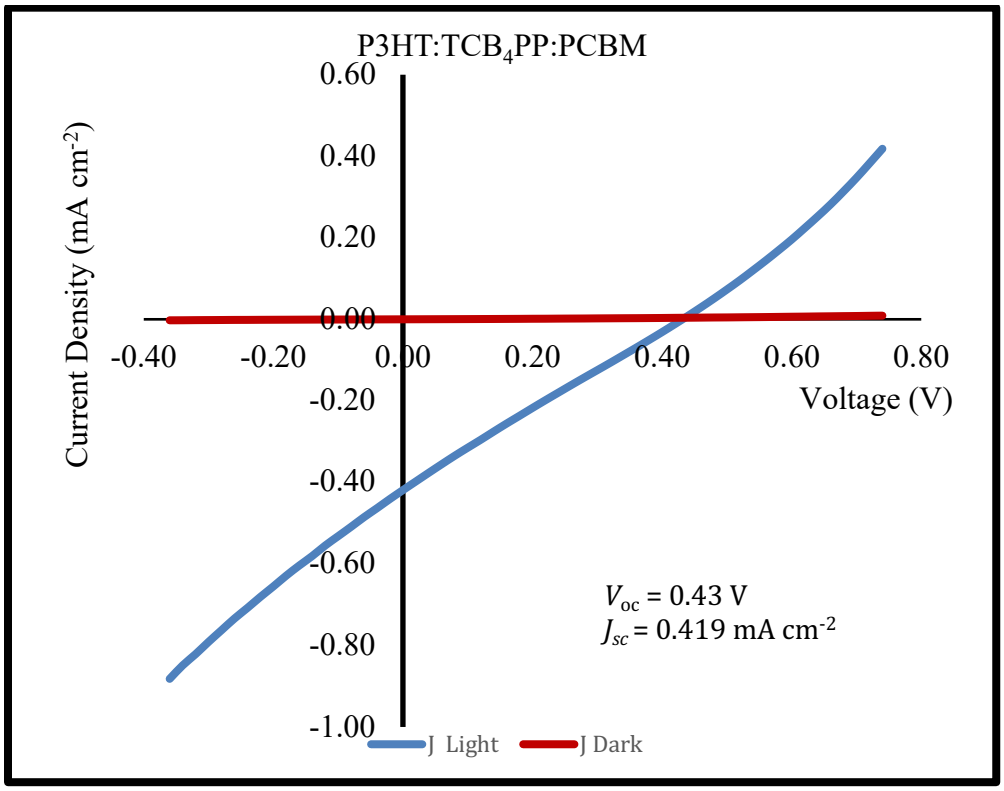

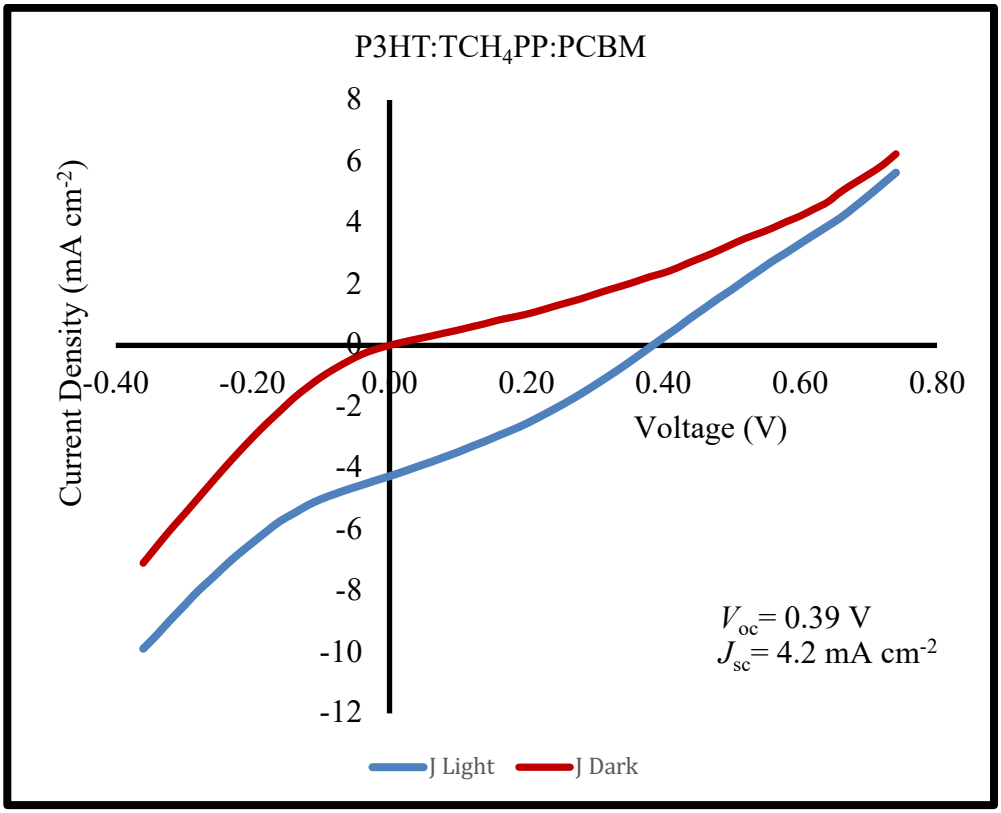

Figure 4.7 J-V curve of ternary blend of ternary blended organic solar cells

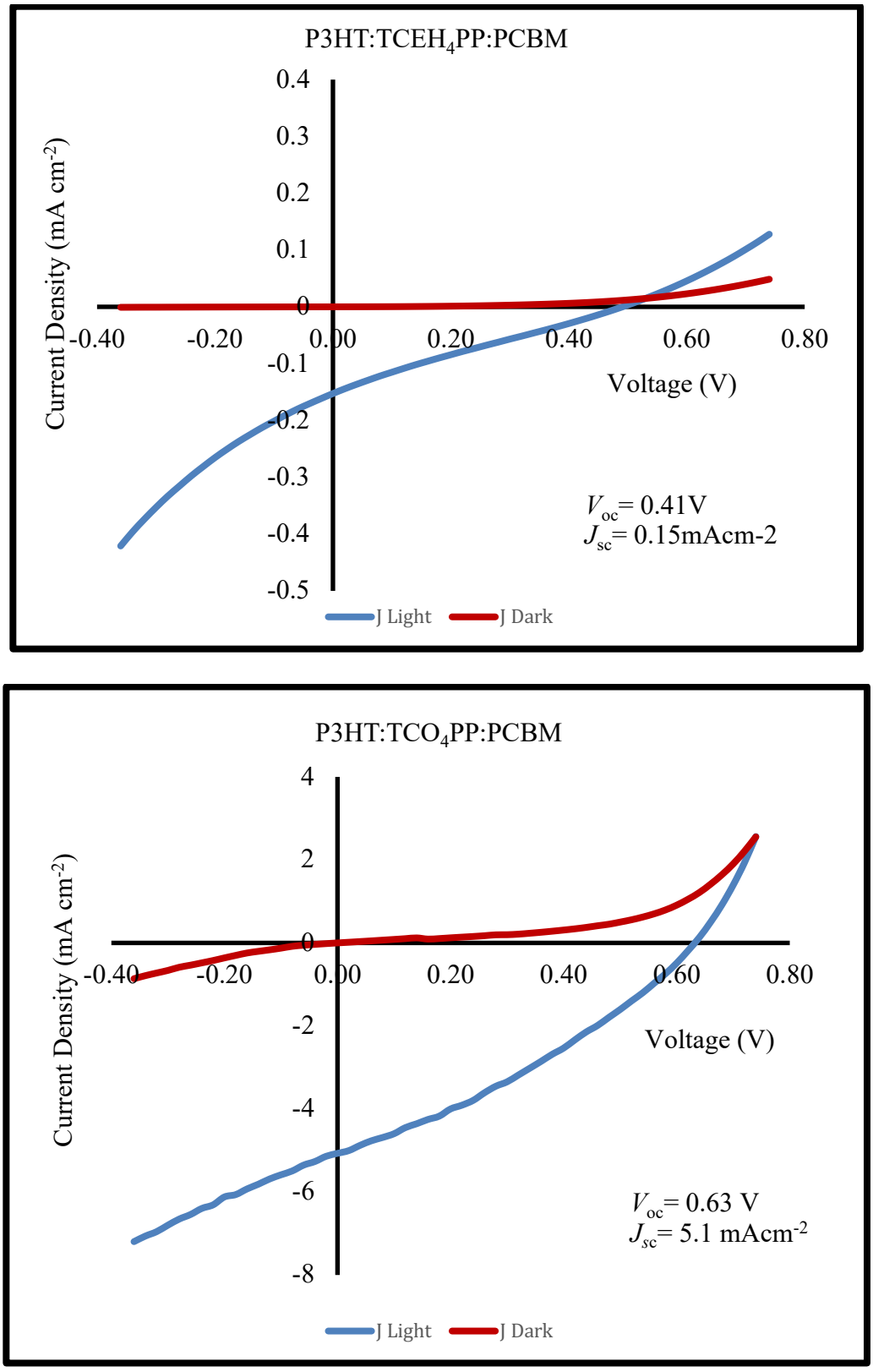

Figure 4.7 J-V curve of ternary blend of ternary blended organic solar cells continued

Table 4.1 Solar cell efficiency data for P3HT: Porphyrin:PCBM devices.

	J_{sc} (mA cm^{-2})	V_{oc} (V)	FF	η (%)
P3HT:TCB_4PP:PCBM	0.419 ± 0.23	0.41 ±0.02	0.22±0.01	0.04±0.02
P3HT:TCH_4PP:PCBM	5.4±0.60	0.39±0.01	0.29±0.01	0.62±0.06
P3HT:$TCEH_4$PP:PCBM	0.152±0.18	0.48±0.07	0.23±0.01	0.02±0.01
P3HT:TCO_4PP:PCBM	5.1 ±0.53	0.63±0.22	0.34±0.05	1.03±0.53

The preliminary data for EQE spectra for the devices made from ternary blends of P3HT:PCBM:Porphyrin and P3HT:PCBM devices with no porphyrin was compared in order to see the contribution of porphyrin towards the photocurrent in the devices as shown in **Figure 4.8**. The preliminary data indicates a small peak observed in the ternary blend at 420 nm in the ternary blended devices which is absent in P3HT: PCBM devices. This added spectral feature of the porphyrin absorption present in the ternary blend which could be contributing to capture incoming photons in that region to increase the spectral response. Overall the efficiency of the ternary solar cells decreased when the porphyrin was added which could be attributed to lower charge carrier mobilities of the porphyrin molecules as compared to the P3HT present in the donor material.

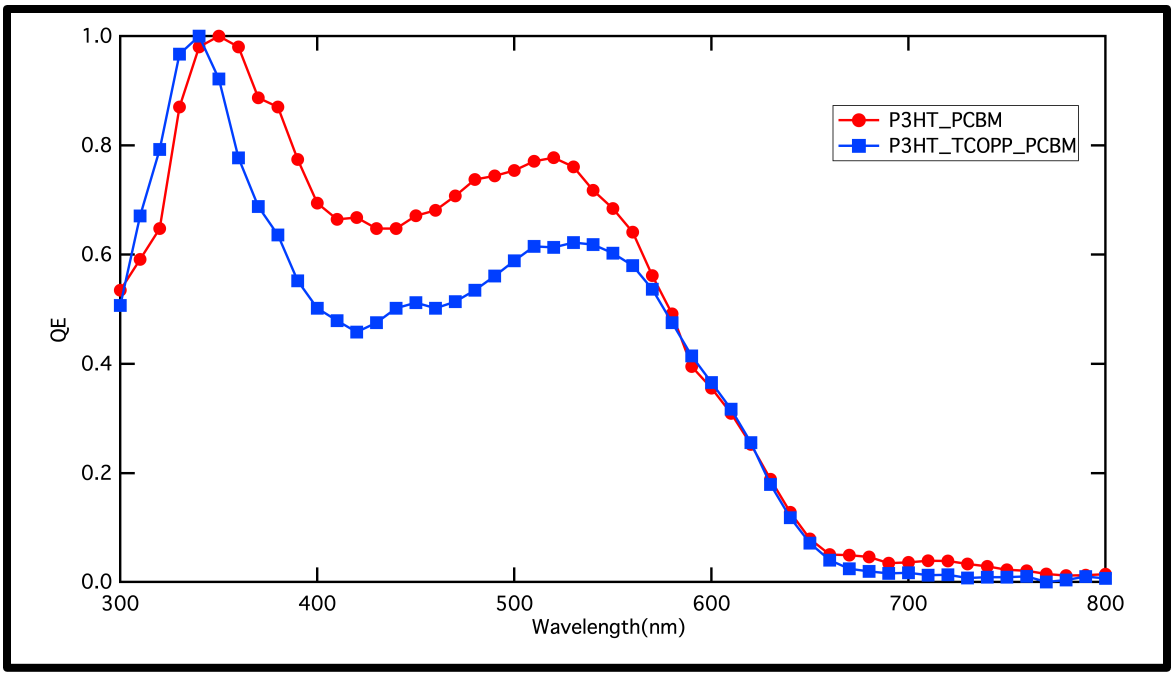

Figure 4.8 EQE spectra of P3HT:PCBM and TCO4PP:P3HT:PCBM

4.3.4 Grazing Incidence Wide-Angle X-Ray Scattering (GIWAXS)

Grazing Incidence Wide Angle X-Ray Scattering is a unique technique used in thin films of porphyrins to probe monolayers of carboalkoxyphenylporphyrins films on the substrate. As the name suggests the GIWAXS is aimed at scattering the incidence beam in a specific way to get information about symmetry, d- spacing, crystalline domain, grain-boundaries etc.[96] GIWAXS is often considered an extension of Grazing Incidence small Angle X-Ray Scattering (GISAXS). The 2D calibrated graphs shows ordering in the thin films in and out of plane. GIWAXS is often confused with GISAXS, the difference lies in the distance between sample and the detector. In GIWAXS the sample and detector are cm apart whereas in GISAXS the sample and detectors are in meters range. By bringing sample closer to the detector larger angular area of the plane is accessible.[97] The spots have been explained from the paper published by Müller-

Buschbaum.[97] **Figure 4.9** shows the calibrated 2D data obtained from the detector. This analysis was done at Diamond Light Source in UK. The GIWAXS insitu X-Ray scattering can provide an insight in to crystalline ordering and unit cell of the thin films of organic semiconducting materials. The GIWAXS with a 2 D area detector shows the reciprocal space information and is useful for our derivatives since they undergo very fast drying kinetics once the solutions have been spin-casted.[98] For the GIWAXS data the glass slides were sonicated and treated with UV ozone with an additional step of scribing at the back in order to cut the slides after spin casting. The final desired film dimensions were 1cm x 1cm and we were able to cut the films for the sample holder of GIWAXS instrument. The GIWAXS data were collected at Oxford University using I07 beamline with diamond light source. Beamline I07 is used to investigate and probe the nanosurfaces and interfaces of soft matter.[99] The beamline operates at 8-30 keV and is a high-resolution diffraction beam at diamond light source (DLS). The other experiments that can be done on this beamline includes surface X-ray diffraction (SXRD), grazing incidence X-Ray diffraction (GIXRD), X-Ray scattering (GISAXS) etc.[99]

The GIWAXS diffraction pattern was collected from TCB_4PP, TCH_4PP, $TCEH_4PP$ and TCO_4PP to obtain the information about nature of crystalline domains on thin films. The well-defined Braggs peaks were seen in TCB_4PP suggesting the lamellar packing of porphyrin molecules shown in **Figure 4.8**. No visible offset of crystal was seen out of plane suggesting mostly ordered packing. Some of the lamellas standing vertical to the substrate with majority of them lying flat. The molecules arranged themselves in layers with both in and out of plane ordering.

In the GIWAXS data for TCH_4PP, the diffraction pattern was seen suggesting more out of plane ordering assembly with some in plane crystallization. There is also some powdered ring features suggesting some texturing in these films. No peaks were seen at higher q values pointing towards large intermolecular spaces. Almost all of the lamellas are lying flat parallel to the substrate which very much coincides with the XRD data from Chapter 2.[96]

$TCEH_4PP$ showed much more in and out of plane growth with diffraction peaks at higher q values suggesting large domain of vertically aligned lamellas like quasi-epitaxial growth. The crystal truncation rods are nearly vertical with a small angular smear at larger q values suggesting the $TCEH_4PP$ molecules are tilting away from surface of the substrate and appear to be mostly vertically aligned.

TCO_4PP has the most out of plane ordering than any of the derivatives and it is very similar to the TCH_4PP with higher out of plane ordering as compared to rest of the derivatives. Some powdered rings were seen in TCO_4PP similar to TCH_4PP suggesting large intermolecular distance at low q values which could be attributed to the longer octyl chains causing various orientations relative to the surface of the substrate.

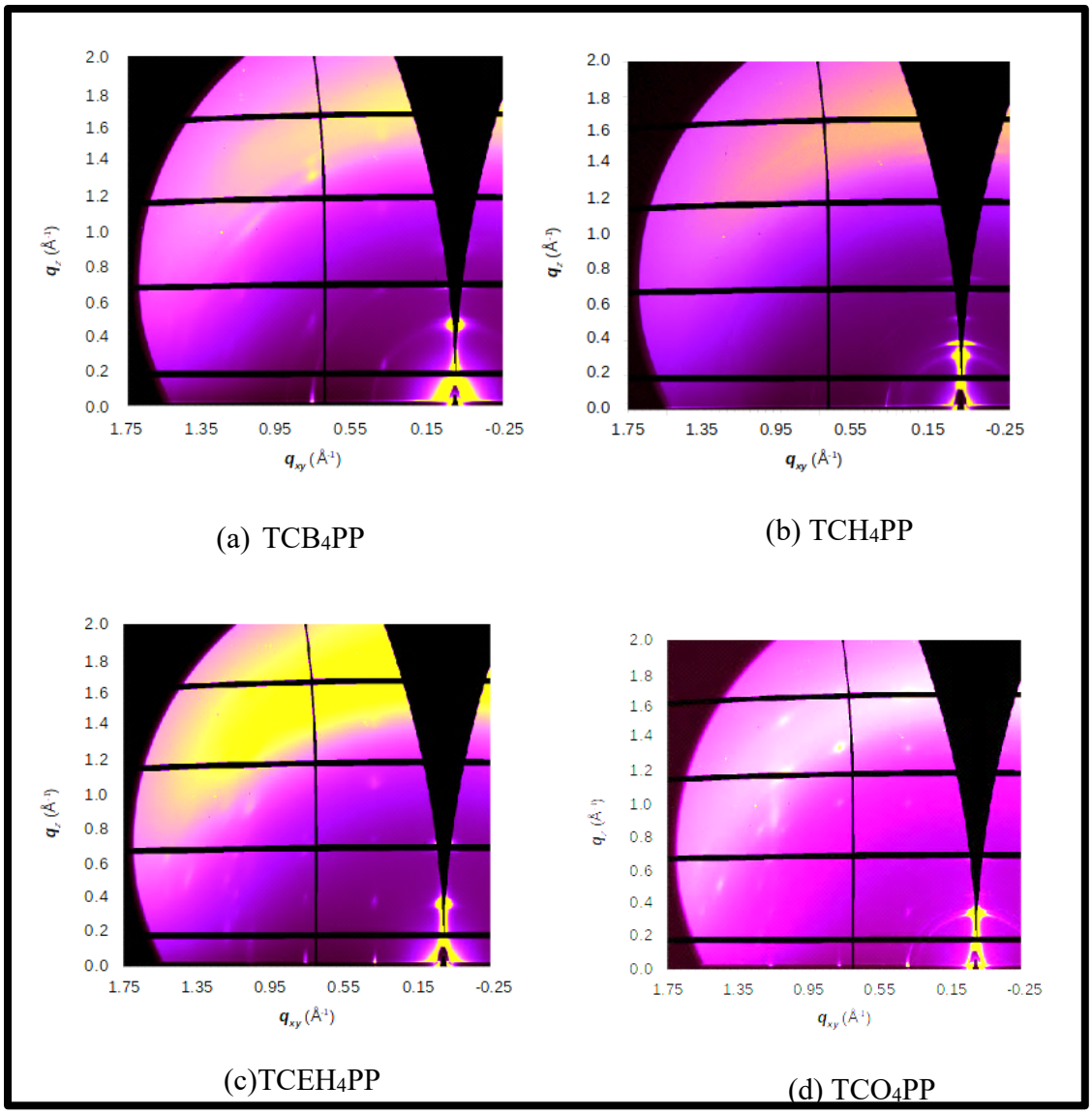

Figure 4.9 GIWAXS pattern for (A) TCB$_4$PP, (B) TCH$_4$PP, (C)TCEH$_4$PP and (D)TCO$_4$PP

4.4 Conclusions:

Ternary blended bulk-heterojunction devices have been fabricated using P3HT: Porphyrin:PCBM composition in the active layer where P3HT and porphyrin are acting as donor materials . The absorption and EQE spectra indicate that porphyrin is contributing in the photo absorption in the active layer of the devices. An improvement in device parameters and performance has been observed as the length of peripheral alkyl

chain in the carboalkoxyphenylporphyrin was increases symmetrically. However, introducing branching on the peripheral alkyl side chains made the devices significantly less efficient. GIWAXS data reemphasizes the fact how the porphyrin derivatives arrange themselves in a monolayer assembly. The porphyrin molecules TCH_4PP and TCO_4PP are oriented in face-on assembly or lying flat mostly parallel to the substrate whereas $TCEH_4PP$ molecules are laying vertical or end-on orientation at a certain angular tilt as compared to the surface of the substrate. This could be attributed to undesired molecular packing and organization of peripheral branched alkyl chains in porphyrin derivatives. This work links our previous findings on exciton diffusion and molecular organization in these very derivatives, where enhanced exciton diffusion parameters were seen in porphyrin derivatives with longer and symmetrical peripheral alkyl groups. The exciton diffusion was more efficient in TCH_4PP, TCO_4PP as compared to $TCEH_4PP$ (branched alkyl chain derivative). Our findings in this chapter validates our previous hypothesis which relates power conversion efficiency and device parameters to exciton diffusion and hence to molecular organization and orientation in a thin film assembly. Porphyrin derivatives with longer PL decay lifetimes (τ_s) and exciton diffusion lengths (L_D) have shown higher photocurrents and improved power conversion efficiencies. Our findings are an important step toward a deeper understanding of the exciton diffusivity and molecular packing relationship.

Chapter 5. CONCLUSIONS AND FUTURE WORK

We have studied the singlet exciton diffusion coefficients for five different alkyls substituted carboalkoxyphenylporphyrins; TCB_4PP (4-carbon), TCH_4PP (6-carbon), $TCEH_4PP$ (branched 6-carbon) and TCO_4PP (8-carbon) using time-resolved photoluminescent studies. We used the TCM_4PP data to compare the longer alkyl chain derivatives to see the effect of increasing alkyl chain length. This study was also performed with porphyrin films quenched by PCBM using two different (0.06%, 00.2%) volume fractions. We see that the singlet exciton diffusion is sensitive to the length of alkyl chain on carboalkoxyphenylporphyrins as this changes the molecular packing and rearrangements in thin cast films. The diffusion lengths of these derivatives increase with increasing alkyl chain up to a certain number of carbon atoms and then decrease with branching. The exciton diffusion lengths for TCH_4PP were longest because of the presence of homeotropic/nematic arrangements of porphyrin molecules in thin films as suggested by XRD peaks. TCH_4PP showed the strongest exciton coupling owing to its homeotropic assembly in thin films whereas branched derivative $TCEH_4PP$ showed the shortest exciton diffusion lengths and exciton diffusivity. This could be explained from the peaks seen in XRD data in Chapter 2, which suggests more slip-stacked arrangement in this particular derivative. When compared with 1-carbon chain derivative TCM_4PP, both TCH_4PP (25 nm) and TCO_4PP (21 nm) showed significantly longer diffusion lengths and photoluminescent lifetimes. This tells us that longer alkyl chain are affecting the exciton diffusion properties. However, it was seen that TCH_4PP has the longest exciton diffusion length and TCO_4PP had the longest lifetime with poor diffusivity. So,

we conclude here that TCH_4PP is likely to be more suited for improving the efficiency of porphyrin based organic solar cells since it demonstrates most promising exciton diffusion properties amongst all the derivatives.

During our second project we studied the bilayer films of pristine thin porphyrin films with C_{60} evaporated on them. This study was performed using our three-high performing (longer L_D's) porphyrin derivatives tetra (4-carbohexoxyphenyl) porphyrin (TCH_4PP), tetra (4-carbo-2-ethylhexoxyphenyl) porphyrin ($TCEH_4PP$), and tetra (4-carbooctoxyphenyl)-porphyrin (TCO_4PP). The bilayer films with porphyrin: C_{60} were constructed and annealed at 150 °C. The bilayer annealed and non-annealed films were tested for their photophysical properties. To study the effects of annealing on the molecular orientation of these derivatives, XRD, differential scanning calorimetry (DSC) experiments were performed. TCH_4PP showed maximum quenching efficiencies for the above stated conditions at room temperature and upon annealing all the films at 150 °C, TCH_4PP films showed greatest structural changes in XRD and in absorbance peaks as compared to $TCEH_4PP$ and TCO_4PP. TCH_4PP also showed decrease in quenching efficiencies upon annealing where as TCO_4PP and $TCEH_4PP$ showed increased quenching efficiencies at elevated temperatures. Future studies for this chapter will include measuring PL decays.

We prepared bulk-heterojunction devices of ternary assembly P3HT and PCBM with our carboalkoxyphenylporphyrin derivatives, since the TCH_4PP and TCO_4PP have long exciton diffusion lengths, almost double the organic semiconductors currently used. The composition of P3HT:Porphyrin:PCBM used in the preliminary data used in this dissertation was 1:1:4. The preliminary data collected showed an increase in

photocurrent as we went up two alkyl chains from TCB_4PP to TCH_4PP and TCO_4PP except for the branched derivative $TCEH_4PP$ which showed decrease in current density and open-circuit voltage as compared to TCH_4PP. This could likely be due to the molecular orientation and exciton diffusion study performed in Chapter 2 where we concluded that branching is not favorable for exciton diffusion pathways in thin films. The GIWAXS data of the thin films also suggests TCH_4PP and TCO_4PP molecules arrange themselves parallel to the surface of the substrate as compared to $TCEH_4PP$ molecules which showed angular tilt with respect to the substrate. The EQE spectra of P3HT:PCBM device was compared to the ternary blended devices with P3HT:Porphyrin:PCBM to examine the contribution of porphyrin to the photocurrent. A very small porphyrin peak was observed at 430 nm in the ternary blend device which indicated that porphyrin is contributing to the photocurrent in our ternary devices. This study helped us validate our initial hypothesis of relating exciton diffusion parameters to the PV characteristics of organic solar cells engineered in a ternary cell assembly.

In our future work, and in order to have better understanding of the porphyrin contribution, devices will be made where composition of P3HT and PCBM will be held constant and composition of porphyrin will be varied. This will help our efforts to understand the impact of varying compositions of porphyrins in the ternary blends. This project will also be extended further to study the effects of thermal annealing on the power conversion efficiencies. Some preliminary absorption data has been collected on thermal annealing of the active layer at 100°C, but more structural and morphology data such as AFM images of the films will be measured in order to have better understanding of the effects of annealing on the surface of thin films.

Recent work has demonstrated that annealing has improved the crystalline domains in some of the organic semiconductors resulting in improved charge mobilities and efficiencies of the devices. Hole mobilities of the ternary blended devices using P3HT: Porphyrin: PCBM will therefore be measured.[23]. Menke et. al. conducted a study on calculating PL quenching while diluting donor layer (thickness) and making a bilayer assembly using the same concentration of acceptor.[100] So far in this project, only the bulk-heterojunction device architecture has been evaluated. Therefore, we will also study the effect of increasing and decreasing the concentration of porphyrin derivative to study more closely the differences in bilayer and bulk heterojunction quenching. This approach is suitable for bilayer solar cell devices because of the use of molecular semiconductors with long L_D's, like the porphyrin derivatives reported in this dissertation.

REFERENCES

(1) Fahrenbruch, A.; Bube, R. *Fundamentals of solar cells: photovoltaic solar energy conversion*; Elsevier, 2012.

(2) Lewis, N. S. Toward cost-effective solar energy use. *science* **2007,** *315* (5813), 798.

(3) Choubey, P.; Oudhia, A.; Dewangan, R. A review: Solar cell current scenario and future trends. *Recent Research in Science and Technology* **2012,** *4* (8).

(4) Koebrich, S., 2019.

(5) Lewis, N. S.; Nocera, D. G. Powering the planet: Chemical challenges in solar energy utilization. *Proceedings of the National Academy of Sciences* **2006,** *103* (43), 15729.

(6) Adams, W. G.; Day, R. The action of light on selenium. *Philosophical Transactions of the Royal Society of London* **1877,** *167*, 313.

(7) Chopra, K.; Paulson, P.; Dutta, V. Thin-film solar cells: an overview. *Progress in Photovoltaics: Research and Applications* **2004,** *12* (2-3), 69.

(8) Miller, S. L.; Google Patents, 1963.

(9) Bhogaita, M.; Shukla, A. D.; Nalini, R. P. Recent advances in hybrid solar cells based on natural dye extracts from Indian plant pigment as sensitizers. *Solar Energy* **2016,** *137*, 212.

(10) Badawy, W. A. A review on solar cells from Si-single crystals to porous materials and quantum dots. *Journal of advanced research* **2015,** *6* (2), 123.

(11) Organics settle down. *Nat Nano* **2009,** *4* (10), 607.

(12) Gratzel, M. Dye-sensitized solar cells. *J. Photochem. Photobiol. C-Photochem. Rev.* **2003,** *4* (2), 145.

(13) Hagfeldt, A.; Boschloo, G.; Sun, L. C.; Kloo, L.; Pettersson, H. Dye-Sensitized Solar Cells. *Chem. Rev.* **2010,** *110* (11), 6595.

(14) Akamatu, H.; Inokuchi, H.; Matsunaga, Y. Organic Semiconductors with High Conductivity. I. Complexes between Polycyclic Aromatic Hydrocarbons and Halogens. *Bulletin of the Chemical Society of Japan* **1956,** *29* (2), 213.

(15) Ayzner, A. L.; Tassone, C. J.; Tolbert, S. H.; Schwartz, B. J. Reappraising the need for bulk heterojunctions in polymer− fullerene photovoltaics: the role of carrier transport in all-solution-processed P3HT/PCBM bilayer solar cells. *The Journal of Physical Chemistry C* **2009,** *113* (46), 20050.

(16) Backer, S. A.; Sivula, K.; Kavulak, D. F.; Fréchet, J. M. High efficiency organic photovoltaics incorporating a new family of soluble fullerene derivatives. *Chemistry of materials* **2007,** *19* (12), 2927.

(17) Nelson, C. A.; Monahan, N. R.; Zhu, X. Y. Exceeding the Shockley-Queisser limit in solar energy conversion. *Energy Environ. Sci.* **2013,** *6* (12), 3508.

(18) Vossier, A.; Gualdi, F.; Dollet, A.; Ares, R.; Aimez, V. Approaching the Shockley-Queisser limit: General assessment of the main limiting mechanisms in photovoltaic cells. *Journal of Applied Physics* **2015,** *117* (1), 015102.

(19) Huang, J.; Carpenter, J. H.; Li, C. Z.; Yu, J. S.; Ade, H.; Jen, A. K. Y. Highly Efficient Organic Solar Cells with Improved Vertical Donor–Acceptor Compositional Gradient Via an Inverted Off-Center Spinning Method. *Advanced Materials* **2016,** *28* (5), 967.

(20) Laquai, F.; Andrienko, D.; Deibel, C.; Neher, D. In *Elementary Processes in Organic Photovoltaics*; Springer, 2017.
(21) Fan, B.; Zhang, D.; Li, M.; Zhong, W.; Zeng, Z.; Ying, L.; Huang, F.; Cao, Y. Achieving over 16% efficiency for single-junction organic solar cells. *Science China Chemistry* **2019**, 1.
(22) Syu, Y. K.; Tingare, Y.; Lin, S. Y.; Yeh, C. Y.; Wu, J. J. Porphyrin Dye-Sensitized Zinc Oxide Aggregated Anodes for Use in Solar Cells. *Molecules* **2016,** *21* (8).
(23) Walter, M. G.; Rudine, A. B.; Wamser, C. C. Porphyrins and phthalocyanines in solar photovoltaic cells. *Journal of Porphyrins and Phthalocyanines* **2010,** *14* (09), 759.
(24) Shirakawa, H. Nobel Lecture: The discovery of polyacetylene film\char22{}the dawning of an era of conducting polymers. *Reviews of Modern Physics* **2001,** *73* (3), 713.
(25) Günes, S.; Neugebauer, H.; Sariciftci, N. S. Conjugated polymer-based organic solar cells. *Chem. Rev.* **2007,** *107* (4), 1324.
(26) Facchetti, A. Semiconductors for organic transistors. *Materials Today* **2007,** *10* (3), 28.
(27) So, F. *Organic electronics: materials, processing, devices and applications*; CRC press, 2009.
(28) Hoppe, H.; Sariciftci, N. S. Organic solar cells: An overview. *J. Mater. Res* **2004,** *19* (7), 1924.
(29) Dimitrakopoulos, C. D.; Mascaro, D. J. Organic thin-film transistors: A review of recent advances. *IBM Journal of research and development* **2001,** *45* (1), 11.
(30) Choy, W. C.; Ho, W. A. A. *Organic solar cells*; Springer, 2013.
(31) Gao, K.; Xiao, L. G.; Kan, Y. Y.; Yang, B. L.; Peng, J. B.; Cao, Y.; Liu, F.; Russell, T. P.; Peng, X. B. Solution-processed bulk heterojunction solar cells based on porphyrin small molecules with very low energy losses comparable to perovskite solar cells and high quantum efficiencies. *Journal of Materials Chemistry C* **2016,** *4* (17), 3843.
(32) Potember, R. S.; Hoffman, R. C.; Poehler, T. O. Molecular electronics. *Johns Hopkins APL Tech. Dig* **1986,** *7*, 129.
(33) He, Y.; Li, Y. Fullerene derivative acceptors for high performance polymer solar cells. *Physical chemistry chemical physics* **2011,** *13* (6), 1970.
(34) Peumans, P.; Uchida, S.; Forrest, S. R. Efficient bulk heterojunction photovoltaic cells using small-molecular-weight organic thin films. *Nature* **2003,** *425* (6954), 158.
(35) McEvoy, A.; Castaner, L.; Markvart, T. *Solar cells: materials, manufacture and operation*; Academic Press, 2012.
(36) Lakowicz, J. R. *Principles of fluorescence spectroscopy*; Springer Science & Business Media, 2013.
(37) Fraiji, L. K.; Hayes, D. M.; Werner, T. Static and dynamic fluorescence quenching experiments for the physical chemistry laboratory. *Journal of chemical education* **1992,** *69* (5), 424.
(38) Kumar, P. *Organic Solar Cells: Device Physics, Processing, Degradation, and Prevention*; CRC Press, 2016.

(39) Xie, W.; Menke, S. M.; Frisbie, C. D.; Holmes, R. J. In *THE WSPC REFERENCE ON ORGANIC ELECTRONICS: ORGANIC SEMICONDUCTORS: Basic Concepts*; World Scientific, 2016.
(40) Feron, K.; Belcher, W. J.; Fell, C. J.; Dastoor, P. C. Organic solar cells: understanding the role of Förster resonance energy transfer. *International journal of molecular sciences* **2012,** *13* (12), 17019.
(41) Rogach, A. L. Fluorescence energy transfer in hybrid structures of semiconductor nanocrystals. *Nano Today* **2011,** *6* (4), 355.
(42) Lattante, S. Electron and hole transport layers: their use in inverted bulk heterojunction polymer solar cells. *Electronics* **2014,** *3* (1), 132.
(43) Kaushal, M.; Ortiz, A. L.; Kassel, J. A.; Hall, N.; Lee, T. D.; Singh, G.; Walter, M. G. Enhancing exciton diffusion in porphyrin thin films using peripheral carboalkoxy groups to influence molecular assembly. *Journal of Materials Chemistry C* **2016,** *4* (24), 5602.
(44) Riede, M.; Uhrich, C.; Widmer, J.; Timmreck, R.; Wynands, D.; Schwartz, G.; Gnehr, W. M.; Hildebrandt, D.; Weiss, A.; Hwang, J. Efficient organic tandem solar cells based on small molecules. *Advanced Functional Materials* **2011,** *21* (16), 3019.
(45) Aranda, E. D.; Galan, J. A. G.; De Cardona, M. S.; Marquez, J. M. A. Measuring the IV curve of PV generators. *IEEE Industrial Electronics Magazine* **2009,** *3* (3), 4.
(46) Picciarelli, V.; Di Gennaro, M.; Stella, R.; Conte, E. A study of university students' understanding of simple electric circuits part 2: Batteries, ohm's law, power dissipated, resistors in parallel. *European Journal of Engineering Education* **1991,** *16* (1), 57.
(47) Narayan, J.; Shukla, V. Formation of Ohmic contacts in semiconducting oxides. *Journal of Applied Physics* **1980,** *51* (6), 3444.
(48) Millikan, R. A.; Bishop, E. S. *Elements of electricity: a practical discussion of the fundamental laws and phenomena of electricity and their practical applications in the business and industrial world*; American Technical Society, 1917.
(49) Sandstrom, J. D. A method for predicting solar cell current-voltage curve characteristics as a function of incident solar intensity and cell temperature. **1967**.
(50) Kadish, K. M.; Smith, K. M.; Guilard, R. *The Porphyrin Handbook: Inorganic, organometallic and coordination chemistry*; Elsevier, 2000.
(51) Yatskou, M. M.; Koehorst, R. B. M.; van Hoek, A.; Donker, H.; Schaafsma, T. J.; Gobets, B.; van Stokkum, I.; van Grondelle, R. Spectroscopic properties of a self-assembled zinc porphyrin tetramer II. Time-resolved fluorescence spectroscopy. *J. Phys. Chem. A* **2001,** *105* (51), 11432.
(52) Giovannetti, R. The use of Spectrophotometry UV-Vis for the Study of Porphyrins. *Edited by Jamal Uddin* **2012,** *87*.
(53) Li, L.-L.; Diau, E. W.-G. Porphyrin-sensitized solar cells. *Chem. Soc. Rev.* **2013,** *42* (1), 291.
(54) Li, L. L.; Diau, E. W. G. Porphyrin-sensitized solar cells. *Chem. Soc. Rev.* **2013,** *42* (1), 291.
(55) Gouterman, M. Spectra of porphyrins. *Journal of Molecular Spectroscopy* **1961,** *6*, 138.

(56) Lee, C. W.; Lu, H. P.; Lan, C. M.; Huang, Y. L.; Liang, Y. R.; Yen, W. N.; Liu, Y. C.; Lin, Y. S.; Diau, E. W. G.; Yeh, C. Y. Novel Zinc Porphyrin Sensitizers for Dye-Sensitized Solar Cells: Synthesis and Spectral, Electrochemical, and Photovoltaic Properties. *Chemistry–A European Journal* **2009,** *15* (6), 1403.
(57) Campbell, W. M.; Burrell, A. K.; Officer, D. L.; Jolley, K. W. Porphyrins as light harvesters in the dye-sensitised TiO2 solar cell. *Coord. Chem. Rev.* **2004,** *248* (13-14), 1363.
(58) Grätzel, M. Dye-sensitized solar cells. *Journal of photochemistry and photobiology C: Photochemistry Reviews* **2003,** *4* (2), 145.
(59) Higashino, T.; Imahori, H. Porphyrins as excellent dyes for dye-sensitized solar cells: recent developments and insights. *Dalton Transactions* **2015,** *44* (2), 448.
(60) Gledhill, S. E.; Scott, B.; Gregg, B. A. Organic and nano-structured composite photovoltaics: An overview. *Journal of Materials Research* **2005,** *20* (12), 3167.
(61) Kaushal, M.; Ortiz, A. L.; Kassel, J. A.; Hall, N.; Lee, T. D.; Singh, g.; Walter, M. G. Enhancing Exciton Diffusion in Porphyrin Thin Films Using Peripheral Carboalkoxy Groups to Influence Molecular Assembly. *J. Mater. Chem. C* **2016,** *4*, 5602.
(62) Huang, Y.; Li, L.; Peng, X.; Peng, J.; Cao, Y. Solution processed small molecule bulk heterojunction organic photovoltaics based on a conjugated donor–acceptor porphyrin. *Journal of Materials Chemistry* **2012,** *22* (41), 21841.
(63) Guldi, D. M. Fullerene–porphyrin architectures; photosynthetic antenna and reaction center models. *Chem. Soc. Rev.* **2002,** *31* (1), 22.
(64) Menke, S. M.; Holmes, R. J. Exciton diffusion in organic photovoltaic cells. *Energy Environ. Sci.* **2014,** *7* (2), 499.
(65) Lin, J. D.; Mikhnenko, O. V.; Chen, J.; Masri, Z.; Ruseckas, A.; Mikhailovsky, A.; Raab, R. P.; Liu, J.; Blom, P. W.; Loi, M. A. Systematic study of exciton diffusion length in organic semiconductors by six experimental methods. *Materials Horizons* **2014,** *1* (2), 280.
(66) Marin, D. M.; Castaneda, J.; Kaushal, M.; Kaouk, G.; Jones, D. S.; Walter, M. G. Spatially resolved micro-photoluminescence imaging of porphyrin single crystals. *Chemical Physics Letters* **2016,** *659*, 137.
(67) Borjesson, K.; Rudquist, P.; Gray, V.; Moth-Poulsen, K. Photon upconversion with directed emission. *Nature Communications* **2016,** *7*.
(68) Duan, P.; Yanai, N.; Kimizuka, N. Photon upconverting liquids: matrix-free molecular upconversion systems functioning in air. *Journal of the American Chemical Society* **2013,** *135* (51), 19056.
(69) Lindsey, J. S.; Schreiman, I. C.; Hsu, H. C.; Kearney, P. C.; Marguerettaz, A. M. Rothemund and Adler-Longo reactions revisited: synthesis of tetraphenylporphyrins under equilibrium conditions. *J. Org. Chem.* **1987,** *52* (5), 827.
(70) Huijser, A.; Savenije, T. J.; Kotlewski, A.; Picken, S. J.; Siebbeles, L. D. Efficient Light-Harvesting Layers of Homeotropically Aligned Porphyrin Derivatives. *Advanced materials* **2006,** *18* (17), 2234.
(71) Milgrom, L. R. The colours of life: an introduction to the chemistry of porphyrins and related compounds. **1997**.

(72) Huijser, A.; Suijkerbuijk, B. M.; Klein Gebbink, R. J.; Savenije, T. J.; Siebbeles, L. D. Efficient exciton transport in layers of self-assembled porphyrin derivatives. *Journal of the American Chemical Society* **2008,** *130* (8), 2485.
(73) Watkins, P. K.; Walker, A. B.; Verschoor, G. L. Dynamical Monte Carlo modelling of organic solar cells: The dependence of internal quantum efficiency on morphology. *Nano letters* **2005,** *5* (9), 1814.
(74) Siebbeles, L. D.; Huijser, A.; Savenije, T. J. Effects of molecular organization on exciton diffusion in thin films of bioinspired light-harvesting molecules. *Journal of Materials Chemistry* **2009,** *19* (34), 6067.
(75) Permyakov, E. A. *Luminescent Spectroscopy of Proteins: 0*; CRC press, 2018.
(76) Hsu, H.-Y.; Vella, J. H.; Myers, J. D.; Xue, J.; Schanze, K. S. Triplet exciton diffusion in platinum polyyne films. *The Journal of Physical Chemistry C* **2014,** *118* (42), 24282.
(77) Ryuzaki, S.; Hasegawa, T.; Onoe, J. X-ray diffraction and infrared multiple-angle incidence resolution spectroscopic studies on the crystal structure and molecular orientation of zinc-porphyrin thin films on a SiO 2/Si substrate. *Journal of Applied Physics* **2009,** *105* (11), 113529.
(78) Huijser, A.; Savenije, T. J.; Meskers, S. C.; Vermeulen, M. J.; Siebbeles, L. D. The mechanism of long-range exciton diffusion in a nematically organized porphyrin layer. *Journal of the American Chemical Society* **2008,** *130* (37), 12496.
(79) Lee, K. H.; Schwenn, P. E.; Smith, A. R.; Cavaye, H.; Shaw, P. E.; James, M.; Krueger, K. B.; Gentle, I. R.; Meredith, P.; Burn, P. L. Morphology of all-solution-processed "bilayer" organic solar cells. *Advanced Materials* **2011,** *23* (6), 766.
(80) Belcher, W.; Wagner, K.; Dastoor, P. The effect of porphyrin inclusion on the spectral response of ternary P3HT: porphyrin: PCBM bulk heterojunction solar cells. *Solar energy materials and solar cells* **2007,** *91* (6), 447.
(81) Sun, Q.; Dai, L.; Zhou, X.; Li, L.; Li, Q. Bilayer-and bulk-heterojunction solar cells using liquid crystalline porphyrins as donors by solution processing. *Applied Physics Letters* **2007,** *91* (25), 253505.
(82) Zhou, X.; Kang, S.-W.; Kumar, S.; Kulkarni, R. R.; Cheng, S. Z.; Li, Q. Self-assembly of porphyrin and fullerene supramolecular complex into highly ordered nanostructure by simple thermal annealing. *Chemistry of Materials* **2008,** *20* (11), 3551.
(83) Sun, S.; Salim, T.; Mathews, N.; Duchamp, M.; Boothroyd, C.; Xing, G.; Sum, T. C.; Lam, Y. M. The origin of high efficiency in low-temperature solution-processable bilayer organometal halide hybrid solar cells. *Energy Environ. Sci.* **2014,** *7* (1), 399.
(84) Ramasseul, R.; Maldivi, P.; Marchon, J.-C.; Taylor, M.; Guillon, D. Phase transitions of long chain esters of meso-tetrakis (para-carboxyphenyl) porphyrin. *Liquid Crystals* **1993,** *13* (5), 729.
(85) Holzwarth, U.; Gibson, N. The Scherrer equation versus the'Debye-Scherrer equation'. *Nature nanotechnology* **2011,** *6* (9), 534.
(86) Cooling, N.; Burke, K. B.; Zhou, X.; Lind, S. J.; Gordon, K. C.; Jones, T. W.; Dastoor, P. C.; Belcher, W. J. A study of the factors influencing the performance

of ternary MEH-PPV: porphyrin: PCBM heterojunction devices: a steric approach to controlling charge recombination. *Solar Energy Materials and Solar Cells* **2011,** *95* (7), 1767.

(87) Cooling, N. A.; Zhou, X.; Sales, T. A.; Sauer, S. E.; Lind, S. J.; Gordon, K. C.; Jones, T. W.; Burke, K. B.; Dastoor, P. C.; Belcher, W. J. A study of the factors influencing the performance of ternary MEH-PPV: porphyrin: PCBM heterojunction devices: Electronic effects in porphyrinoid ternary blend bulk heterojunction photovoltaic devices. *Solar Energy Materials and Solar Cells* **2012,** *98*, 308.

(88) Khlyabich, P. P.; Burkhart, B.; Thompson, B. C. Efficient ternary blend bulk heterojunction solar cells with tunable open-circuit voltage. *Journal of the American Chemical Society* **2011,** *133* (37), 14534.

(89) Stoltzfus, D. M.; Kesters, J.; Kelchtermans, M.; Verstappen, P.; Cardinaletti, I.; Cornelissen, R.; D'Haen, J.; Lutsen, L.; Vanderzande, D.; Manca, J. Improved efficiency of polymer-fullerene bulk heterojunction solar cells by the addition of Cu (II)-porphyrin-oligothiophene conjugates. *Synthetic Metals* **2016,** *218*, 1.

(90) Huang, J.-S.; Goh, T.; Li, X.; Sfeir, M. Y.; Bielinski, E. A.; Tomasulo, S.; Lee, M. L.; Hazari, N.; Taylor, A. D. Polymer bulk heterojunction solar cells employing Förster resonance energy transfer. *Nature Photonics* **2013,** *7* (6), 479.

(91) Ismail, Y. A.; Soga, T.; Jimbo, T. The contribution of coumarin 6 in light harvesting and photocurrent of P3HT: PCBM bulk heterojunction solar cell. *Solar Energy Materials and Solar Cells* **2010,** *94* (8), 1406.

(92) Rahimi, K.; Botiz, I.; Agumba, J. O.; Motamen, S.; Stingelin, N.; Reiter, G. Light absorption of poly (3-hexylthiophene) single crystals. *RSC Advances* **2014,** *4* (22), 11121.

(93) Shafiee, A.; Salleh, M. M.; Yahaya, M. Determination of HOMO and LUMO of [6, 6]-phenyl C61-butyric acid 3-ethylthiophene ester and poly (3-octyl-thiophene-2, 5-diyl) through voltametry characterization. *Sains Malaysiana* **2011,** *40* (2), 173.

(94) Leonat, L.; Sbarcea, G.; Branzoi, I. V. Cyclic voltammetry for energy levels estimation of organic materials. *UPB Sci Bull Ser B* **2013,** *75*, 111.

(95) Ortiz, A. L.; Collier, G. S.; Marin, D. M.; Kassel, J. A.; Ivins, R. J.; Grubich, N. G.; Walter, M. G. The effects of heavy atoms on the exciton diffusion properties in photoactive thin films of tetrakis(4-carbomethoxyphenyl)porphyrins. *Journal of Materials Chemistry C* **2015,** *3* (6), 1243.

(96) Perlich, J.; Rubeck, J.; Botta, S.; Gehrke, R.; Roth, S. V.; Ruderer, M. A.; Prams, S. M.; Rawolle, M.; Zhong, Q.; Korstgens, V.et al. Grazing incidence wide angle x-ray scattering at the wiggler beamline BW4 of HASYLAB. *Rev. Sci. Instrum.* **2010,** *81* (10), 7.

(97) Müller-Buschbaum, P. The active layer morphology of organic solar cells probed with grazing incidence scattering techniques. *Advanced Materials* **2014,** *26* (46), 7692.

(98) Liman, C. D.; Choi, S.; Breiby, D. W.; Cochran, J. E.; Toney, M. F.; Kramer, E. J.; Chabinyc, M. L. Two-Dimensional GIWAXS Reveals a Transient Crystal Phase in Solution-Processed Thermally Converted Tetrabenzoporphyrin. *The Journal of Physical Chemistry B* **2013,** *117* (46), 14557.

(99) Nicklin, C.; Arnold, T.; Rawle, J.; Warne, A. Diamond beamline I07: a beamline for surface and interface diffraction. *Journal of Synchrotron Radiation* **2016,** *23* (5).
(100) Menke, S. M.; Luhman, W. A.; Holmes, R. J. Tailored exciton diffusion in organic photovoltaic cells for enhanced power conversion efficiency. *Nature materials* **2013,** *12* (2), 152.

APPENDIX-I

^{1}H N-MR of Carboalkoxyphenyl porphyrin Derivatives

(a) TCB_4PP

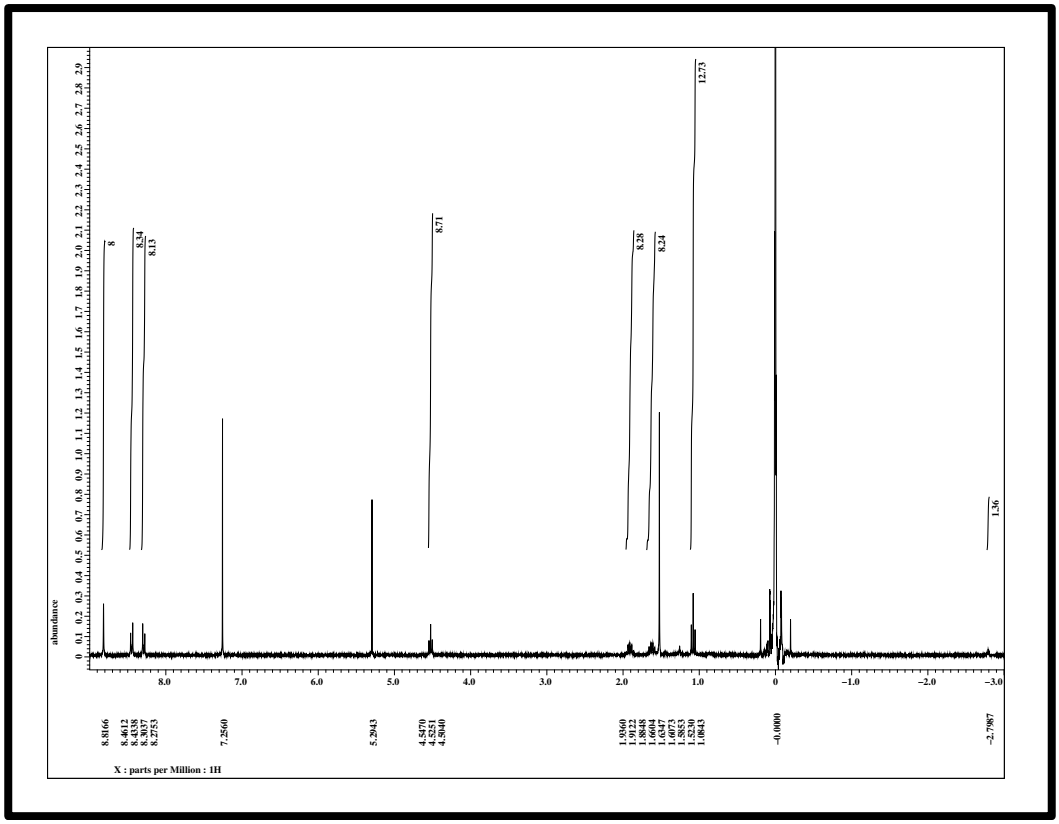

^{1}H NMR (300 MHz, CH_2Cl_2, TMS, δ): 8.86 (s, 8H), 8.44 (d, *J* = 8.0 Hz, 8H), 8.31 (d, *J* = 8.3 Hz, 8H), 4.50 (t, *J* = 6.5 Hz, 8H), 1.90 (pnt, *J* = 7.0 Hz, 8H), 1.62 (sxt, *J* = 7.4 Hz, 8H), 1.07 (t, *J* = 7.3 Hz, 12H), -2.84 (s, 2H)

APPENDIX-II

^{1}H NMR of Carboalkoxyphenyl porphyrin Derivative

(b) TCH_4PP

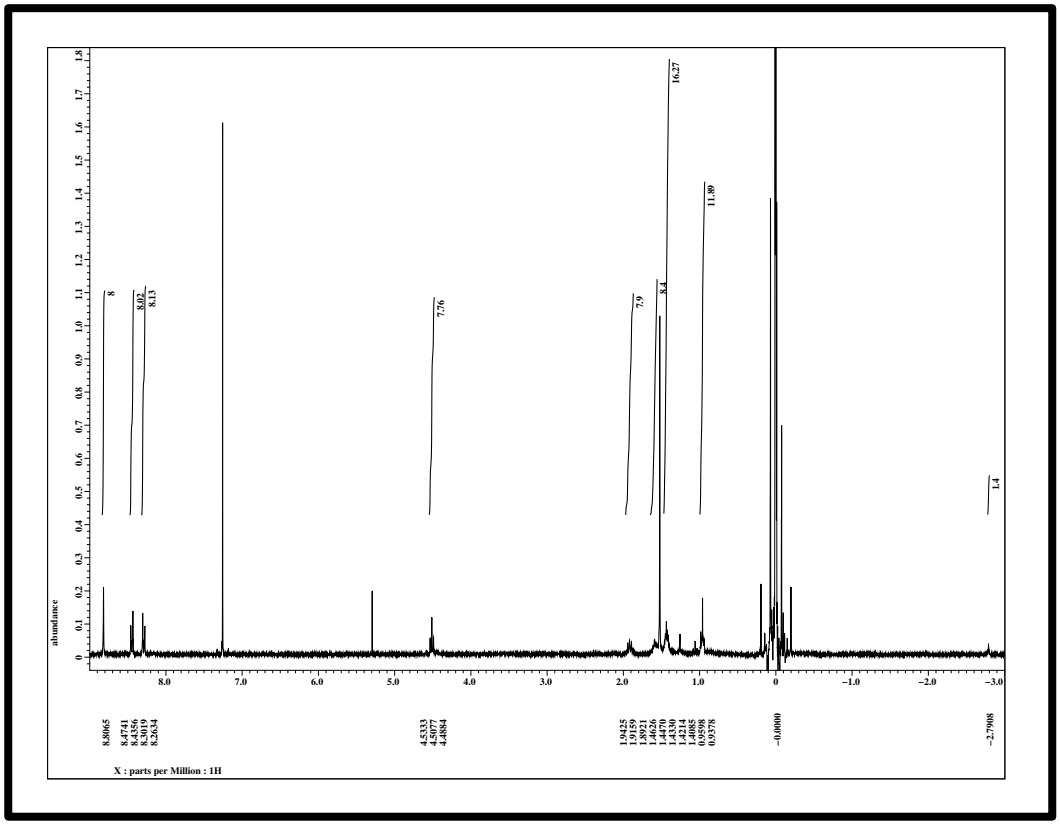

^{1}H NMR (300 MHz, CH_2Cl_2, TMS, δ): 8.86 (s, 8H), 8.44 (d, *J* = 8.0 Hz, 8H), 8.31 (d, *J* = 8.0 Hz, 8H), 4.49 (t, *J* = 6.6 Hz, 8H), 1.91 (pnt, *J* = 7.04 Hz, 8 H), 1.59 (m, 8H), 1.43 (m, 16H), 0.96 (t, *J* = 7.0 Hz, 12H), -2.84 (s, 2H)

APPENDIX-III

^{1}H NMR of Carboalkoxyphenyl porphyrin Derivatives

(c) TCO_4PP

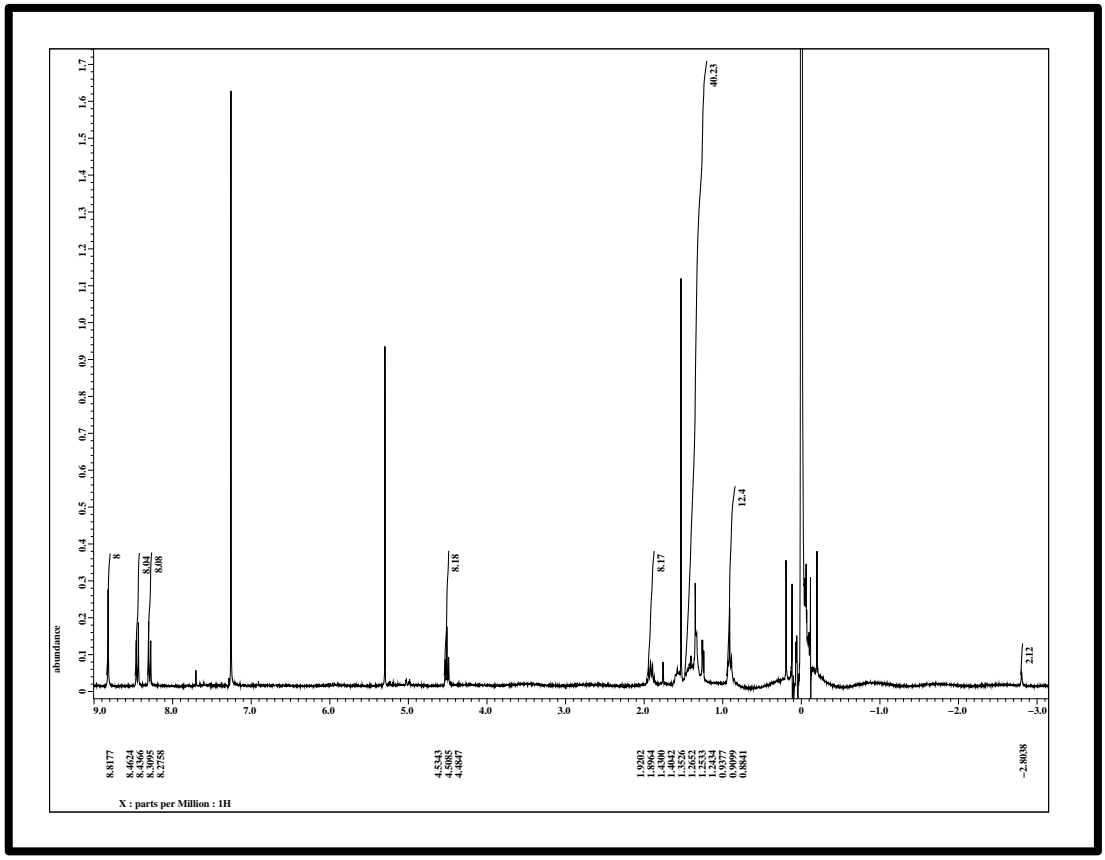

^{1}H NMR (300 MHz, CH_2Cl_2, TMS, δ): 8.86 (s, 8H), 8.44 (d, *J* = 8.3 Hz, 8H), 8.31 (d, *J* = 8.5 Hz, 8H), 4.49 (t, *J* = 6.6 Hz, 8H), 1.91 (pnt, *J* = 7.2 Hz, 8H), 1.6-1.38 (m, 40H), 0.91 (t, *J* = 6.8 Hz, 12H), -2.84 (s, 2H)

APPENDIX-IV

MALDI-MS of Carboalkoxyphenyl porphyrin Derivatives

(a) TCB_4PP – Molar Mass 1014.5 g/mol

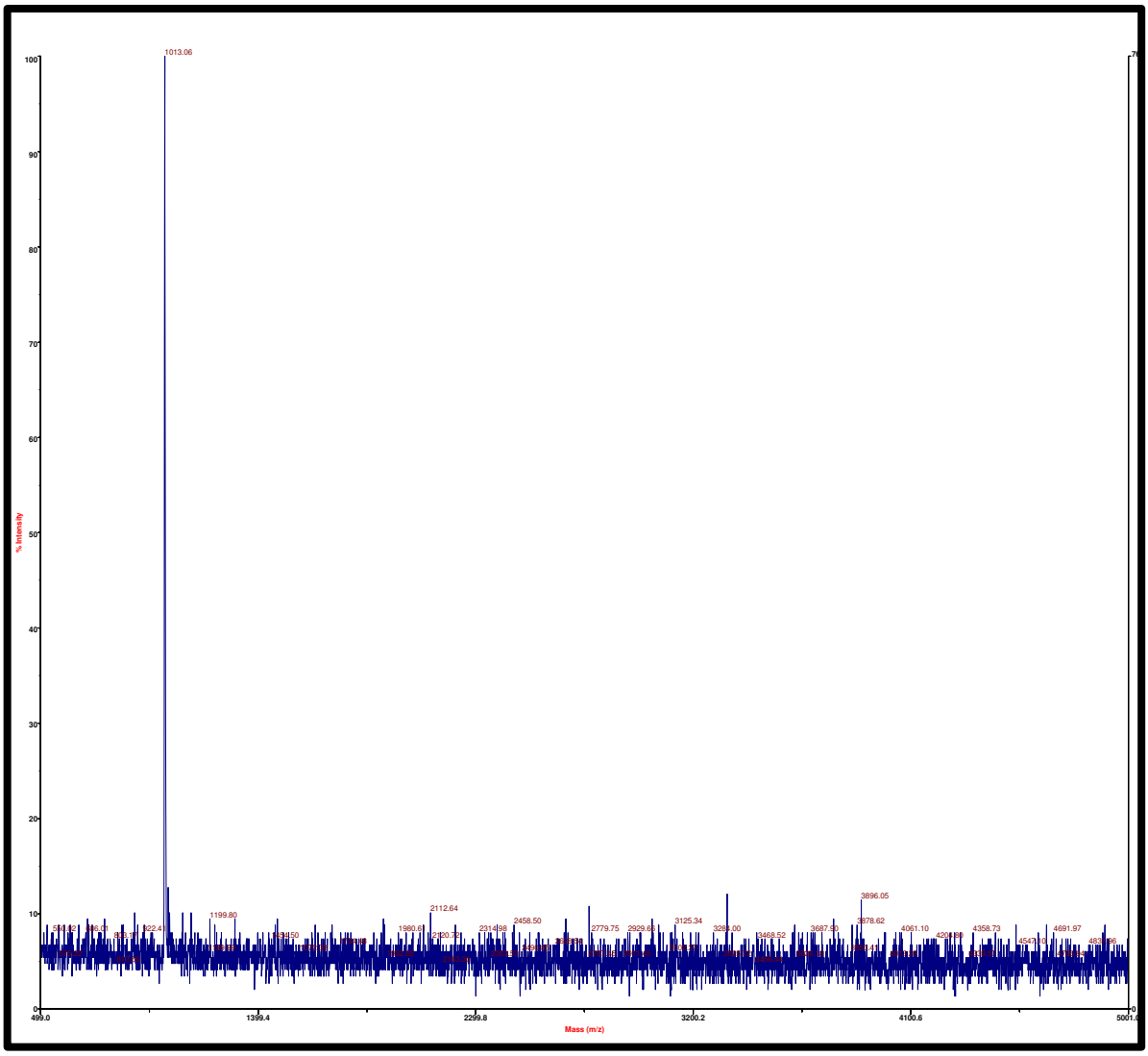

APPENDIX-V

MALDI-MS of Carboalkoxyphenyl porphyrin Derivatives

(b) TCH_4PP- Molar Mass 1126.6 g/mol

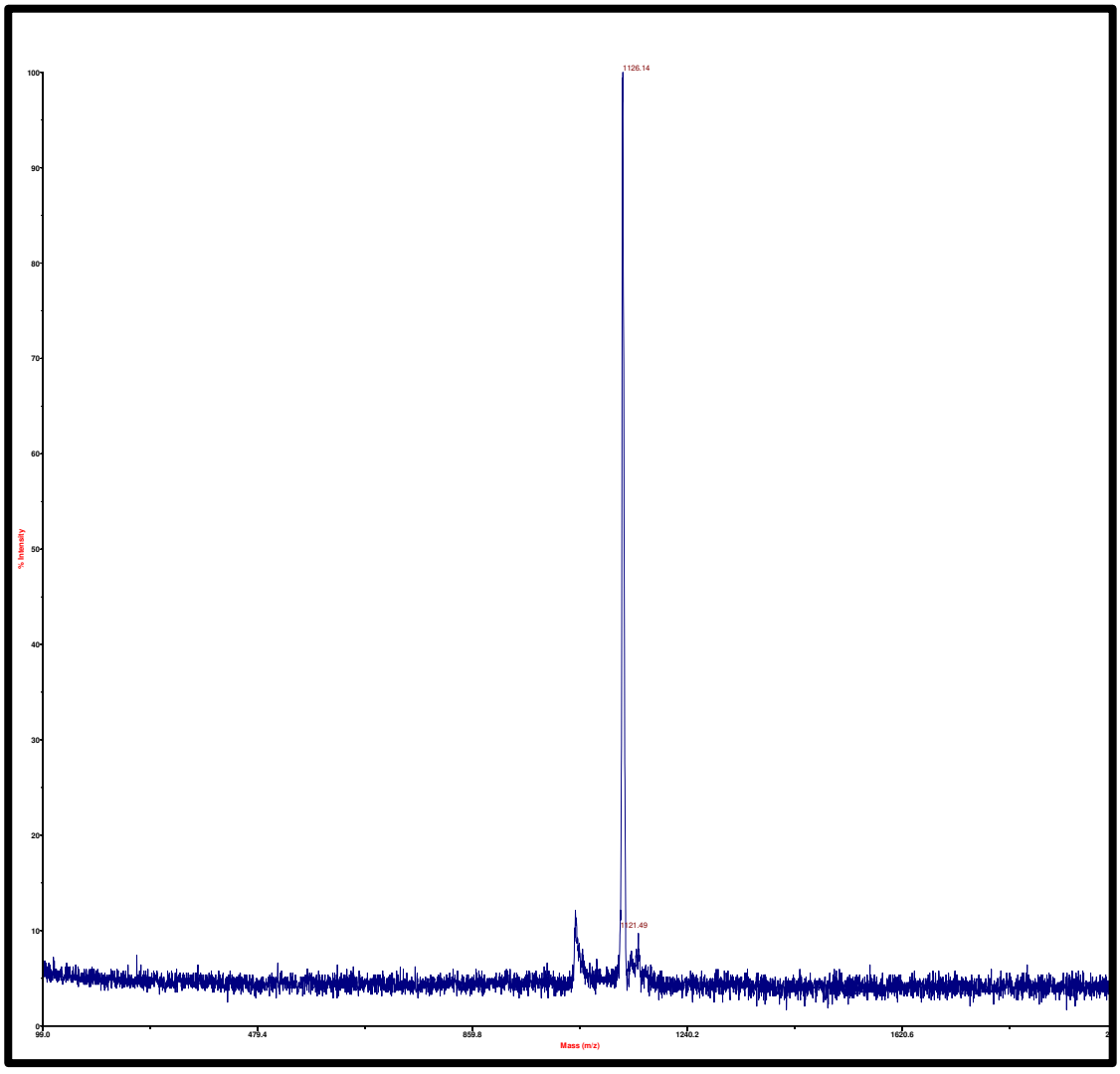

APPENDIX -VI

MALDI-MS of Carboalkoxyphenyl porphyrin Derivatives

(c) $TCEH_4PP$- Molar Mass 1237.2 g/mol

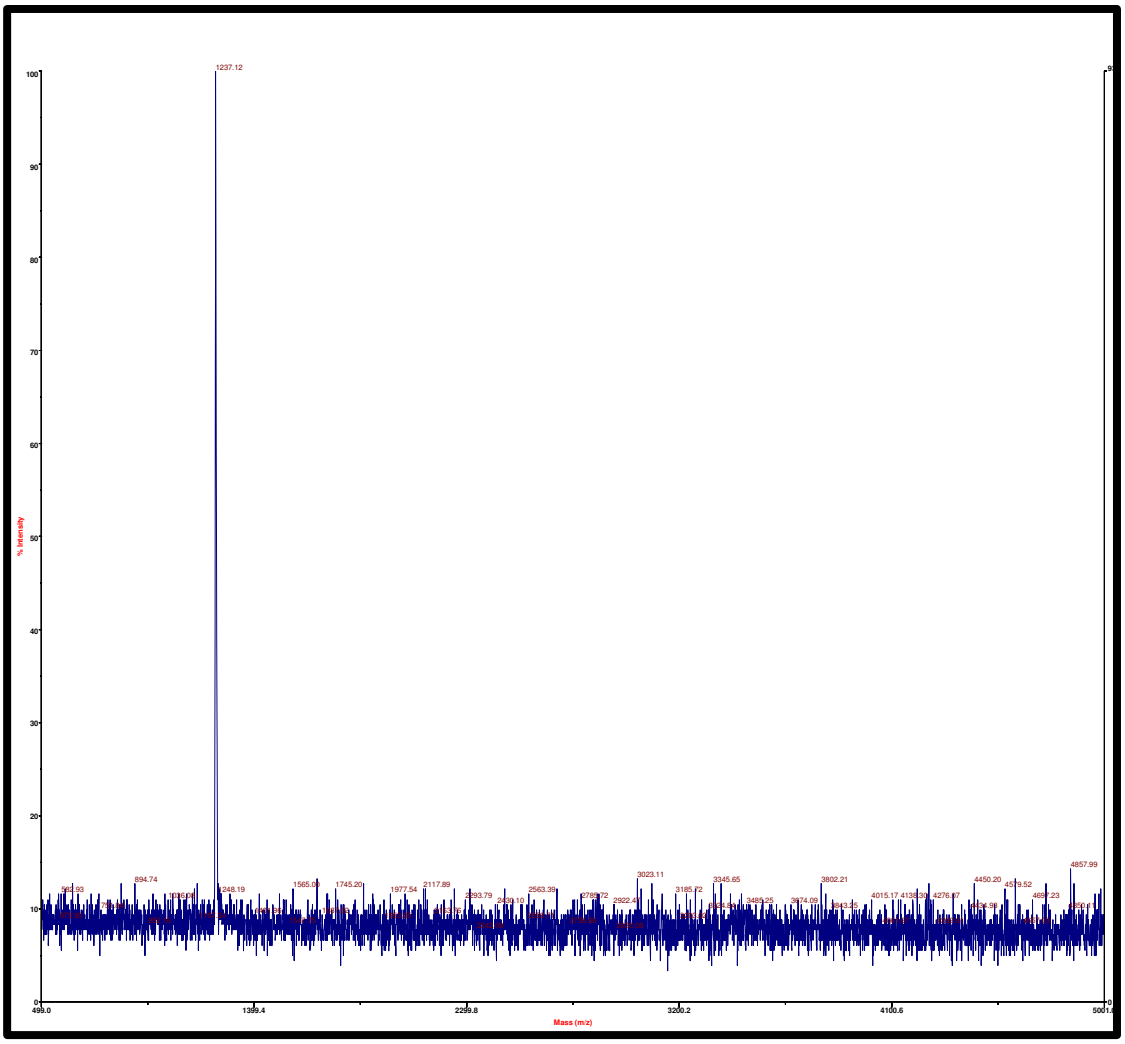

APPENDIX -VII

MALDI-MS of Carboalkoxyphenyl porphyrin Derivatives

(d) TCO_4PP- Molar Mass 1237.5 g/mol